Let Wind Rise – Harnessing Bulk Energy Storage under Increasing Renewable Penetration Levels

by

Nan Li

A Dissertation Presented in Partial Fulfillment
of the Requirements for the Degree
Doctor of Philosophy

Approved September 2016 by the
Graduate Supervisory Committee:

Kory W. Hedman, Chair
Gerald T. Heydt
Lalitha Sankar
Daniel J. Tylavsky

ARIZONA STATE UNIVERSITY

December 2016

ABSTRACT

With growing concern regarding environmental issues and the need for a more sustainable grid, power systems have seen a fast expansion of renewable resources in the last decade. The uncertainty and variability of renewable resources has posed new challenges on system operators. Due to its energy-shifting and fast-ramping capabilities, energy storage (ES) has been considered as an attractive solution to alleviate the increased renewable uncertainty and variability.

In this dissertation, stochastic optimization is utilized to evaluate the benefit of bulk energy storage to facilitate the integration of high levels of renewable resources in transmission systems. A cost-benefit analysis is performed to study the cost-effectiveness of energy storage. A two-step approach is developed to analyze the effectiveness of using energy storage to provide ancillary services. Results show that as renewable penetrations increase, energy storage can effectively compensate for the variability and uncertainty in renewable energy and has increasing benefits to the system.

With increased renewable penetrations, enhanced dispatch models are needed to efficiently operate energy storage. As existing approaches do not fully utilize the flexibility of energy storage, two approaches are developed in this dissertation to improve the operational strategy of energy storage. The first approach is developed using stochastic programming techniques. A stochastic unit commitment (UC) is solved to obtain schedules for energy storage with different renewable scenarios. Operating policies are then constructed using the solutions from the stochastic UC to efficiently operate energy storage across multiple time periods. The second approach is a policy function approach. By incorporating an offline analysis stage prior to the actual operating

stage, the patterns between the system operating conditions and the optimal actions for energy storage are identified using a data mining model. The obtained data mining model is then used in real-time to provide enhancement to a deterministic economic dispatch model and improve the utilization of energy storage. Results show that the policy function approach outperforms a traditional approach where a schedule determined and fixed at a prior look-ahead stage is used. The policy function approach is also shown to have minimal added computational difficulty to the real-time market.

To my mother Li Li and my father Chenghui Li,

for your unconditional love.

You have always been the brightest stars during my darkest time.

ACKNOWLEDGMENTS

I would like to express my sincere thanks and gratitude to my advisor, Dr. Kory Hedman, for his guidance and mentorship throughout these years. His patience to help students, passion for work, and dedication to perfection have encouraged and inspired me to face and solve the hardest problems in research and the toughest tasks in life. I could not be more grateful for his invaluable help and support. This dissertation would have never been possible without the help of him.

I would like to thank Dr. Daniel Tylavsky for his advice and support during my Master's degree. He has spent countless hours working with me and guiding me throughout my research work, for which I am truly grateful and indebted.

I am also grateful to my committee members, Dr. Gerald Heydt and Dr. Lalitha Sankar for their valuable time and suggestions.

I would like to express my sincere thanks to Dr. Audun Botterud, who invited me to work as an intern at Argonne National Laboratory. He has been a mentor as well as a friend to me, providing me with valuable suggestions and inspirations on my research. I would also like to thank Dr. John Birge, Canan Uckun, and Emil Constantinescu, for their help and feedback on portions of this research.

Thank you Di Shi, for providing me with the opportunity to work as an intern at GEIRINA. Your advice and help provided me the courage when I needed it the most.

In addition, I would like to thank the Power Systems Engineering Research Center, Consortium for Electric Reliability Technology Solutions, and National Renewable Energy Laboratory for their financial support.

Finally, I would like to thank all my friends and my colleagues. They are always standing by my side when I need them. Especially, I would like to thank Fengyu Wang, Song Zhang, Nikita Singhal, Qiuhua Huang, Yuting Ji, Joshua Lyon, Chao Li, and Pranav Balasubramanian for their help and support. The time we spent together will be one of the most unforgettable memories in my life.

TABLE OF CONTENTS

Page

LIST OF TABLES

Table Page

Table Page

LIST OF FIGURES

Figure Page

NOMENCLATURE

AGC	Automatic Generation Control
ARIMA	Autoregressive integrated moving average
b	Index of energy storage units
c	Index of contingencies
Cnt	Number of contingency scenarios
c_{bt}^{In}	Cost to violate the proxy limits (determined by the policy function) on the absorbing power of energy storage *b* in period *t*
c_g^l (c_b^l)	Slope for segment *l* of piecewise linear cost function for generator *g* (energy storage *b*)
c_{bt}^{Low}	Cost to violate the lower proxy energy limit determined for energy storage *b* in period *t*
C_g (C_b)	Variable cost function for generator *g* (energy storage *b*)
c_g^{NL} (c_b^{NL})	No load cost for generator *g* (energy storage *b*)
c_{bt}^{Out}	Cost to violate the proxy limits (determined by the policy function) on the generation power of energy storage *b* in time period *t*
c_g^R (c_b^R)	Ramping cost for generator *g* (energy storage *b*)
c_g^{SU} (c_b^{SU})	Startup cost for generator *g* (energy storage *b*)
c_{gst}^{Total}	Total cost for generator *g* in scenario *s* and period *t*
c_{bt}^{Up}	Cost to violate the upper proxy energy limit determined for energy storage *b* in period *t*
C_{bm}	Expected system total cost for the benchmark approach that the policy function based approach is compared with
C_{ref}	Expected system total cost for the reference approach
C_{EAC}	Expected hourly average cost per generator
C_{PFA}	Expected system total cost for the policy function based approach

CAES	Compressed air energy storage
CG	Conventional generator
d_{nt}	Real power demand at node *n* in period *t*
DAM	Day-ahead market
DOD	Depth of discharge
DT_g	Minimum down time for unit *g*
e	Index for "buckets" used in stochastic unit commitment
E_{bst}	State of charge of energy storage *b* in scenario *s* and period *t*
$\bar{E}_{b,t}$	State of charge of energy storage *b* in period *t*, determined from the day-ahead UC
E_{bs0}	Initial storage level of energy storage unit *b*
E_{bsT}	Final storage level of energy storage unit *b*
E^G_{gst}	Energy produced by generator *g* in scenario *s* and period *t*
$E^{Low}_{b,t}$	Lower proxy energy limit on SOC determined for energy storage *b* in period *t*
E^{Min}_{b}	Minimum storage capacity of energy storage *b*
E^{Max}_{b}	Maximum storage capacity of energy storage *b*
$\bar{\boldsymbol{E}}^{\boldsymbol{s_m}}_{\boldsymbol{b}}$	Battery schedule determined for scenario s_m, which is a vector with each element representing a target SOC in each time period for energy storage *b*
$\bar{E}^{s_m}_{b,t}$	Target SOC determined for energy storage *b* in time period *t* and scenario s_m
$E^{Up}_{b,t}$	Upper proxy energy limit on SOC determined for energy storage *b* in period *t*
EI	Eastern Interconnection
$ETCH$	Expected total generator commitment hours

EMS	Energy management system
ES	Energy storage
$ExpLifeTime$	Expected life time
g	Index of generators
GP	Gaussian process
i_d	Discount factor
ISO	Independent System Operator
k	Index of transmission lines
l	Index of line segments of the piecewise linear function
L	Number of line segments of the piecewise linear function
L_{bt}^{In}	Lower proxy limit on the absorbing power of energy storage b, determined by the policy function
L_{bt}^{Out}	Lower proxy limit on the generation power of energy storage b, determined by the policy function
LMP	Locational marginal price
m	Index
MMS	Market management system
MILP	Mixed-integer linear programming
n	Index of buses
N_g^c	Parameter indicating if generator g is in contingency condition in contingency scenario c (0 for contingency, 1 otherwise)
N_k^c	Parameter indicating if transmission line k is in contingency condition in contingency scenario c (0 for contingency, 1 otherwise)
N^{On}	Number of units dispatched in the system
NaS	Sodium-sulfur
NWP	Numerical weather prediction

$p_X(x)$:	Probability density function of *x*
P_{gst} (P_{g0t})	Power output of generator *g* in scenario *s* (base case scenario 0) and period *t*
$\bar{P}_{gt}$	Desired dispatch point for generator *g* in period *t*, determined by previous generation scheduling stage
P_{kst}	Real power flow on transmission line *k* in scenario *s* and period *t*
P_{bt}^{ES}	Net output for storage *b* in period *t* (positive value indicates production; negative value indicates consumption).
$P_b^{In\_ea}$	Maximum pumping power for each motor at pumped hydro storage facility *b*
P_{bst}^{In}	Power absorbed by energy storage unit *b* in scenario *s* and period *t*
$P_b^{In\_max}$	Maximum power absorption for energy storage *b*
$P_b^{In\_\min}$	Minimum power absorption for energy storage *b*
P_g^{Max}	Maximum real power output for generator *g*
P_k^{Max}	Capacity (Rate A) for transmission line *k*
P_k^{MaxC}	Emergency capacity (Rate C) for transmission line *k*
P_g^{Min}	Minimum real power output for generator *g*
$P_b^{Out\_max}$	Maximum power output for energy storage *b*
$P_b^{Out\_\min}$	Minimum power output for energy storage *b*
P_{bst}^{Out}	Power generated by energy storage *b* in scenario *s* and period *t*
$\bar{P}_{bt}^{Out}$	Scheduled generation output for energy storage *b* in period *t*, determined from previous generation scheduling stage
P_{wst}^{Wind}	Power output for wind generator *w* in scenario *s* and period *t*
PFA	Policy function approximation
PHS	Pumped hydro storage

$PTDF_{n(g),k}$	Power transfer distribution factor for bus *n* (where generator *g* is located) on transmission line *k*
PV_+	Present value of the cost saving obtained by using battery storage
$PV\_$	Present value of the capital cost of battery storage
Q_{st}^{OR}	System-wide operating reserve requirement in scenario *s* and period *t*
Q_{st}^{R+}	System-wide up regulation requirement in scenario *s*, period *t*
Q_{st}^{R-}	System-wide down regulation requirement in scenario *s*, period *t*
r_{gst}^{S} (r_{bst}^{S})	Spinning reserve provided by generator *g* (energy storage *b*) in scenario *s* and period *t*
$\bar{r}_{gt}^{S}$ ($\bar{r}_{bt}^{S}$)	Scheduled spinning reserve for generator *g* (energy storage *b*) in period *t*, determined by previous generation scheduling stage
r_{gst}^{R+} (r_{bst}^{R+})	Up regulation reserve provided by generator *g* (energy storage *b*) in scenario *s* and period *t*
r_{gst}^{R-} (r_{bst}^{R-})	Down regulation reserve provided by generator *g* (energy storage *b*) in scenario *s* and period *t*
$\bar{r}_{gt}^{R+}$ ($\bar{r}_{bt}^{R+}$)	Scheduled up regulation reserve for generator *g* (energy storage *b*) in period *t*, determined by previous generation scheduling stage
$\bar{r}_{gt}^{R-}$ ($\bar{r}_{bt}^{R-}$)	Scheduled down regulation reserve for generator *g* (energy storage *b*) in period *t*, determined by previous generation scheduling stage
R_g^{NS} (R_b^{NS})	Maximum non-spinning reserve ramp rate for generator *g* (energy storage *b*)
R_g^{SD}	Maximum shut-down ramp rate for generator *g*
R_g^{SU}	Maximum start-up ramp rate for generator *g*
R_{sys}^{+} ($R_{sys\_DA}^{+}$)	System-wide available capability to provide up reserves in the current scenario (day-ahead solution)
R_{sys}^{-}	System-wide available capability to provide down reserves in the current scenario
$R_g^{2.5+}$	Maximum 2.5-minute ramp up rate for generator *g*

$R_g^{2.5-}$	Maximum 2.5-minute ramp up rate for generator *g*
R_g^{5+}	Maximum 5-minute ramp up rate for generator *g*
R_g^{5-}	Maximum 5-minute ramp down rate for generator *g*
R_g^{10+}	Maximum 10-minute ramp up rate for generator *g*
R_g^{10-}	Maximum 10-minute ramp down rate for generator *g*
R_g^{60+}	Maximum hourly ramp up rate for generator *g*
R_g^{60-}	Maximum hourly ramp down rate for generator *g*
$RltP_i\%$	Relative performance
RTM	Real-time market
s	Index of scenarios
s_{nst}^{L}	Involuntary load shedding at node *n* in scenario *s* and period *t*
$s_{b,t}^{Low}$	Slack variable to relax the lower energy proxy limit on the SOC of energy storage *b* in period *t*
s_{st}^{R+}	Slack variable to relax system up regulation requirement in scenario *s* and period *t*
s_{st}^{R-}	Slack variable to relax system down regulation requirement in scenario *s* and period *t*
s_{bt}^{In+}	Slack variable to relax the upper proxy limit on the absorbing power of energy storage *b* in time period *t*
s_{bt}^{In-}	Slack variable to relax the lower proxy limit on the absorbing power of energy storage *b* in time period *t*
s_{bt}^{Out+}	Slack variable to relax the upper proxy limit on the generation power of energy storage *b* in time period *t*
s_{bt}^{Out-}	Slack variable to relax the lower proxy limit on the generation power of energy storage *b* in time period *t*
s_{st}^{OR}	Slack variable to relax system operating reserve requirement in scenario *s* and period *t*

s_{st}^{SP}	Slack variable to relax system reserve mix requirement in scenario *s* and period *t*
$s_{b,t}^{Up}$	Slack variable to relax the upper energy proxy limit on the SOC of energy storage *b* in period *t*
s_{wst}^{W}	Wind curtailment for wind farm *w* in period *t* and scenario *s*
S	Number of scenarios
SCUC	Security-constrained unit commitment
SOC	State of charge
SVM	Support vector machine
t	Index of time periods
t'	The current time period in a look-ahead dispatch model
T	Number of time periods
T_{LA}	Number of look-ahead time periods in a look-ahead model
u_{gst} (u_{g0t})	Binary unit commitment variable for generator *g* in scenario *s* (base case scenario 0) and period *t* (0 down, 1 online)
U_{bt}^{In}	Upper proxy limit on the absorbing power of energy storage *b*, determined by the policy function
U_{bt}^{Out}	Upper proxy limit on the generation power of energy storage *b*, determined by the policy function
UC	Unit commitment
UT_g	Minimum up time for generator *g*
$U_{\%}$	Utilization rate for conventional generators in percent
v_{gst} (v_{g0t})	Startup variable for generator *g* in scenario *s* (base case scenario) and period *t* (1 for startup, 0 otherwise)
w	Index of wind generators
w_{gst} (w_{g0t})	Shutdown variable for generator *g* in scenario *s* (base case scenario) and period *t* (1 for shutdown, 0 otherwise)

y_{gst}^{on}	Variable indicates if generator *g* is online in scenario *s* and period *t*
z_{bst}	Binary variable for energy storage *b* in period *t* and scenario *s*, when both minimum production and consumption level are assumed to be *zero* (1 for production, 0 for consumption)
$z_{b,m,t}^{In}$	Binary variable for the m^{th} motor at the pumped hydro storage facility *b* in period *t*, when minimum production/consumption level is assumed to be *nonzero* (1 for consumption, 0 for idle)
z_{bt}^{In}	Binary variable for energy storage *b* in period *t* and scenario *s*, when minimum production/consumption level is assumed to be *nonzero* (1 for consumption, 0 for idle)
z_{bt}^{Out}	Binary variable for energy storage *b* in period *t* and scenario *s*, when minimum production/consumption level is assumed to be *nonzero* (1 for production, 0 for idle)
α_b^{Conv}	Coefficient converting energy to power for energy storage *b*
α_b^R	Minimum duration of time (hour) that the regulation reserve has to be maintained by energy storage *b*
α_b^S	Minimum duration of time (hour) that the spinning reserve has to be maintained by energy storage *b*
$\beta(s,t)$	Bucket assignment that assigns scenario *s* to its corresponding bucket in period *t*
γ_b^{DF}	Parameter used to estimate the actual regulation deployment in real-time operation for energy storage *b*
θ_{kt}^{+}	Bus angle for the "from" bus of line *k*
θ_{kt}^{-}	Bus angle for the "to" bus of line *k*
λ	Ramping cost coefficient associated with generators during ramping process
η_b^{In}	Efficiency of the absorbing cycle of energy storage unit *g*
η_b^{Out}	Efficiency of the generating cycle of energy storage unit *g*
π_s	Probability of scenario *s*
$\delta_k^{+}(n)$	For any transmission line *k* with "to" bus *n*

$\delta_k^-(n)$	For any transmission line *k* with "from" bus *n*
Γ_{gt}^c	Reserve activation factor for generator *g* period *t* and contingency scenario *c*
μ	Mean value
σ	Standard deviation
$\boldsymbol{\omega_s}$, $\boldsymbol{\omega_0}$	A vector representing the wind path in scenario *s* (scenario 0 which is used in day-ahead UC).
$\phi(\cdot)$	Probability density function for standard Gaussian distribution
$\Phi(\cdot)$	Cumulative distribution function for standard Gaussian distribution
Ω_G	Set of conventional generators
Ω_{G^c}	Set of critical generators
Ω_{Gs}	Set of slow-start generators
Ω_{Gf}	Set of fast-start generators
Ω_{L^c}	Set of critical transmission lines
Ω_P	Set of pumped hydro storage units
Ω_C	Set of compressed air energy storage units
$\forall(n)$	For any generating unit at bus *n*

CHAPTER 1.

INTRODUCTION

1.1. Overview

For the past decades, power systems have been relying on fossil fuels to supply electric power, such as coal, oil and natural gas. With the growing concern regarding climate change and environmental issues, renewable energy is playing an increasingly important role in power systems. By the end of 2012, the worldwide installed wind capacity has reached 282.5 GW [1], [2], while the solar installed capacity reached 100 GW [3]. In the U.S, both the government policies and the concerns regarding environmental problem have speeded up the integration of renewable energy. As of January 2012, thirty States have enforced Renewable Portfolio Standards (RPS) or other mandated renewable capacity policies. In California, the RPS requires that electric utilities should have 33% of their retail sales derived from eligible renewable energy resources by 2020 [4]. By 2012, 60 GW of wind power capacity has been installed in the U.S., while the total installed capacity for solar power is 7.2 GW [5]. With the fast expansion of renewable resources, reliable and efficient operation of power systems has become an increasingly complex and challenging task. As renewable penetration increases, flexible resources are needed to maintain the reliable supply of power with increasing uncertainties. Under such circumstances, new interests have been focused on energy storage in recent years.

The utilization of energy storage in power systems has a long history. Back in the 1880s, lead-acid batteries have been used in the New York City area as the original nighttime load solution [6]. Starting in late 20th century, with the rapid development in storage technologies, energy storage has been used in a variety of power-system

applications, such as peak shaving, load leveling and frequency regulation. By absorbing excess clean energy and shifting it to hours when scheduled generation cannot meet demand, energy storage can effectively address the intermittency in renewable generation. Meanwhile, due to its fast ramping capability, energy storage can provide high quantities of ancillary services in a short time period. The energy-shifting and fast-ramping capabilities make energy storage an attractive solution to facilitate the integration of high penetration levels of renewable resources.

In this dissertation, the benefit of energy storage in systems with renewable resources is investigated. The impact of increasing renewable penetrations on the attractiveness of energy storage in comparison to conventional generators is evaluated using stochastic optimizations. The cost-effectiveness of energy storage in systems with increased renewable penetrations is analyzed. The effectiveness of using energy storage to provide ancillary services is evaluated.

While there are growing interests in energy storage, existing energy management systems (EMS) and market management systems (MMS) do not make full use of storage flexibility. Today, schedules for energy storage are frequently determined and fixed at a look-ahead time stage with limited real-time adjustments. Since such approaches do not fully capture the characteristics of storage, enhanced models are needed to effectively utilize the flexibility of energy storage. Toward this goal, two approaches are developed in the dissertation. In the first approach, a flexible operating range is determined for energy storage using a two-stage stochastic program. The obtained flexible operating range is then utilized to efficiently manage energy storage across multiple time periods. The second approach is a policy function approach. Different from the first approach which re-

quires solving a stochastic program, the policy function approach shifts the most computationally challenging tasks to an offline analysis stage and makes operational decisions for energy storage in real-time based on the knowledge obtained offline. The primary motivation to use the policy function approach is to provide enhancement to deterministic economic dispatch models with minimal added computational difficulty.

The main contributions of this dissertation are: 1) evaluate the attractiveness of energy storage under increasing renewable penetrations in comparison to conventional generators; 2) analyze the benefits of using energy storage to provide ancillary services in system with renewable resources; 3) develop enhanced dispatch models for energy storage to improve its utilization in systems with renewable resources, while maintaining the added computational difficulty at minimum.

1.2. Summary of Chapters

This dissertation is structured as follows. In chapter 2, existing and emerging bulk energy storage technologies are reviewed. Operating characteristics, storage technology principles and power-system applications are discussed for different energy storage technologies.

Chapter 3 reviews previous studies on different power-system applications of energy storage, including peak shaving, load leveling, price-arbitrage opportunity, integration of renewable resources, transmission congestion mitigation and transmission expansion deferral.

In chapter 4, two formulations of unit commitment are reviewed, namely the deterministic unit commitment and the stochastic unit commitment. The advantages and disadvantages of the two unit commitment formulations are discussed and compared.

In chapter 5, an economic assessment is conducted to compare the short-term profitability of conventional generators and energy storage under increasing renewable penetration levels. The impact of increasing renewable penetrations on the attractiveness of energy storage and conventional generators is studied. The result shows that as renewable penetrations increase, conventional generators will have increased average costs, decreased capacity factors as well as decreased return on investments. However, the benefits of energy storage will increase as higher levels of renewable resources are integrated into the system.

In chapter 6, the benefit of using flywheels to provide regulation services in systems with renewable resources is investigated. A two-step approach is designed for regulation reserve scheduling and its deployment in real-time operation. Testing on the RTS 24-bus test system demonstrates that flywheels can effectively provide fast regulation reserves to the system and compensate for renewable uncertainties.

In chapter 7, a stochastic programming framework is developed to study the benefit of battery storage in systems with renewable resources. A flexible operating range approach is proposed to improve the operational scheme of energy storage in real-time operations. Results show that battery storage can reduce system operating costs and improve system reliability. The proposed flexible operating range approach is demonstrated to be more effective than a traditional approach (a fixed-schedule approach) where the schedule for energy storage is determined and fixed at a prior look-ahead planning stage.

In chapter 8, a policy function approach is proposed to enhance the utilization of pumped hydro storage (PHS) in real-time operation. The policy function is constructed offline using stochastic simulations and data mining techniques. Testing on the RTS 24-

bus test case shows that the policy function approach outperforms a traditional fixed-schedule approach. Results in the case study also demonstrate that the policy function approach has minimal added computational difficulty to the real-time market.

In chapter 9, conclusions to this dissertation and directions for future work are presented.

CHAPTER 2.

ENERGY STORAGE TECHNOLOGIES

In this chapter, available and emerging bulk energy storage technologies are introduced. Operating characteristics, technology maturity and commercial availability of different energy storage technologies are discussed. A summary of power-system applications for energy storage technologies is presented.

2.1. Introduction to Bulk Energy Storage Technologies

Among all types of energy storage technologies, PHS has the largest installed capacity of 127,000 MW. Following PHS is compressed air energy storage (CAES) with 440-MW installed capacity. Sodium-sulfur (NaS) batteries have a total installed capacity of 316 MW, which is the third largest existing storage technology. In the same time, another 606 MW of sodium-sulfur batteries have been planned or announced. Worldwide installed capacities for different energy storage technologies are summarized in Fig. 2.1 [8].

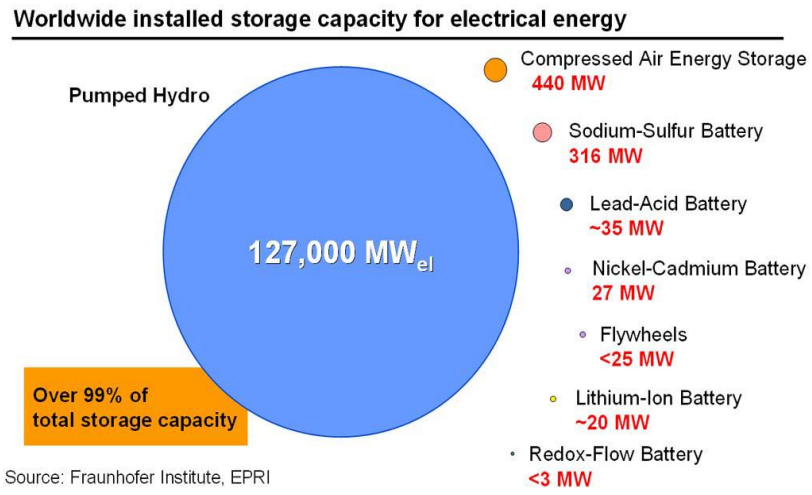

Fig. 2.1. Worldwide Installed Capacity for Different Energy Storage Technologies [8]

2.1.1. Pumped Hydro Energy Storage

The first use of pumped hydroelectric energy storage can be traced back to 1890 in Italy and Switzerland. After a hundred years, more than two hundred PHS facilities are now in operation or under planning worldwide. During off-peak periods or when excessive renewable resources are available, PHS absorbs energy from grid to pump water from its lower reservoir to its higher reservoir. During on-peak hours or when renewable resources are not available, PHS supplies energy back to grid by running water to drive a water turbine. A PHS facility can have more than 3000 MW of power capacity and store 30,000 MWh of energy. The round-trip efficiency for PHS is typically from 75% to 85%. The life-cycle is long for PHS, which ranges from 50 to 60 years. Pumped hydro storage also has a fast ramping capability. It can be turned on and ramped up to full capacity within several minutes and transition between pumping and generation mode in less than ten minutes. The main drawbacks with PHS are its negative impact on environments and the large requirements of land use. For a PHS facility to hold enough water to generate 10,000 MWh, the upper reservoir has to be one kilometer in diameter, twenty-five meters deep and having an average head of 200 meters.

As the most widely used bulk energy storage technology, PHS technologies have been advanced significantly since its first introduction. The advances in PHS technology include the use of reversible pump-turbines, integration of power electronic devices and improvement in energy-conversion efficiencies. Since the 1990s, a newer PHS technology named adjustable-speed PHS has been developed and used in commercial operation. Different from the traditional fixed-speed technology whose input power is fixed during the pumping process, adjustable-speed PHS units are able to adjust the

power consumed in the pumping mode. This novel feature enables adjustable-speed PHS units to provide frequency regulation services in both pumping and generation modes and gain higher round-trip efficiencies [10]. Globally, there are around 270 PHS stations currently either in operation or under construction, where 36 of them are equipped with adjustable-speed machines.

2.1.2. Compressed Air Energy Storage

A CAES facility works in a similar way as a PHS. During off-peak hours, a CAES facility absorbs power to compress air into an underground cavern. During peak hours, air is withdrawn from the cavern and heated with natural gas in a chamber, where the expansion in volume is used to drive a combustion turbine. A CAES plant burns two-thirds the natural gas of a conventional combustion turbine during generation process, which results in a lower fuel cost compared to a conventional gas-fired combustion turbine plant [11]. Currently several technologies are available for CAES. The aforementioned one is referred to as the first-generation CAES system. For a more advanced CAES system, no natural gas is needed during the generation process. Instead, the compressed air is heated using the heat recovered from the compression process. However, the second-generation CAES system is still under test and has not been used for utility-scale applications.

Compressed air energy storage has a fast ramping capability. It can be started up and ramp up to full load within ten minutes. However, the transition process between generation and compression mode is relatively slow, which will take more than ten minutes. One drawback with CAES is that the first-generation system requires the use of natural gas during generation process. If natural gas price increases, the economic

benefits for CAES may be reduced. Another drawback is that CAES has strict siting requirements. It requires specific locations to build the cavern to store the compressed air.

As of 2015, there are only three utility-scale CAES plants in operation: one 290 MW plant built in 1979 in Huntorf, Germany; one 110 MW plant built in 1991 in Alabama, USA, and one 2 MW plant built in 2012 in Texas, USA [12].

2.1.3. Battery Energy Storage

Battery storage is a developing and promising storage technology. Compared to PHS and CAES, batteries have smaller capacities and require much less land use. However, the life cycle for battery storage is much shorter. Factors like temperature, rate of discharge and depth of discharge (DOD) may all have an impact on the life cycle of batteries. Right now the main barrier preventing grid-scale batteries from being widely used in power systems is their relative high investment costs. Contemporarily several battery storage technologies are available, such as lead-acid batteries, sodium-sulfur batteries, lithium-ion (Li-ion) batteries and nickel-cadmium batteries.

Lead-acid batteries are the oldest and most commercially mature battery storage technology. It has been used in a wide range of applications, such as automotive, marine and uninterruptable power supply (UPS) systems. Generally, lead-acid batteries are designed either for power application or energy application. For a lead-acid battery manufactured by Xtreme Power [13], its life cycle is about 500,000 cycles at 1% DOD and 1,000 cycles at 100% DOD. Several concerns about lead-acid exist. One is the environmental and safety hazards related to lead. Other concerns with lead-acid battery technology are its limited life cycle, low power density and self-discharge issues.

Compared with lead-acid batteries, lithium-ion batteries are a newer family of battery storage technology. Li-ion battery systems have the merits of high power densities and a low weight. Li-ion batteries also have long life cycles and high round-trip efficiencies up to 85% to 90%. Compared to other battery storage technologies, Li-ion batteries pose less negative environmental impact as they do not contain toxic metals such as lead or cadmium. However, Li-ion batteries are sensitive to over temperature and over discharge. The life cycle and the performance of a Li-ion battery may degrade as a result of over temperature and over discharge.

Sodium-sulfur (NaS) battery storage is a more mature technology compared to Li-ion batteries. The round-trip efficiencies for sodium-sulfur batteries are about 80%. Sodium-sulfur batteries have long rated-power discharge durations as high as six hours, which is a great potential for power grid applications. The power densities for sodium-sulfur batteries are high. The estimated life cycle for a sodium-sulfur battery is approximately 4500 cycles at 90% depth of discharge. However, since sodium-sulfur batteries contain metallic sodium which is combustible if exposed to water, more safety protection features are required to keep the safe operation of sodium-sulfur battery facilities. Meanwhile, sodium-sulfur batteries require a high-temperature operating condition, which is in the range of 300℃ to 350℃.

With the development in battery technologies and the increasing need for flexible generation resources, battery energy storage is gaining its popularity in power-system applications. In Alaska, a 1 MW/1.5 MWh lead-acid battery has been operating for 12 years to provide load-leveling services to the area of Metlakatla [14]. In 2003, a 27 MW/6.75 MWh nickel-cadmium battery was installed in Fairbanks, Alaska, which is

used to provide backup power during outages. In 2011, a 32 MW/8 MWh Li-ion battery that operates along with a wind farm was installed in Laurel Mountain, West Virginia. This battery is primarily used to provide reserves and to moderate the output of the wind farm at Laurel Mountain.

2.1.4. Flywheel Energy Storage

Flywheel energy storage is a short energy duration technology. Flywheels store energy in spinning rotors in the form of kinetic energy and convert kinetic energy to electric power through power conversion systems. Flywheels have fast response times and high efficiencies. The response time for flywheels can be as short as four milliseconds and the efficiencies can be as high as 93%. High peak power can be provided by flywheels in short time-intervals without over heating concerns. Life cycles are long for flywheels, which can exceed 100,000 cycles at 100% depth of discharge. Flywheels have power densities five to ten times that of batteries and pose much less adverse environmental impact than batteries. However, a flywheel facility should be built with enough safety features to prevent damage and injuries in case flywheels crack and break off during rotation. Another drawback with flywheels is their limited energy capacities, which constrains their power-system applications primarily to frequency regulations and power quality services. Currently a 20 MW/5 MWh flywheel facility is in operation in Stephentown, New York.

2.1.5. Other Bulk Energy Storage Technologies

In recent years, a number of new storage technologies have emerged, in spite of the fact that most of which are still under development or undergoing testing. One of the

emerging storage technologies is thermal energy storage. For a thermal energy storage facility, solar energy is first stored as thermal energy and is then converted to power when needed. In 2011, the world's first commercial-scale solar thermal plant that uses the central tower receiver and molten salt heat storage technology was built and commissioned in Seville, Spain. The plant is named Gemasolar solar thermal plant. The solar thermal plant is rated at 19.9 MW and can provide power up to 15 hours without solar feed. The plant is equipped with more than 2600 heliostats and has a surface area of 185 hectares [15]. When solar is available, the heliostats reflect and concentrate the solar radiation to a receiver located at the top of a tower. Molten salt flows in the tower and is heated in the receiver. Then the heated salts flow through a chamber at the bottom of the tower where steam is generated to power a steam turbine. Excessive heat is stored in a hot tank located under the tower [16]. The panoramic view of the Gemasolar solar thermal plant is shown in **Error! Reference source not found.** [15]. In 2013, another thermal plant project was completed in Ivanpah, California [17]. The Ivanpah solar thermal plant also utilizes a tower solar thermal system and has a power capacity of 377 MW.

Flow batteries are another emerging storage technology. A flow battery utilizes two electrolytes that circulate through an electrochemical cell. Chemical energy is converted to electricity when the two electrolytes flow through the electrochemical cell. Flow batteries have the advantage of long life cycles. However, the downsides are that they have relative low power densities and require additional equipment, such as a pump, in order to operate a flow battery facility.

Cryogenic energy storage utilizes low temperature liquids, such as liquid air or liquid nitrogen, to store energy. During off-peak hours, electricity is used to liquefy air and store the liquid air in an insulated tank at low pressure. During on-peak hours, liquid air is pumped at high temperature to a heat exchanger. In the heat exchanger, heat is applied to turn liquid air back to gas. During the phase change of the air, the increase in pressure and volume is used to drive a turbine [18], [19]. Currently a 300 kW/ 2.5MWh pilot cryogenic energy storage system is in operation in the United Kingdom [20].

2.2. Power-System Applications of Bulk Energy Storage Technologies

Depending on the power rating, energy capacity and response time, bulk energy storage can be used in a wide range of power-system applications. The applications of energy storage technologies with different power ratings and energy capacities (expressed in discharge time at rated power) are illustrated in Fig. 2.2 [11]. As shown in Fig. 2.2, PHS and CAES have the largest power ratings and energy capacities. These two types of energy storage can be used for energy arbitrage opportunities, peak shaving, load leveling, and providing ancillary services such as spinning reserve and frequency regulations.

Batteries have the medium power ratings and energy capacities. Contemporarily most of the utility-scale batteries are used to provide operating reserves and frequency regulation services. Some batteries are installed at wind farm locations to moderate the intermittent wind generation outputs. Other batteries have also been used to provide short-term power support and to stabilize power grid during occurrence of contingencies. Such projects include the 27 MW nickel-cadmium batteries deployed by Golden Valley Electric Association in Alaska, and the 20 MW lithium-ion batteries operated by Sistema

Interconnectado del Norte Grande (SING) in the Northern Chilean grid [22]. Flywheels have small to medium power ratings and small energy capacities. Due to their limited energy capacities, flywheels are primarily used to provide frequency regulation and power quality services.

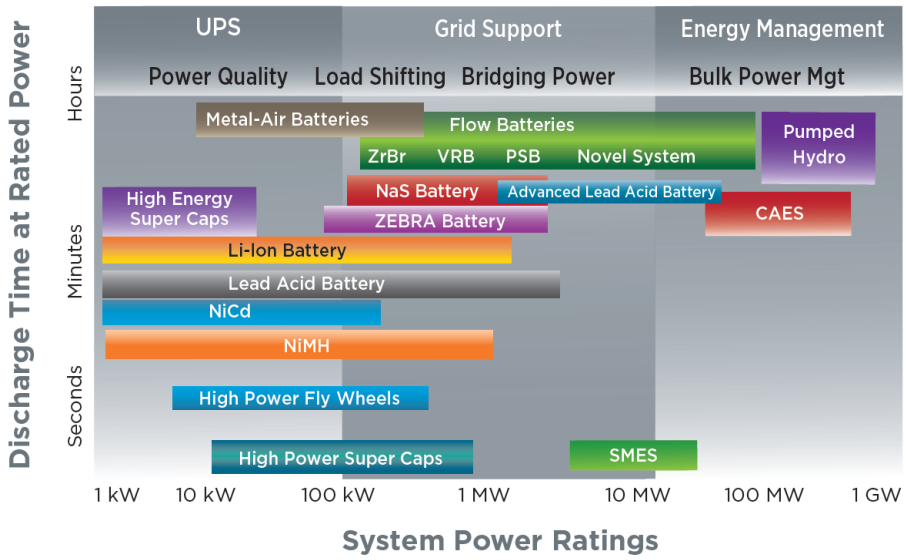

Fig. 2.2. Applications of Energy Storage Technologies with Different Power Ratings and Energy Capacities [11]

2.3. Summary

Due to the fast-ramping and energy-shifting capabilities, energy storage is gaining its popularity in power-system applications. While several types of energy storage technologies are available today, the capital costs for most of the energy storage technologies are still high compared to conventional generators. With the increasing needs for flexible resources and the potential reduction in investment costs, energy storage is expected to find more of its applications in power systems.

CHAPTER 3.

ENERGY STORAGE LITERATURE REVIEW

For the past decades, energy storage has been used in a variety of applications in power systems, such as peak shaving, load leveling, price-arbitrage, integration of renewable resources, transmission congestion mitigation and transmission expansion deferral. In this chapter, previous studies on different applications of bulk energy storage are reviewed and discussed.

3.1. Peak Shaving and Load Leveling

Peak shaving and load leveling [23]-[27] are two traditional applications of energy storage. In the case of peak shaving, energy stored during low-demand hours is used to supply demand during on-peak hours so that the peak load is reduced. Peak shaving can reduce the dispatch of the expensive "peaking" units and improve the system load factor. In the case of load leveling, the same process is used except that the goal is to flatten the load profile rather than shaving the peak load. In [23], a dc optimal power flow (OPF) model was used to study the peak shaving value of pumped hydro storage. By using PHS for peak shaving, $47 million was saved in system operating costs for the Arizona transmission system. In [24], the load-leveling application of PHS and battery storage was studied. Results in [24] showed that using PHS for load leveling could lead to a saving of $22 million per year. However, because of the high capital costs, using battery storage for load leveling has yet demonstrated to be economic [24].

3.2. Price-Arbitrage Applications

Price arbitrage is another popular application for energy storage. In the case of price arbitrage, the profit of energy storage is maximized by buying power in low-price hours and selling to the grid during high-price hours. In [28], a study was conducted to analyze the price-arbitrage value of energy storage in the PJM markets. The study showed that energy storage may reduce the price differences between off-peak and on-peak hours, which may consequently reduce the profits that energy storage obtained from price arbitrage. Reference [28] also pointed out that the value of energy storage is not limited to price-arbitrage opportunities; other services provided by energy storage should also be considered when evaluating the value of energy storage. In [29], the application of Sodium-sulfur batteries and flywheels in the New York City region was studied. The results showed that there was a strong economic case for batteries to participate in the electricity market within New York City, by price arbitrage and, for flywheels to participate as well, by providing frequency regulation services. In [30], a stochastic simulation methodology was developed to evaluate the impact of energy storage in systems with wind resources. The energy storage was assumed to be controlled by the Independent System Operator (ISO), with the goal of maximizing the total social welfare in the system. The study demonstrated the benefits of energy storage in systems with deepening penetration of wind resources, such as reducing the wholesale purchase payments by the buyers and providing improvements in system reliability.

3.3. Integration of Renewable Resources

With the increasing penetration of intermittent renewable resources, the need for flexible generation resources is greater than ever. In recent years, studies have been

focused on using energy storage to facilitate the integration of high levels of renewable resources. In [31], the impact of pumped hydro storage on the Irish power system under high wind penetration levels was studied. The results indicated that with PHS in the system, more wind could be integrated into the grid and the system total costs could be reduced by more than 40%. However, with the current wind penetration target in the Irish grid, the savings in total system costs are not enough to justify the costs to build new PHS facilities.

In [32], a two-step approach was proposed to determine the inter-temporal reservoir targets for PHS in a system with significant wind generation. The first-step of the approach determines the weekly reservoir targets by using a stochastic unit commitment model, while the second-step schedules the daily reservoir usage through a rolling-horizon approach. The result showed that the proposed method was able to provide more efficient and economical schedules for PHS than the traditional weekly refill method.

In [33], a stochastic security-constrained UC model was used to evaluate the benefits of energy storage in enhancing renewable dispatchability. It is illustrated in [33] that with PHS in the system, the total operation costs and corrective action costs were reduced while the dispatchability of wind generation was improved.

In [34], the impact of high wind penetrations on investments in CAES was studied. A stochastic electricity market model was proposed to evaluate the economic value of CAES. The results showed that CAES can be a competitive investment option under high renewable penetration levels. In [35], a security-constrained UC model was used to study the impact of CAES on systems with renewable resources. The results showed that CAES

was able to reduce total system cost and reduce the dispatch of the more expensive "peaking" units in the system.

Reference [36] analyzed the benefits of battery storage in systems with wind generation. The results showed that with battery storage in system, the expensive units were dispatched less frequently and the total system costs were reduced. It is also shown in [36] that locating battery near to the wind farms has better effects than locating battery storage away from the wind farms.

While most of the previous works studied energy storage from the viewpoint from a centralized entity, the work in [37] takes on the viewpoint of the owner of an energy storage. In [37], a stochastic UC model was used to maximize the profits of a generation company who owned a wind farm and a PHS unit. With uncertainties in market prices and wind generation, the result confirmed that the co-optimization of wind farm and PHS could increase the profits and decrease the penalty costs that the company paid when failing to provide the required quantities.

The studies on the value of energy storage in providing frequency regulation services are reported in [38]- [40]. In [38], a control scheme was proposed to coordinate wind generators and a flywheel energy storage system to provide frequency regulation services. The result showed that the proposed method reduced deviations in grid frequency and increased the profits for the wind generators and the flywheels.

In [39], a multi-time-scale framework was proposed to study the value of flywheels and battery energy storage systems over multiple time horizons. The proposed framework evaluated the benefits of energy storage in primary control, secondary frequency regulation and economic dispatch applications. The results demonstrated that energy

storage was effective in providing primary and secondary frequency regulations and reducing the total frequency regulation costs in the system.

In [40], the performance and economic value of flywheels in providing frequency regulation services was studied. A strategy of coordinating flywheels with a hydro plant to provide frequency regulations was proposed. The results illustrated that the proposed method can improve the quality of the frequency regulation services provided by the flywheels and increase the profits of the flywheels.

3.4. Review of Other Applications

Besides the aforementioned applications, energy storage can also be used to mitigate transmission line congestion [41], [42] and to defer investments in transmission [43], [44]. In [41], a security-constrained UC model was used to determine the short-term scheduling of a PV/battery system. By locating energy storage on the load side of the congested line, the congestion on the transmission line was significantly mitigated during peak-load hours. In [43], a mixed-integer linear programming (MILP) model considering investments in transmission and energy storage was proposed. The results showed that the use of energy storage could defer the investments in new transmission lines and reduce total system investment costs.

CHAPTER 4.

REVIEW OF UNIT COMMITMENT

In this chapter, two different UC formulations, namely the deterministic UC formulation and the stochastic UC formulation, are presented. Previous studies on the two UC formulations are reviewed. The advantages and challenges associated with the two formulations are compared and discussed.

4.1. Overview of Unit Commitment

Power systems face variations in demand every day. Though load profiles have daily patterns, load can also fluctuate largely in real time. With the objective of meeting power demand at minimum costs, UC plays a significant role in power system operation and planning. Unit commitment is a decision making process to schedule the on/off status for generators over a defined period [45]. The aim of UC is to find the most cost-effective combinations of generators to reliably supply electric power to customers with minimum production costs. Unit commitment is generally modeled as a mixed integer program (MIP) subject to a set of network and security constraints. Due to the large size of real-world power systems and the non-convexities of MIP, UC is a complicated optimization problem with high computational difficulty.

4.2. Deterministic Unit Commitment Methods

Traditionally, UC is solved with deterministic loads and uses certain rules to determine the required reserves in the system. In such deterministic models, the commitment schedules are obtained using the forecast information and uncertainties are addressed by keeping reserves in the system. The quantity of the reserves needed in the

system is generally determined by ad-hoc rules, which are the rules obtained from historical information or operating experiences. In [47], the authors proposed a post-stage methodology to assess the required reserve level in the system. A risk index was developed to determine a balance between the cost and the reliability of the system. The method was demonstrated to be effective in reducing excess spinning reserves. In [50], a UC problem with transmission and environmental constraints was proposed. In this model, deterministic requirements were used to schedule the reserves in the system. The UC model was solved by augmented Lagrangian relaxation.

Today, deterministic UC models are widely used by the system operators to efficiently plan and manage the resources in the system. However, one main drawback with deterministic methods is that deterministic methods only consider certain expected operating conditions. If the realized system operating conditions significantly deviate from the expected operating condition, the obtained solution may not be economical or reliable.

4.3. Stochastic Unit Commitment

Compared to deterministic UC, stochastic UC is a relative new approach, not in terms of research but in terms of implementation. Stochastic programming models endogenously incorporate a set of uncertain scenarios, which is often obtained by pre-sampling of discrete uncertainty realizations. Results obtained using stochastic programming models are robust with respect to multiple possible realizations of uncertainties modeled within the mathematical program, not only for the expected value.

Most stochastic UC problems are formulated as a two-stage scenario based stochastic program. In a two-stage stochastic program, a set of decisions are made in the first-stage,

which cannot be changed within the second-stage. In the second-stage, random events may occur and recourse decisions are made to compensate any negative effect that the random events have. These recourse actions, which are represented by the second-stage decision variables, are generally linked to the first-stage decisions. The optimal policy from such a model is the first-stage decisions and a set of correction actions corresponding to each random event [53]. In a stochastic UC model, the first-stage decisions generally are commitment status. For the second-stage, depending on the different assumptions and formulations, decisions can be only generation dispatch [54], or both generation dispatch and commitment status (the commitment status of fast-start units are allowed to differ between the second-stage decisions and the first-stage decisions) [32].

To compare the differences between deterministic UC and stochastic UC, two figures are presented in Fig. 4.1 (a) and (b). In Fig. 4.1 (a), each dotted purple hexagon represents the operating state for each time period, and the dashed blue circles are the reserves scheduled for each period. With deterministic UC, only one state is modeled in each time period, and the transition between each state is constrained by hourly ramp rate constraints for generators, as well as minimum up and down time restrictions. However, for stochastic UC, multiple scenarios are modeled in each time period as shown in Fig. 4.1 (b). The dotted purple hexagons in Fig. 4.1 (b) represent the states in the base scenario, which represents the actual forecast system operating condition. The solid blue circles represent the scenarios with uncertainties incorporated, such as wind forecast errors or system element failures. The transitions between the states in the base scenario are constrained by hourly ramp rate limits and minimum up and down time constraints. The second-stage scenarios are linked to the first-stage by short-term ramp rate

constraints such as 10-minute ramp rate constraints. It should be noted that Fig. 4.1 (b) only represents one possible formulation of stochastic UC models. Other variants of stochastic UC models can be found in [57]-[63].

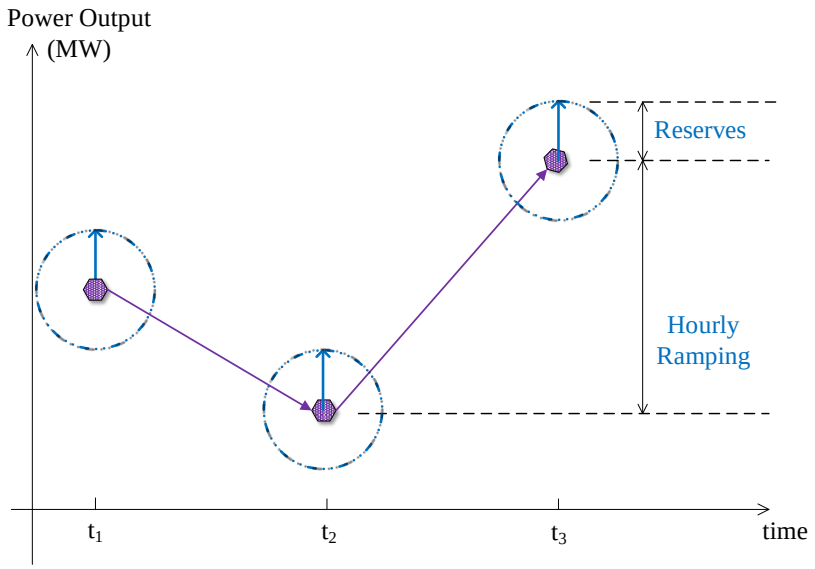

(a) Deterministic UC

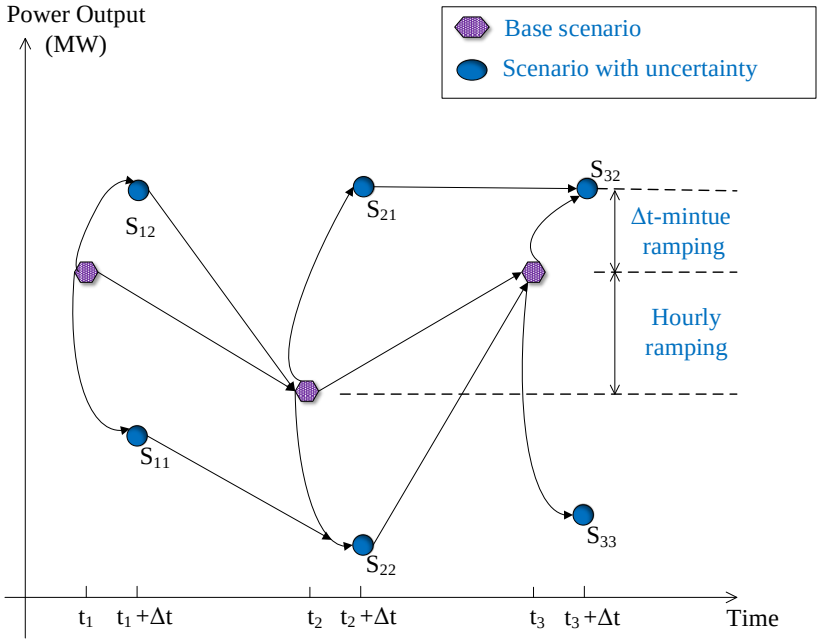

(b) Stochastic UC

Fig. 4.1. Comparison of Deterministic UC and Stochastic UC

The scenarios in stochastic UC can be modeled to represent different uncertainties. In [60] and [61], scenarios were modeled as single transmission line and generator contingencies. In [62], scenarios were used to represent uncertainties in demand and wind generation. Reserve requirements, which are meant to satisfy system *N*-1 compliance, can be modeled either implicitly or explicitly in stochastic UC models. Implicit modeling of such reserve requirements relies on deterministic policies, which are generally heuristic policies or approximations. For an explicit approach, the loss of major elements is endogenously modeled as scenarios. This is similar to an extensive form of security-constrained unit commitment [55], [56], where discrete failures of network elements are explicitly represented. Sometimes the failures of single element in the system are also modeled along with other uncertainties such as volatile wind generation in stochastic UC models [57]. Such an approach can account for different uncertainties and ensure the *N*-1 reliability of the system simultaneously. However, it may significantly increase the computational complexity of the problem to the point that it is nearly impossible to solve for large-scale systems.

By simultaneously considering multiple realizations of uncertainties, stochastic UC has been demonstrated to be more reliable and cost-effective than deterministic UC in many applications. In [52], the authors demonstrated that stochastic UC can provide significant cost savings in managing demand uncertainties and generator outages compared to a deterministic UC model. In [63], a two-stage stochastic UC was proposed to determine reserve requirements in the presence of wind generation. The results showed that the proposed method provided more efficient reserve schedules and reduced total system costs compared to a deterministic UC.

Despite its attractive advantages, two major challenges exist with stochastic UC models. One is the selection of scenarios and the determination of their corresponding probabilities, as it is a difficult task to use only a few realizations to adequately represent a large set of uncertain events. The other challenge associated with stochastic UC models is its computational complexity. As a stochastic UC model optimizes over multiple scenarios simultaneously, a stochastic UC model is much more computationally challenging to solve than a deterministic UC model. While the industry still solves a deterministic UC formulation today, algorithms for stochastic UC are receiving increased attention and advances in techniques are being made. In [63], the authors used a Lagrange relaxation procedure to deal with the non-anticipativity constraints that bind the decisions in the first-stage to be consistent (for slow units) with the second-stage, the recourse stage. In [57], the authors proposed the use of Benders' decomposition as a mechanism to improve performance. The primary strength in Benders' decomposition is that the master problem often requires less memory initially but there is no guarantee that, after multiple iterations, the master problem grows in size to the extent that it is as difficult to solve as the original problem. In [66], the authors developed a progressive hedging framework and applied it to large-scale models with up to 100 scenarios. The progressive hedging algorithm is a heuristic since it does not guarantee a global optimal solution for MIPs; however, as [66] has shown, progressive hedging algorithm performs rather well for large-scale stochastic UC problems by producing a feasible solution with a small optimality gap.

CHAPTER 5.

ECONOMIC ASSESSMENT OF BULK ENERGY STORAGE WITH HIGH LEVELS OF RENEWABLE RESOURCES

In this chapter, a stochastic UC model is designed to evaluate the short-term profitability of conventional generators and energy storage under increasing renewable penetration levels. The stochastic UC model takes into account renewable uncertainties as well as the cost of ramping for conventional generators. The impact of increasing renewable penetration levels on the attractiveness of bulk energy storage in comparison to conventional generators (CG) is studied.

5.1. Background and Motivation

Traditionally, conventional generators have been used as the solution to compensate variability and uncertainty in renewable generation. However, under high levels of renewable resources, the role of conventional generators will transition from primarily supplying energy to providing reserves and backup generation for intermittent renewable resources. As a result, conventional generators will be operating at low output levels or be used as standby generation. At low operating levels, most conventional generators will have higher average costs and lower marginal costs as shown in Fig. 5.1 [67]. As the locational marginal prices (LMPs) reflect the marginal cost of the "marginal unit" in the system, the LMPs in the system are likely to decrease. On the other hand, since the fuel costs of wind generation can be considered to be zero, the increase in penetration of renewable resources is expected to further drive down energy prices, which may decrease the profits that conventional generators receive on top of having an increase in average

costs and a reduction in the overall utilization of the generator. Under high levels of variable resources, conventional generators may have to frequently adjust their outputs to provide system operating reserve and frequency regulation services. This imposed ramping requirement on conventional generators may degrade the efficiency and increase the emissions per MWh of conventional generators. The above factors may substantially decrease the incentive to invest in conventional generation under high levels of renewable penetration.

With the stringent fleet challenges introduced by renewable resources, the need for flexible resources in power systems is higher than ever. Since energy storage can absorb excess clean energy and shift it to hours when scheduled generation cannot meet demand, bulk energy storage has the potential to become competitive under high renewable penetration levels. Meanwhile, their fast ramping capability provides energy storage the ability to better manage the uncertainty and intermittency in renewable generation. Yet the primary barrier with bulk energy storage is their high investment costs. California is the first US state to create an energy storage target [7]; note, however, that there is a specified MW target but no specified MWh target. In this chapter, studies are conducted to evaluate and compare the attractiveness of conventional generators and energy storage under increasing renewable penetration levels.

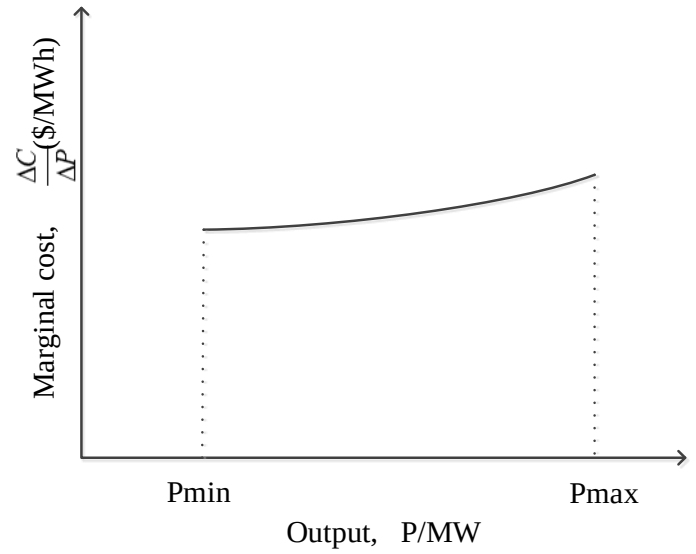

(a) Generator marginal cost curve

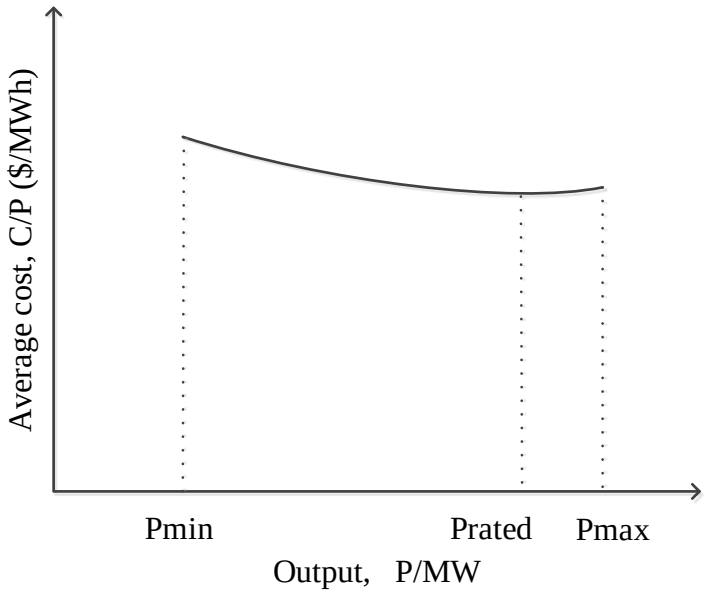

(b) Generator average cost curve

Fig. 5.1. Typical Conventional Generator Cost Curves [67]

5.2. Mathematical Formulation and Methodology

In this dissertation, a two-stage stochastic UC model is developed. The model represents a traditional day-ahead generation scheduling problem with an hourly based

interval. By using the stochastic UC model, the uncertainties in wind generation are endogenously captured in the formulation.

5.2.1. Energy Storage Model

Pumped hydro storage and compressed air energy storage are included in this study, since they are the two most attractive large-scale options with low capital costs, low maintenance costs, and long life expectancies [68]. Since PHS and CAES are operated in similar ways, they can be modeled as shown in (5.1)-(5.5). The constraints include reservoir balance constraint (5.1), lower and upper limits of power absorption and generation (5.2)-(5.3), lower and upper limits of the energy capacity (5.4), and a binary variable indicating whether the energy storage unit is in generation mode (z_{bst}=1) or pumping/compression mode (z_{bst}=0),

$$E_{bst} = E_{bs,t-1} + P_{bst}^{In}\eta_g^{In} - P_{bst}^{Out}/\eta_b^{Out}, \forall b \in \{\Omega_C, \Omega_P\}, s, t \quad (5.1)$$

$$P_b^{In\_min}(1 - z_{bst}) \le P_{bst}^{In} \le P_b^{In\_max}(1 - z_{bst}), \forall b \in \{\Omega_C, \Omega_P\}, t, s \quad (5.2)$$

$$P_b^{Out\_min} z_{bst} \le P_{bst}^{Out} \le P_b^{Out\_max} z_{bst}, \forall b \in \{\Omega_C, \Omega_P\}, s, t \quad (5.3)$$

$$E_b^{Min} \le E_{bst} \le E_b^{Max}, \forall b \in \{\Omega_C, \Omega_P\}, s, t \quad (5.4)$$

$$z_{bst} \in \{1,0\}, \forall b \in \{\Omega_C, \Omega_P\}, s, t. \quad (5.5)$$

5.2.2. Stochastic Unit Commitment Model

The stochastic UC model is formulated as a mixed integer linear program (MILP). The model is assumed to be lossless. The objective function (5.6) of the UC model is to minimize system total cost, which includes generator operating costs, no-load costs, startup costs and ramping costs. The ramping cost terms in the objective function, $c_g^R(P_{gst})$ and $c_b^R(P_{bst}^{Out})$, are calculated using (5.11) and (5.12) respectively. The ramping

cost terms represent the cost associated with the 10-minute ramping process of generators. Since generators may have different efficiencies when operating at a constant output compared to when they ramp, a ramping coefficient λ is used to approximate the inefficiencies of generators during the ramping process. The complete UC model is shown in (5.1)-(5.30):

Minimize:

$$\sum_s \pi_s \sum_s \{\sum_{g\in\Omega_G}[C_g(P_{gst}) + c_g^R(P_{gst})] + \sum_{b\in\Omega_C}[C_b(P_{bst}^{Out}) + c_b^R(P_{bst}^{Out})] + \sum_{g\in\Omega_G}[c_g^{NL}u_{gst} + c_g^{SU}v_{gst}] + \sum_{b\in\Omega_C}[c_b^{NL}z_{gst} + c_b^{SU}v_{bst}]\} \quad (5.6)$$

Subject to:

$$\sum_{\forall g(n)}^{g\in\Omega_G} P_{gst} + \sum_{\forall b(n)}^{b\in\{\Omega_C,\Omega_P\}}(P_{bst}^{Out} - P_{bst}^{In}) + \sum_{\delta^+(n)} P_{kst} - \sum_{\delta^-(n)} P_{kst} = d_{nt} - \sum_{\forall w(n)} P_{wst}^{Wind}, \forall n, s, t \quad (5.7)$$

$$P_{kst} = B_k(\theta_{kst}^+ - \theta_{kst}^-), \forall k, s, t \quad (5.8)$$

$$-P_k^{Max} \le P_{kst} \le P_k^{Max}, \forall k, s, t \quad (5.9)$$

$$P_g^{Min}u_{gst} \le P_{gst} \le P_g^{Max}u_{gst} - r_{gst}^S,\ \forall g \in \Omega_G, s, t \quad (5.10)$$

$$c_g^R(P_{gkt}) = \sum_{l=1}^{L}(1+\lambda)c_g^l[\frac{(2l-1)(P_{gk,t}-P_{g0t})}{2L} + P_{g0t}],\ \forall g \in \Omega_G, s, t \quad (5.11)$$

$$c_b^R(P_{bst}^{Out}) = \sum_{l=1}^{L}(1+\lambda)c_b^l[\frac{(2l-1)(P_{bs,t}^{Out}-P_{b0t}^{Out})}{2L} + P_{b0t}^{Out}],\ \forall b \in \Omega_C, s, t \quad (5.12)$$

$$v_{g0t} - w_{g0t} = u_{g0t} - u_{g0,t-1},\ \forall g \in \Omega_G, t \quad (5.13)$$

$$v_{b0t} - w_{b0t} = u_{b0t} - u_{b0,t-1},\ \forall b \in \Omega_C, t \quad (5.14)$$

$$\sum_{q=t-UT_g+1}^{t} v_{g0q} \le u_{g0t},\ \forall g \in \Omega_G, t \in \{UT_g, \dots, T\} \quad (5.15)$$

$$\sum_{q=t-DT_g+1}^{t} w_{g0q} \le 1 - u_{g0t},\ \forall g \in \Omega_G, t \in \{DT_g, \dots, T\} \quad (5.16)$$

$$r_{gst}^S \ge 0,\ \forall g \in \Omega_G, s, t \quad (5.17)$$

$$r_{gst}^{S} \leq R_g^{10+} u_{gst}, \forall g \in \Omega_G, s, t \tag{5.18}$$

$$r_{bst}^{S} \geq 0, \ \forall b \in \{\Omega_C, \Omega_P\}, s, t \tag{5.19}$$

$$r_{bst}^{S} \leq P_b^{Out\_max} z_{bst} - P_{bst}^{Out} + P_{bst}^{In}, \forall b \in \Omega_C, s, t \tag{5.20}$$

$$r_{bst}^{S} \leq P_b^{Out\_max} - P_{bst}^{Out} + P_{bst}^{In}, \forall b \in \Omega_P, s, t \tag{5.21}$$

$$r_{bst}^{S} \leq \alpha_b^{Conv} \eta_b^{Out} E_{bst}, \forall b \in \{\Omega_C, \Omega_P\}, s, t \tag{5.22}$$

$$r_{bst}^{S} \leq \alpha_b^{Conv} \eta_b^{In} E_{bs,t-1} + P_{bst}^{In}, \forall b \in \{\Omega_C, \Omega_P\}, s, t \tag{5.23}$$

$$0 \leq r_{gst}^{NS} \leq R_g^{NS}(1 - u_{gst}), \forall g \in \Omega_G, s, t \tag{5.24}$$

$$P_{g0t} - P_{g0,t-1} \leq R_g^{+} u_{g0,t-1} + R_g^{SU} v_{g0t}, \ \forall g \in \Omega_G, t \tag{5.25}$$

$$P_{g0,t-1} - P_{g0,t} \leq R_g^{-} u_{g0,t} + R_g^{SD} w_{g0,t}, \ \forall g \in \Omega_G, t \tag{5.26}$$

$$-R_g^{10-} \leq P_{gst} - P_{g0,t} \leq R_g^{10+}, \ \forall g \in \Omega_G, s, t \tag{5.27}$$

$$u_{gst}, \in \{0,1\}, \ \forall g \in \Omega_G, s, t \tag{5.28}$$

$$0 \leq v_{gst} \leq 1, \ 0 \leq w_{gst} \leq 1, \ \forall g \in \Omega_G, s, t \tag{5.29}$$

$$0 \leq v_{bst} \leq 1, \ 0 \leq w_{bst} \leq 1, \ \forall b \in \Omega_C, s, t. \tag{5.30}$$

The nodal balance constraint is shown in (5.7), where bus injections are assumed to be positive and withdrawals negative. Constraints (5.8) and (5.9) represent the dc line-flow constraints; line losses are neglected. The upper and lower limits on the generator output are shown in (5.10). The minimum up and down time constraints for conventional generators are shown in (5.13)-(5.15). Minimum up and down time constraints are not required for PHS and CAES, since they are considered to be fast unit which can be turned on within one hour. Fast units are defined to be the units that have minimum up and down time smaller or equal to one hour and can be turned on within ten minutes, while slow units are generators with minimum up and down time longer than one hour.

The system reserve requirements used in the above formulation follows the one that used in the California ISO system. It is required that the spinning reserve in the system should account for 50% of the system operating reserve. Operating reserve in the system should be greater than 5% of the hydro generation plus 7% of generation from other fuel types, or the single largest generator contingency in the system, whichever is greater [70].

Constraints (5.17) and (5.18) formulate the spinning reserves provided by conventional generators. Constraints (5.19)-(5.23) represent the spinning reserves provided by PHS and CAES units. Since transition time between compression and generation mode is longer than 10 minutes for CAES, constraint (5.20) indicates that the maximum spinning reserve that CAES can provide is either P_{bst}^{In} in compression mode, or $P_b^{Out\_max} - P_{bst}^{Out}$ in generation mode. However, a PHS unit can ramp up to full capacity from offline within ten minutes. Therefore, as shown in (5.21), if a PHS unit is in pumping mode, the maximum reserve it can provide is $P_b^{Out\_max} + P_{bst}^{In}$, which indicates that a PHS unit can provide spinning reserve by stop pumping and transition to generation mode to provide up reserves. If a PHS unit is in generation mode, the maximum spinning reserve it can provide is $P_b^{Out\_max} - P_{bst}^{Out}$. Constraints (5.22) and (5.23) guarantee that energy storage should have enough energy to provide spinning reserve for the required time duration. The non-spinning reserve constraints for conventional generators are shown in (5.24).

The ramp rate constraints for conventional generators are shown in (5.25)-(5.27). Constraints (5.25) and (5.26) are hourly ramp rate constraints, and constraint (5.27) represents 10-minute ramp rate constraint. Ramp rate constraints for PHS and CAES units are omitted, since they have fast-ramping capabilities and neither the hourly ramp rate

constraints nor the 10-minute ramp rate constraints will be binding for them. The non-negativity for commitment variables are presented in (5.28)-(5.30).

5.2.3. Modeling of Ramp Rate Constraints and Uncertainties

While stochastic UC can provide robust solutions, the large number of constraints that couple the scenarios together make stochastic UC computationally challenging to solve. Therefore, the accuracy and computation complexity should be balanced. The modeling of the ramp rate constraints and uncertainties in the proposed stochastic UC is illustrated in Fig. 5.2.

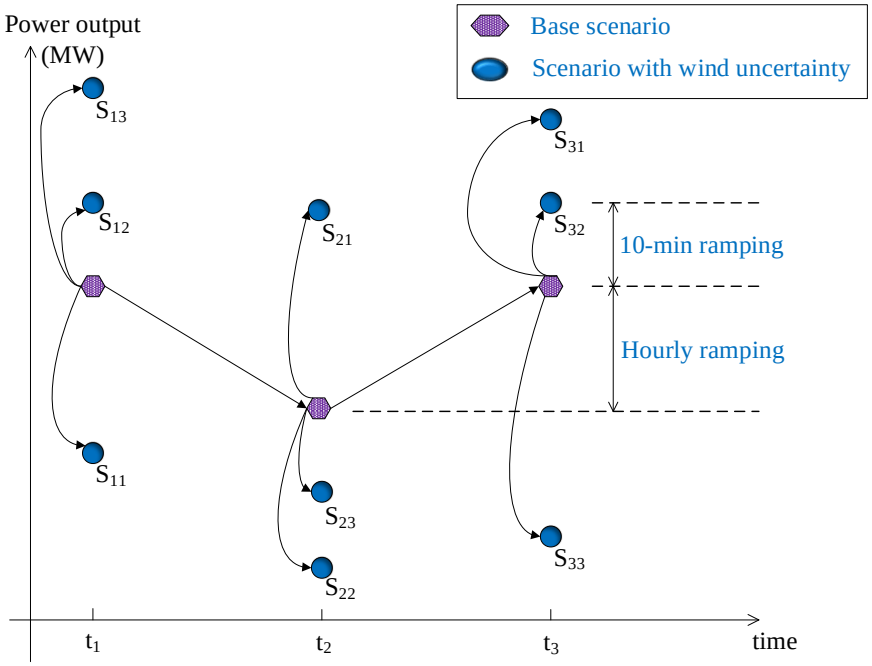

Fig. 5.2. Modeling of Ramp Rate Constraints and Wind Uncertainties

In Fig. 5.2, the dotted purple hexagons represent the base scenario with the actual wind forecast, while the solid blue circles represent possible wind generation realizations. To adequately represent renewable uncertainties while not significantly increasing computational complexity of the model, hourly ramp rate constraints are only enforced

between base case scenarios in the proposed model, i.e., only between the dotted purple hexagons in Fig. 5.2. And the 10-minute ramp rate constraints are only modeled between the base case and the possible wind realizations in the same time period, i.e., between the dotted purple hexagon and the solid blue circles in the same time period *t*. Such a formulation assumes that if the system has enough flexibility to manage the scenario transitions captured in the formulation, the system will also have enough flexibility to address the ramping requirements that are omitted in the formulation.

5.3. Renewable Modeling

5.3.1. Brief Review on Wind Forecast Methods

Wind scenarios can be generated using wind forecast models. Numeric weather prediction (NWP) is a physical model using weather data and advanced meteorological techniques for wind forecasting [72]-[73]. Due to the high computational complexity of NWP, it is usually used for day-ahead forecast. Statistical models, such as autoregressive integrated moving average (ARIMA) models and their variants, [74]-[75], can also be used in wind scenario generation. Such models use historical data, pattern identification, and mathematical approaches to produce forecast. The implementation of such models, for wind scenario generation, is discussed in [63]. Spatial correlation models take the spatial relationship of different wind farms into account. The spatial correlation method is usually combined with other methods, such as the method combing fuzzy logic and spatial correlation, [76], and the ANFIS-based method using spatial correlation, [77].

5.3.2. Wind Scenario Generation

Wind generation data for different wind farms were obtained from NREL Wind Integration Datasets [78]. The approach described in [79] was implemented to generate wind scenarios. One thousand wind scenarios were generated using Monte-Carlo simulations. For each time period *t*, the wind forecast error was assumed to follow a truncated Gaussian distribution $N(0,\sigma^2)$ with zero mean and variance σ^2 [79]. A truncated normal distribution with $a_1 \le x \le a_2$ can be expressed as

$$p_X(x) = \begin{cases} 0 & ,x < a_1 \\ \frac{\frac{1}{\sigma}\phi\left(\frac{x-\mu}{\sigma}\right)}{\frac{1}{\sigma}\Phi\left(\frac{a_2-\mu}{\sigma}\right)-\frac{1}{\sigma}\Phi\left(\frac{a_1-\mu}{\sigma}\right)} & ,a_1 \le x \le a_2 \\ 0 & ,x > a_2 \end{cases} \tag{5.31}$$

where $\phi(x)$ is the probability density function for standard normal distribution, and $\Phi(x)$ is the corresponding cumulative distribution function. The normal distribution is truncated such that 1) the forecast errors were within three standard deviations of the corresponding distribution, which accounts for 99.7% of the values; 2) the resulted wind generation was between zero and the maximum capacity of the wind generator. In [80] and [81], the typical forecast error for day-ahead forecasting was reported to be 10% to 20%. To reflect the practical forecast error reported in literature, σ was chosen to create an error of roughly 16%.

Note that the forecast error distribution for a particular wind farm may not necessarily be Gaussian. Rayleigh distribution, Weibull distribution and Beta distribution have also been previously used [82]-[84]. The assumption of a Gaussian distribution in the case study is to approximate the wind forecast error without overcomplicating the scenario generation process. More accurate distributions can be adopted in future work.

While including a large number of scenarios in a stochastic program can result in more robust solutions, such an approach may significantly increase computational difficulty of the stochastic program. To keep the computational complexity of the stochastic UC tractable, a scenario reduction technique was used to reduce the number of scenarios to a predetermined number. The primary objective of scenario reduction is to use a subset of selected scenarios to approximate the original scenario set such that the distribution of the selected scenarios is closest to the initial distribution [64]. In this work, a backward reduction method introduced in [64] and [86] was employed to select ten scenarios out of one thousand to be used in the stochastic UC. The backward reduction technique deletes the scenarios that have the minimum distance of the scenario pair. Scenarios with low probabilities are eliminated and scenarios that are similar are combined. The probability of deleted scenarios is allocated to the remaining scenario [64].

5.4. Description of Simulation Procedure

First, 1000 wind scenarios are generated based on the approach outlined above. Ten scenarios are selected using the scenario reduction technique [64]. Second, the stochastic UC is solved for increasing renewable penetration levels. Third, the obtained UC solutions are tested against all the wind scenarios generated (via stochastic simulations) to determine if the solutions can satisfy load under all wind scenarios for the corresponding penetration levels. After the wind scenario analysis, the *N*-1 contingency analysis, combined with selected wind scenarios, is conducted to test if the system can withstand the loss of any single element while compensating for potential wind deviations as well. A flowchart summarizing the simulation procedure is presented in Fig. 5.3.

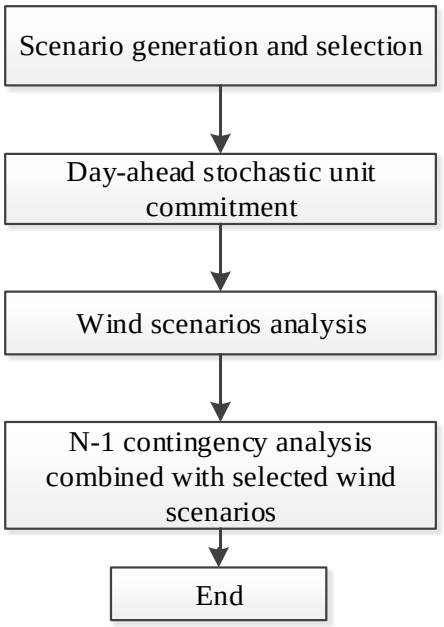

Fig. 5.3. Flowchart of the Simulation

5.4.1. Mathematical Formulation of Wind Scenario Analysis

Wind scenario analysis is conducted to test if the day-ahead solutions can reliably supply the system demand with different wind scenarios. With desired dispatch points and commitment statuses obtained from the day-ahead UC solution, operating reserves are deployed in wind scenario analysis to address the deviations in wind generation from its forecast value. If violations (e.g. involuntary load shedding) occur, security corrections should be performed to correct such violations in the system. Wind scenario analysis is formulated as a dc OPF problem with the objective to minimize total operating costs, ramping costs and security correction costs. The complete formulation of the wind scenario analysis is presented in (5.32)–(5.43),

Minimize:

$$\sum_{g\in\Omega_G}\left[C_g(P_g)+c_g^R(P_g)\right]+\sum_{b\in\Omega_C}[C_b(P_b^{Out})+c_b^R(P_b^{Out})]+\sum_n c_n^{vL}\,s_n^L \tag{5.32}$$

Subject to:

$$P_g^{Min}\bar{u}_{gt}\le P_g\le P_g^{Max}\bar{u}_{gt},\forall g\in\Omega_{Gs} \tag{5.33}$$

$$\bar{P}_{gt}-\bar{r}_{gt}^S\le P_g\le\bar{P}_{gt}+\bar{r}_{gt}^S,\forall g\in\Omega_{Gs} \tag{5.34}$$

$$0\le P_g\le P_g^{Max},\forall g\in\Omega_{Gf} \tag{5.35}$$

$$\bar{P}_{gt}-R_g^{10-}\le P_g\le\bar{P}_{gt}+R_g^{10+}\bar{u}_{gt}+R_g^{NS}(1-\bar{u}_{g,t-1}),\forall g\in\Omega_{Gf} \tag{5.36}$$

$$\sum_{\forall g(n)}^{g\in\Omega_G}P_g+\sum_{\forall b(n)}^{b\in\{\Omega_P,\Omega_C\}}(P_b^{Out}-P_b^{In})+\sum_{\delta^+(n)}P_k-\sum_{\delta^-(n)}P_k=d_n-\sum_{\forall w(n)}^{w\in\Omega_W}(P_w^{Wind}-$$

$$s_w^W)-s_n^L,\forall n \tag{5.37}$$

$$c_g^R(P_g)=\sum_{l=1}^{L}(1+\lambda)c_g^l\left[\frac{(2l-1)(P_g-\bar{P}_{gt})}{2L}+\bar{P}_{gt}\right],\forall g\in\Omega_G \tag{5.38}$$

$$c_b^R(P_b^{Out})=\sum_{l=1}^{L}(1+\lambda)c_b^l\left[\frac{(2l-1)(P_b^{Out}-\bar{P}_{bt}^{Out})}{2L}+\bar{P}_{bt}^{Out}\right],\ \forall b\in\Omega_C \tag{5.39}$$

$$P_k=B_k(\theta_k^+-\theta_k^-),\forall k \tag{5.40}$$

$$-P_k^{Max}\le P_k\le P_k^{Max},\forall k \tag{5.41}$$

$$0\le s_n^L\le d_n,\forall n \tag{5.42}$$

$$0\le s_w^W\le P_w^{Wind},\forall w. \tag{5.43}$$

Constraints (5.33)-(5.36) represent the operating ranges for conventional generators. In the formulation, variables with a bar above are parameters whose value is obtained from the day-ahead UC solution. Constraint (5.33) represents the power output limits for slow generators. Variable $\bar{u}_{gt}$ in (5.33) is the commitment status determined from day-ahead UC solution. The operating range for a slow unit is its scheduled generation (desired dispatch point) plus and minus its scheduled reserve, as shown in (5.34).

Variable $\bar{P}_{gt}$ is the desired dispatch point for generator g obtained from the day-ahead base case scenario. Since fast units can be turned on within ten minutes, their lower generation limits are assumed to be zero. The maximum output level for a fast unit in wind scenario analysis is constrained by its desired dispatch point plus 10-minute ramp rate, or its non-spinning reserve ramp rate, depending on the commitment status of the generator in the previous time period. The constraints on the operating ranges for fast units are shown in (5.35) and (5.36). The nodal balance constraint is shown in (5.37). Variables s_n^L and s_w^W are slack variables representing involuntary load shedding and wind power curtailment at each bus. Constraints (5.38) and (5.39) represent the ramping costs incurred during the 10-minute ramping process. Constraint (5.40) formulates the dc power flow on each line and (5.41) is the line-flow limit for each transmission line. Constraints (5.42) and (5.43) represent the limits on slack variables s_n^L and s_w^W.

A flowchart describing the procedure of wind scenario analysis is shown in Fig. 5.4. Day-ahead solution is first obtained from the stochastic UC. Then a dc OPF is solved to test the day-ahead solution against each wind scenario *s* in each time period *t*. After all the wind scenarios are tested, reliability metrics are computed, such as expected costs for violations, expected wind spillage and number of violations during wind scenario analysis.

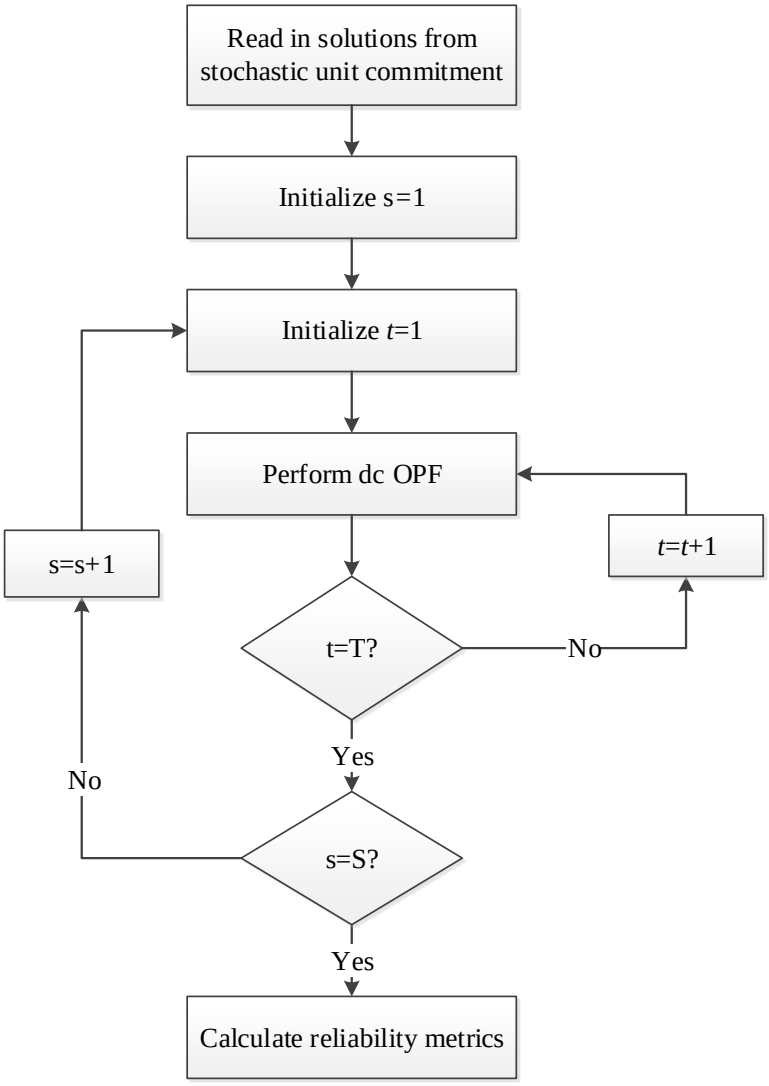

Fig. 5.4. Flowchart for Wind Scenario Analysis

5.4.2. Mathematical Formulation of *N*-1 Contingency Analysis

The *N*-1 contingency analysis simulates the post-contingency operating condition within ten minutes of the occurrence of a single transmission line or generator outage in the system. The *N*-1 contingency analysis is performed in combination with the selected wind scenarios to test if the system can withstand the loss of a single transmission line or generator under wind uncertainties. Similar to the wind scenario analysis, the *N*-1

contingency analysis is formulated as a dc OPF problem. The complete formulation is shown in (5.44)-(5.55),

Minimize:

$$\sum_{g\in\Omega_G}\left[C_g(P_g)+c_g^R\left(P_g\right)\right]+\sum_{b\in\Omega_C}[C_b(P_b^{Out})+c_b^R(P_b^{Out})]+\sum_n c_n^{vL}\,s_n^L \tag{5.44}$$

Subject to:

$$P_g^{Min}\bar{u}_{gt}N_g^c \le P_g \le P_g^{Max}\bar{u}_{gt}N_g^c, \forall g \in \Omega_{Gs} \tag{5.45}$$

$$(\bar{P}_{gt}-\bar{r}_{gt}^S)N_g^c \le P_g \le (\bar{P}_{gt}+\bar{r}_{gt}^S)N_g^c, \forall g \in \Omega_{Gs} \tag{5.46}$$

$$0 \le P_g \le P_g^{Max}N_g^c, \forall g \in \Omega_{Gf} \tag{5.47}$$

$$\left(\bar{P}_{gt}-R_g^{10-}\right)N_g^c \le P_g \le \left[\bar{P}_{gt}+R_g^{10+}\bar{u}_{gt}+R_g^{NS}\left(1-\bar{u}_{g,t-1}\right)\right]N_g^c, \forall g \in \Omega_{Gf} \tag{5.48}$$

$$\sum_{\forall g(n)}^{g\in\Omega_G} P_g+\sum_{\forall b(n)}^{b\in\{\Omega_P,\Omega_C\}}(P_b^{Out}-P_b^{In})+\sum_{\delta^+(n)}P_k-\sum_{\delta^-(n)}P_k=d_n-\sum_{\forall w(n)}^{w\in\Omega_W}(P_w^{Wind}-s_w^W)-s_n^L, \forall n \tag{5.49}$$

$$c_g^R\left(P_g\right)=\sum_{l=1}^{L}(1+\lambda)c_g^l\left[\frac{(2l-1)\left(P_g-\bar{P}_{gt}\right)}{2L}+\bar{P}_{gt}\right], \forall g \in \Omega_G \tag{5.50}$$

$$c_b^R(P_b^{Out})=\sum_{l=1}^{L}(1+\lambda)c_b^l\left[\frac{(2l-1)\left(P_b^{Out}-\bar{P}_{bt}^{Out}\right)}{2L}+\bar{P}_{bt}^{Out}\right],\ \forall b \in \Omega_C \tag{5.51}$$

$$P_k=B_kN_k^c(\theta_k^+-\theta_k^-), \forall k \tag{5.52}$$

$$-P_k^{Max}N_k^c \le P_k \le P_k^{Max}N_k^c, \forall k \tag{5.53}$$

$$0 \le s_n^L \le d_n \tag{5.54}$$

$$0 \le s_w^W \le P_w^{Wind}, \forall w. \tag{5.55}$$

The constraints in the above formulation include power output limits for generators (5.45)-(5.48), nodal power balance constraint (5.49), ramping costs constraint (5.50) and (5.51), dc power flow on each line (5.52), transmission line capacity constraint (5.53), and constraints on involuntary load shedding and wind spillage variables (5.54) and

(5.56). Except for (5.45)–(5.48), (5.52) and (5.53), all the other constraints are identical to those used in the formulation of the wind scenario analysis. The parameter N_g^c in (5.45)–(5.48) indicates whether if generator *g* is in contingency state in contingency scenario *c*. Similarly, the parameter N_k^c in constraints (5.52) and (5.53) indicates whether transmission line *k* is in contingency state in contingency scenario *c*. A flowchart describing the procedures used in the *N*-1 contingency analysis is shown in Fig. 5.5.

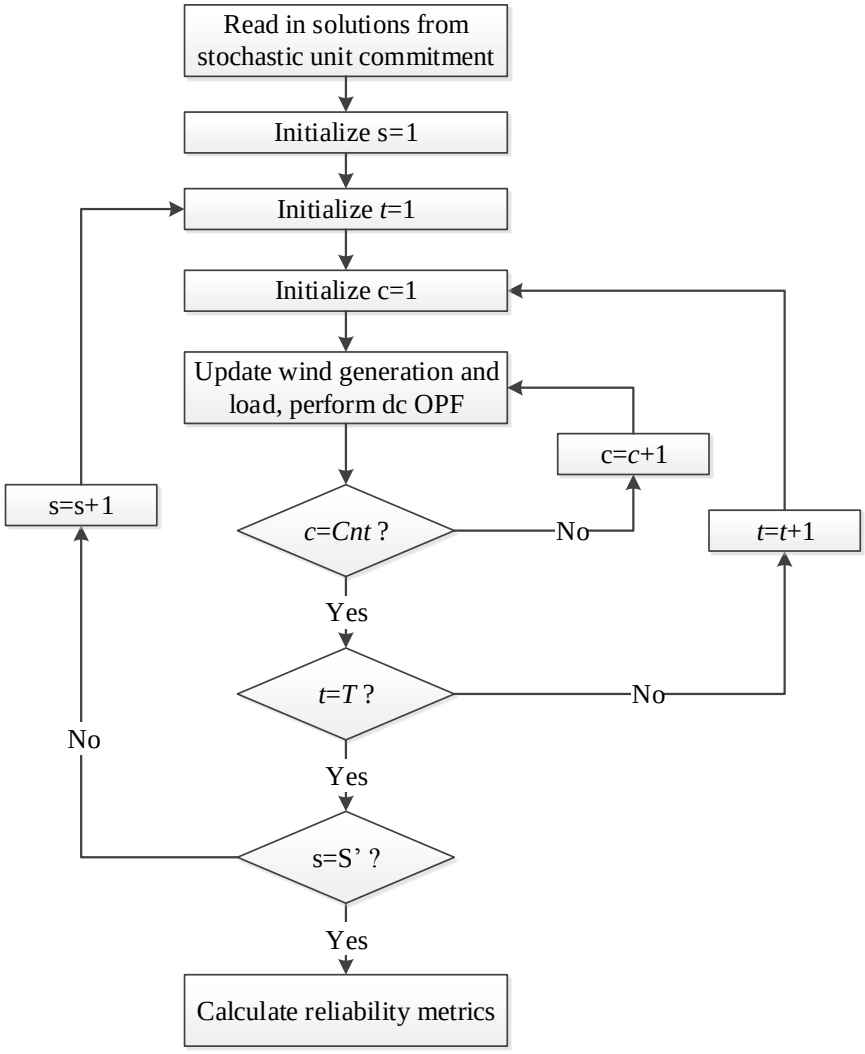

Fig. 5.5. Flowchart for *N*-1 Contingency Analysis

5.5. Numerical Results

A modified RTS96 one-zone model [87], [88] is used in the case study. The original one-zone model has 32 generators, 24 buses and 17 loads. The total generation capacity in the system is 3402 MW, and the system peak load is 2850 MW. The six hydro generators in the system are replaced with one oil-fired and one coal-fired generator; the total generation capacity remained the same as before. The ramping coefficient λ is assumed to be 0.05. Wind penetration levels from 30% to 70% with 10% increments are studied, where the wind penetration level is defined as the ratio of total daily wind generation to the total system daily demand.

As wind penetration levels increase, it is imperative to accurately model the correlations of the renewable production. Under high wind penetration levels, the geographical spreading of wind farms is likely to increase. Since wind speed has relative weak correlation for long distances [63], geographical diversity will attenuate the system-wide wind forecast uncertainty. To represent the smoothing effect resulting from the widely dispersed wind farms, wind generation is not scaled up using a multiplier as penetration levels increase. Instead, for each 10% penetration increment, a wind farm with a different wind profile and different wind scenarios is added. Wind data for January 3rd, 2016 is collected from NREL Wind Integration Datasets. The original 10-min wind data are averaged into hourly data and are used as the predicted wind power output in the simulation. Wind spillage is allowed in the UC model.

5.5.1. Impact of Increasing Wind Penetration Levels on Conventional Generators

The primary interest in this subsection is to quantify the economic efficiencies of conventional generators under high wind penetration levels. The day-ahead stochastic UC

problem is solved for increasing wind penetration levels and the results are reported in Table 5.2. The first column in Table 5.2 shows the targeted wind penetration levels. As wind spillage is allowed, the actual wind generation dispatched in the system is presented in Table 5.1. Since the test bed system has limited capability to accommodate large amounts of wind generation, the actual wind generation dispatched in the system is less than the targeted wind penetration levels. Although the actual wind dispatched in the system did not achieve the targeted penetration levels, the actual dispatched wind generation increases as the targeted wind penetration level increases. To accommodate more wind generation into the system, more flexible generation should be incorporated into the study. The results in this chapter can be interpreted as the evaluation of economic efficiencies for conventional generators under increasing "actual" wind penetration levels.

TABLE 5.1. ACTUAL WIND GENERATION DISPATCHED IN THE SYSTEM

Wind %	Without ES	With ES
30%	27%	29%
40%	35%	38%
50%	42%	45%
60%	45%	49%
70%	48%	51%

In Table 5.2, four metrics are used to evaluate the economic efficiencies of conventional generators, namely the expected hourly average cost per generator, the expected capacity factor per generator, the expected hourly utilization rate per generator, and the total number of dispatched units in the system. The expected hourly average cost is calculated as

$$C_{EAC} = \sum_g \frac{\sum_t \sum_s (\frac{c_{gst}^{Total}}{E_{gst}^G})\pi_s}{\sum_t \sum_s y_{gst}^{on} \pi_s} \Big/ N^{On} \quad (5.56)$$

where E_{gst}^G and c_{gst}^{Total} are the energy produced by generator *g* and the total cost for generator *g* in time period *t* and scenario *s* respectively. N^{On} is the number of conventional generators dispatched in the system. Variable y_{gst}^{on} takes on value "1" if generator *g* is online in period *t* scenario *s*, and "0" otherwise. The term c_{gst}^{Total} is the total cost for generator *g* in period *t* scenario *s*, which includes variable costs, no-load costs, startup costs, and ramping costs. The expected utilization rate is calculated as

$$U_{\%} = \sum_g \frac{\sum_t \sum_k (\frac{P_{gst}}{P_g^{Max}})\pi_s}{\sum_t \sum_s y_{gst}^{on} \pi_s} \Big/ N^{On} \cdot 100\%. \quad (5.57)$$

This metric is used to measure the hourly utilization levels of the dispatched conventional generators. Variables used in (5.57) are the same as those used in (5.56).

TABLE 5.2. EXPECTED AVERAGE COSTS AND UTILIZATION OF CONVENTIONAL GENERATORS

Wind Level%	Expected Hourly Average Cost Per CG ($/MWh)	Expected Capacity Factor Per CG	Expected Hourly Utilization Rate Per CG	Number of CG Dispatched
30%	83.5	39.0%	65.5%	20
40%	88.5	30.3%	59.4%	23
50%	86.2	27.3%	58.1%	21
60%	86.8	25.2%	55.5%	21
70%	87.2	23.5%	54.8%	21

As shown in Table 5.2, the expected hourly average cost for a conventional generator increases in general as the wind penetration level increases. This result is consistent with the typical fossil-fuel fired generator average cost curve as shown in Fig. 5.1. Under high wind penetration levels, conventional generators will operate at low output levels and

mainly be used as backup generation. Due to large fixed costs, fossil-fuel fired generators have higher average costs and lower marginal costs at low output levels. Note that, in market settings, there are uplift payments made to generators if they do not recover their costs across a day; such required side payments are expected to increase, which is also not desirable.

One thing to note in Table 5.2 is that the expected hourly average cost for 40% wind penetration level is higher than those in all the other penetration levels. This is due to the different wind farm profiles that are modeled in the system, which cause more expensive units to be dispatched in the 40% penetration level. Under high wind penetration levels, because of the geographical diversity of wind profiles, the expected hourly average costs for conventional generators may not necessarily increase monotonically. However, the results in Table 5.2 show that the expected average costs for conventional generators, in general, increase as more wind is integrated in the system. As the wind penetration level increases, both the capacity factor and expected hourly utilization rate for conventional generator decrease, which indicates that conventional generators are utilized less efficiently under high wind penetration levels.

The total number of generators dispatched in the system for each penetration level is shown in the fourth column in Table 5.2. It can be found that more generators are dispatched in the system in higher wind penetration levels than when the penetration level is 30%. Under high wind penetration levels, the increased uncertainty and variability in renewable generation requires more generators to be dispatched. However, to provide backup generation and ancillary services, these generators have to be operated with higher average costs, lower capacity factors, and lower hourly utilization rates.

These observations indicate that conventional generators may have a decrease in profit under high renewable penetration levels.

5.5.2. Economic Assessment of Energy Storage under High Wind Penetration Levels

Three energy storage units are included in the study, with one being CAES and the other two PHS. A summary of the parameters used for energy storage units is presented in Table 5.3. The parameters for energy storage were obtained from [90] and [91].

TABLE 5.3. ENERGY STORAGE PARAMETERS

Type	$P_b^{In\_\min}$, $P_b^{Out\_\min}$ (MW)	$P_b^{In\_max}$, $P_b^{Out\_max}$ (MW)	E_b^{Max} (MWh)	η_b^{In}	η_b^{Out}
CAES	0	100	1000	0.7	0.6
PHS	0	100	1000	0.8	0.8

The solution from stochastic UC with energy storage is presented in Table 5.4 and the actual wind generation dispatched for each targeted wind penetration level is shown in Table 5.1. As wind penetration levels increase, the expected hourly average costs for conventional generators generally increase, while the expected capacity factors and hourly expected utilization rates decrease. Comparing the results in Table 5.4 with those in Table 5.2, it can be found that, with energy storage in the system, the expected hourly average costs for conventional generators are lower than those in the cases without energy storage. Also, with energy storage, the expected capacity factors and hourly utilization rates are higher than those in the cases without energy storage.

TABLE 5.4. EXPECTED AVERAGE COSTS AND UTILIZATION OF CONVENTIONAL GENERATORS WITH ENERGY STORAGE

Wind Level %	Expected Hourly Average Cost Per CG ($/MWh)	Expected Capacity Factor Per CG	Expected Hourly Utilization Rate Per CG	Number of CG Dispatched
30%	79.2	44.6%	82.6%	17
40%	79.9	38.5%	75.2%	17
50%	80.8	31.1%	69.7%	17
60%	80.3	27.2%	69.2%	17
70%	83.6	23.8%	63.6%	18

Another observation can be made from the comparison is that by including energy storage, fewer generators are dispatched in the system. This is because energy storage can store and shift excess wind power, which moderates the renewable generation in the system. Meanwhile, because energy storage has high flexibility, it can provide more spinning and non-spinning reserves with higher quality than conventional generators. Therefore, with energy storage in the system, fewer conventional generators are needed as backup generation and the dispatched generators have lower average costs and higher capacity factors and utilization rates. These important observations indicate that energy storage can improve the efficiencies of conventional generators under high renewable penetration levels.

To further demonstrate the benefits of energy storage under high renewable penetration levels, the expected system total operating costs and expected generator daily profits for the cases with and without energy storage are presented in Table 5.5. As wind penetration levels increase, the expected daily profits for conventional generators decrease in both the cases with and without energy storage. Since wind can be considered as a “free” energy with zero fuel cost, the increase of wind generation will decrease the LMPs in the system. At the same time, the average costs of conventional generators

increase as wind integration levels increase. As a result, the profits for conventional generators will decrease as more wind generation is integrated in the system. Comparing the expected system total costs in the cases with and without energy storage, it can be found that the expected system total costs are lower when energy storage is included in the system. The cost savings achieved by integrating energy storage is about 20% for each wind penetration level. These results again show that the benefits of energy storage increase with the increase in renewable penetration levels.

TABLE 5.5. EXPECTED DAILY SYSTEM TOTAL COSTS AND GENERATOR PROFITS

Wind Level %	Without Energy Storage		With Energy Storage		System Total Cost Savings
	Expected System Total Operating Cost ($)	Expected Profit per CG ($)	Expected System Total Operating Cost ($)	Expected Profit per CG ($)	
30%	656974	48552	532434	37529	19.0%
40%	566646	32711	449361	19588	20.7%
50%	447600	17684	359312	13582	19.7%
60%	418355	13963	330503	11920	21.0%
70%	377683	13491	294813	11179	21.9%

5.5.3. Results for Wind Scenario Analysis and *N*-1 Contingency Analysis

After the stochastic UC is solved, wind scenario analysis and *N*-1 contingency analysis, combined with selected wind scenarios, are performed and the results are reported in Table 5.6 and Table 5.7 respectively. A price of $3000/MWh was used to approximate the costs to correct the security violations.

TABLE 5.6. RESULTS FOR SECURITY CORRECTIONS WITH WIND SCENARIO ANALYSIS[1]

Wind %	Cost for Violations ($K)	Hourly Wind Spillage (MW)	Expected Violation Costs Plus Operating Cost ($K)	Number of Violations
With Energy Storage				
30%	0.04 (41.6)	163.7 (834.2)	403.2	1
40%	0.2 (120.6)	194.2 (941.0)	346.7	2
50%	1.9 (353.6)	276.8 (1258.8)	290.3	15
60%	1.9 (402.5)	422.6 (1721.6)	269.8	11
70%	11.4 (1053.8)	589.1 (2360.7)	252.3	49
Without Energy Storage				
30%	3.6 (255.9)	59.7 (479.4)	561.4	43
40%	6.8 (462.7)	98.1 (756.2)	485.6	69
50%	17.3 (681.4)	171.6 (1074.1)	392.6	104
60%	1.4 (354.9)	315.6 (1536.9)	349.0	15
70%	26.2 (1231.6)	468.1 (2175.9)	342.9	119

TABLE 5.7. RESULTS FOR SECURITY CORRECTIONS WITH *N*-1 CONTINGENCY ANALYSIS[1]

Wind %	Cost for Violations ($K)	Hourly Wind Spillage (MW)	Expected Violation Costs Plus Operating Cost ($K)	Number of Violations
With Energy Storage				
30%	1.6 (712.5)	3.7 (734.6)	13.1	497
40%	2.4 (748.8)	4.5 (989.0)	12.3	624
50%	2.3 (904.4)	7.1 (1252.8)	10.5	189
60%	1.7 (913.3)	11.0 (1669.6)	9.3	262
70%	1.0 (973.3)	15.4 (2309.0)	7.7	179
Without Energy Storage				
30%	4.5 (928.2)	1.0 (562.4)	20.0	517
40%	4.0 (794.3)	2.2 (804.2)	17.3	469
50%	3.2 (1140.0)	4.3 (1067.9)	13.7	235
60%	2.1 (1173.2)	8.1 (1484.7)	11.7	163
70%	1.9 (946.2)	12.3 (2124.2)	10.4	147

[1] α (β): α represents the expected daily costs for violations (expected hourly wind spillage); β represents hourly maximum costs for violations (hourly maximum wind spillage).

From Table 5.6 and Table 5.7, it can be seen that both the expected and maximum costs for correcting violations are lower in the cases with energy storage. Also, with energy storage in the system, the expected operating costs plus violation costs are lower than the cases without energy storage. These results show that energy storage can reduce the total system operating costs as well as improve the reliability of the system. Similar results can also be observed for the number of violations, where the use of energy storage significantly reduces the occurrence of violations in wind scenario analysis.

However, the wind spillage is large in both the cases with and without energy storage, which is a result of the limited capability of the system to accommodate intermittent renewable resources. Also, wind spillage is higher in the cases with energy storage. This is because the use of energy storage reduces the number of generators dispatched in the system. As the system only has limited number of fast units, more wind has to be curtailed in the cases when the flexibility of energy storage is maxed out or the reserve provided by energy storage cannot be delivered due to congestions in the system.

Note that the results presented in Table 5.6 and Table 5.7 are based on the assumption of a security violation price of 3000 $/MWh. If a different penalty price is used, the results reported in Table 5.6 and Table 5.7 may not be the same. However, it is expected the same trend of the result will be maintained, which is that energy storage can reduce system total operating costs and improve the reliability of the system.

5.6. Conclusions

As renewable penetration levels increase, conventional generators will have higher average costs, lower capacity factors, increased ramping, and decreased utilization rates. These facts indicate that conventional generators will have lower profits and, hence,

produce lower returns on investments as the renewable penetration levels increase. However, by integrating energy storage into the system, the average costs of conventional generators decrease, while fewer generators are committed in the system with higher capacity factors compared to the cases without energy storage. As such, energy storage improves the utilization of the conventional generators in the system. Furthermore, the benefits of energy storage have been shown to increase with the increasing levels of renewables. While most forms of energy storage are still considered to be too expensive and not competitive with conventional generators, the result shows that the attractiveness of conventional generators decreases as the renewable penetration levels increase whereas the attractiveness of energy storage increases with the increase in renewable resources. As the cost for energy storage is projected to be further reduced during the next five to ten years [6], [8], it is expected that there will be a break point where energy storage becomes competitive with conventional generating resources, resulting in increased deployment of energy storage technologies.

CHAPTER 6.

UTILIZING FLYWHEELS TO PROVIDE REGULATION SERVICES FOR SYSTEMS WITH RENEWABLE RESOURCES

With the increasing penetration of renewable resources in power systems, more operational flexibility is required to deal with the uncertainty of renewable generation. In particular, fast acting regulation reserves are needed to maintain the load-generation balance. In this chapter, the benefits of energy storage in providing regulation services for real-time operation are evaluated. Among the various storage technologies, flywheels have fast-ramping capabilities and are, thus, very attractive for providing regulation services. In this chapter, a two-step framework is proposed for scheduling regulation reserve and dispatching it in real-time operations.

6.1. Introduction

In power systems, generation and load should match in order to maintain the required grid frequency. However, the exact match of generation and load can only be achieved for a short period of time and a normal frequency deviation is allowed. In the Eastern Interconnection (EI), the maximum required standard deviation of frequency is 18 mHz from the nominal 60 Hz [92]. As load varies from minute to minute, it is a challenging task to balance load and generation continuously and instantaneously. Traditionally, the variation in load mainly results from the random turning on and off of different individual loads. With the rapid integration of renewable energy, another source of variability and uncertainty has been added into power systems. The tasks of balancing load and

generation to maintain system frequency continuously have become increasingly complex and difficult.

Due to the energy-shifting and fast-ramping capabilities, energy storage has been considered as a competitive and attractive resource for regulating power system frequency. Mandated by FERC order No. 890 issued in 2007, non-generation technologies are allowed to participate in the deregulated market for ancillary services [93]. While most of the energy storage technologies can provide regulation services, flywheels are one of the most attractive technologies in such applications, due to their fast-ramping and quick-response capabilities. The response time for a flywheel can be as short as four milliseconds. Even though flywheels have limited energy capacity, their fast ramping capability and short response time make them a competitive source for regulating frequency and following Automatic Generation Control (AGC) instructions in real-time. In this chapter, a two-step approach is proposed to analyze the benefits of flywheels in systems with renewable resources. The proposed approach simulates the scheduling and activation of regulation reserves during real-time operations. The attractiveness of flywheels to provide regulation services in real-time operation is analyzed.

6.2. Mathematical Formulations

The performance of a regulation resource should be measured by two aspects: the regulation capacity it can provide and its accuracy in following the AGC signals. A desired flexible resource should not only have the capability to provide high capacity of regulation reserves, but also be able to follow the AGC signal accurately. The proposed

two-step framework evaluates the regulation services that flywheels can provide from the aforementioned two aspects.

In this section, the two-step energy and ancillary services scheduling model is formulated. In the first-step, a 15-minute real-time generation scheduling problem is formulated to schedule the generation dispatch and regulation reserves for each unit. In the second-step, a regulation reserve dispatch problem is used to simulate the deployment of regulation reserves under renewable uncertainties. As in real-time operations, regulation reserves are deployed based on the AGC signals. In the following formulations, terms with a bar represent parameters; these parameters are either fixed from the previous step or given as an input to the optimization program. Since a flywheel has limited energy capacity, it does not qualify for providing an energy product and its primary application is to provide regulation reserves [94]. Therefore, in this study, it is assumed that flywheels will only provide regulation reserves and are not allowed to provide an energy product.

6.2.1. Real-Time Generation Scheduling Model

In the first-step, the real-time scheduling problem is formulated with three time periods, each representing a 5-minute time interval. The lossless dc power flow formulation is utilized. Note that the nodal balance constraint does not include the flywheel's production as it is not providing an energy product at the look-ahead time stage. The objective of the real-time generation scheduling problem, shown in (6.1), is to minimize system operating cost and the costs to correct security violations (e.g., the cost to correct involuntary load shedding and violations of the reserve requirements). The complete formulation is as follows:

Minimize:

$$\sum_t \left[\sum_g c_g\left(P_{gt}\right) + \sum_n c^{vL} s_{nt}^{L} + c^{vR+} s_t^{R+} + c^{vR-} s_t^{R-} + c^{vOR} s_t^{OR}\right] \quad (6.1)$$

Subject to:

$$\sum_{\forall g(n)} P_{gt} + \sum_{k\in\delta^{+}(n)} P_{kt} - \sum_{k\in\delta^{-}(n)} P_{kt} = d_{n,t} - s_{nt}^{L} - \sum_{\forall w(n)} (P_{wt}^{Wind} - s_{wt}^{W}), \forall n, t \quad (6.2)$$

$$P_{kt} - B_k(\theta_{kt}^{+} - \theta_{kt}^{-}) = 0, \forall k, t \quad (6.3)$$

$$-P_k^{Max} \leq P_{kt} \leq P_k^{Max}, \forall k, t \quad (6.4)$$

$$P_g^{Min}\bar{u}_{gt} + r_{gt}^{R-} \leq P_{gt} \leq P_g^{Max}\bar{u}_{gt} - r_{gt}^{R+} - r_{gt}^{S}, \forall g, t \quad (6.5)$$

$$r_{gt}^{R+} \leq R_g^{5+}\bar{u}_{gt}, r_{gt}^{Rd} \leq R_g^{5-}\bar{u}_{gt}, r_{gt}^{S} \leq R_g^{10+}\bar{u}_{gt}, \forall g, t \quad (6.6)$$

$$-R_g^{5-} \leq P_{gt} - P_{g,t-1} \leq R_g^{5+}, \forall g, t \quad (6.7)$$

$$\sum_g r_{gt}^{R+} + \sum_b r_{bt}^{R+} \geq Q_t^{R+} - s_t^{R+}, \forall t \quad (6.8)$$

$$\sum_g r_{gt}^{R-} + \sum_b r_{bt}^{R-} \geq Q_t^{R-} - s_t^{R-}, \forall t \quad (6.9)$$

$$\sum_g r_{gt}^{S} \geq P_{gt} + r_{gt}^{S} - s_t^{OR}, \forall \mathrm{g}, t \quad (6.10)$$

$$r_{bt}^{R+} \leq P_b^{Out\_max} - P_{bt}^{ES}, \forall b, t \quad (6.11)$$

$$r_{bt}^{R-} \leq P_b^{In\_max} + P_{bt}^{ES}, \forall b, t \quad (6.12)$$

$$r_{bt}^{R+} \leq 12\left(E_{b,t} - E_b^{Min}\right), \forall b, t \quad (6.13)$$

$$r_{bt}^{R-} \leq 12(E_b^{Max} - E_{b,t}), \forall b, t \quad (6.14)$$

$$-P_b^{In\_max} \leq P_{bt}^{ES} \leq P_b^{Out\_max}, \forall b, t \quad (6.15)$$

$$E_b^{Min} \leq E_{bt} \leq E_b^{Max}, \forall b, t \quad (6.16)$$

$$E_{bt} = E_{b,t-1} - \frac{P_{bt}^{ES}}{12} + \frac{\gamma_b^{DF}(r_{bt}^{R-} - r_{bt}^{R+})}{12}, \forall b, t. \quad (6.17)$$

In the above formulation, the nodal balance constraint is shown in (6.2). Constraint (6.3) represents the dc power flow on each line and (6.4) is the line-flow limit constraint.

Constraints (6.5) and (6.6) represent the limits on power output and ancillary services, including spinning and regulation reserves, for each generator. The ramp rate constraints are presented in (6.7). Constraints (6.8) and (6.9) represent the system regulation requirements. In the model, the regulation requirement is set to be 2% of the load. The sum of spinning reserves in the system is required to be greater or equal to the single largest generator contingency, as shown in (6.10). The reserve requirement constraints can be violated for a predetermined penalty price. Since the focus of the work is on the scheduling and dispatch of regulation reserves, non-spinning reserve is omitted in the formulation for simplicity.

The flywheel model is presented by (6.11)-(6.17). Constraints (6.11)-(6.14) formulate the up and down regulation reserves provided by flywheels. The coefficient "12" is used to convert energy (MWh) to power (MW), where it is assumed that the flywheels should have enough energy to provide the scheduled regulation reserve for five minutes. Constraint (6.15) represents the limits on consumption and production, where negative value indicates consumption and positive value indicates production. The capacity constraint for the state of charge is presented in (6.16). The energy balance constraint for flywheels is shown in (6.17). To approximate the change in the state of charge when regulation reserve is deployed, up and down regulation reserves are included in the energy balance constraint. The inclusion of up and down regulation reserves in the energy balance constraint provides an estimation of how much energy is needed when the scheduled regulation reserve is deployed. Parameter γ_b^{DF} is a tuning parameter between 0 and 1, which is to estimate the actual regulation deployment in time period *t* [94]. This parameter implies that the scheduled regulation capacity may not be fully used during the

deployment of the reserves. Note that, in the first-step, only the capacity of the regulation reserves are determined for the flywheels and, thus, the optimization program does not know how much regulation reserve will actually be deployed. If this deployment factor is omitted, the optimization program may over- or under-schedule regulation reserves.

6.2.2. Regulation Reserve Dispatch Model

In the second-step, a regulation reserve dispatch model is used to simulate the deployment of the regulation reserves scheduled in the first-step. The regulation reserve dispatch model is solved to test if the scheduled regulation reserves are able to balance generation and load in real-time under different wind scenarios. In this step, the energy products from the flywheels are included in the nodal balance constraint, based on the activation of regulation reserves. Each dispatch run is solved for two consecutive time periods: the current time period and the next time period. Each time period represents a 2.5-mintue interval. The main function of the look-ahead period is to ensure the feasibility of the problem, since generators should be able to ramp to the desired dispatch point in the next time period. The regulation reserve dispatch problem will be solved sequentially using this 5-minute rolling window. The total simulation length of the second-step is 15 minutes. The objective function of the regulation reserve dispatch problem is to minimize the total system operating costs and the costs to correct system violations. The complete formulation is as follows:

Minimize:

$$\sum_t \left[\sum_g c_g\left(P_{gt}\right) + \sum_n c^{vL} s_{nt}^{L} + c^{vR+} s_t^{R+} + c^{vR-} s_t^{R-} + c^{vOR} s_t^{OR}\right] \quad (6.18)$$

Subject to:

$$\sum_{k\in\delta^{+}(n)} P_{kt} - \sum_{k\in\delta^{-}(n)} P_{kt} + \sum_{b} P_{bt}^{ES} + \sum_{\forall g(n)} P_{gt} = d_{n,t} - s_{nt}^{L} - \sum_{\forall w(n)}(P_{wt}^{Wind} - s_{wt}^{W}), \forall n, t \quad (6.19)$$

$$P_{kt} - B_k(\theta_{kt}^{+} - \theta_{kt}^{-}) = 0, \forall k, t \quad (6.20)$$

$$-P_k^{Max} \leq P_{kt} \leq P_k^{Max}, \forall k, t \quad (6.21)$$

$$P_g^{Min}\bar{u}_{gt} \leq P_{gt} + r_{gt}^{S} \leq P_g^{Max}\bar{u}_{gt}, \forall g, t \quad (6.22)$$

$$(\bar{P}_{gt} - \bar{r}_{gt}^{R-})\bar{u}_{gt} \leq P_{gt} \leq (\bar{P}_{gt} + \bar{r}_{gt}^{R-})\bar{u}_{gt}, \forall g, t \quad (6.23)$$

$$-R_g^{2.5-} \leq P_{gt} - P_{g,t-1} \leq R_g^{2.5+}, \forall g, t \quad (6.24)$$

$$\sum_{g\in\Omega_G} r_{gt}^{S} \geq P_{gt} + r_{gt}^{S} - s_t^{OR}, \forall \mathrm{g}, t \quad (6.25)$$

$$-P_b^{In\_max} \leq P_{bt}^{ES} \leq P_b^{Out\_max}, \forall b, t \quad (6.26)$$

$$\bar{P}_{bt}^{ES} - \bar{r}_{bt}^{R-} \leq P_{bt}^{ES} \leq \bar{P}_{bt}^{ES} + \bar{r}_{bt}^{R-}, \forall b, t \quad (6.27)$$

$$E_b^{Min} \leq E_{bt} \leq E_b^{Max}, \forall b, t \quad (6.28)$$

$$E_{bt} = E_{b,t-1} - P_{bt}^{ES}/24, \forall b, t. \quad (6.29)$$

Constraints (6.22) and (6.23) indicate that the operating range for generators in the second-step will be bounded by the desired dispatch point plus and minus the regulation reserve determined in the first-step. The operating range for the flywheel is modeled similarly as shown in (6.26) and (6.27), which is also limited by the desired dispatch point plus and minus the regulation reserve scheduled in the first-step. The other constraints in the second-step formulation are similar to those in the first-step.

6.2.3. Renewable Modeling

In order to generate wind scenarios for the case study, the method described in [79] is adopted. For each time period *t*, the wind forecast error is assumed to follow a truncated Gaussian distribution $N(0, \sigma^2)$ with zero mean and variance σ^2. The wind scenarios are

generated as a scenario tree. Fig. 6.1 shows a scenario tree over two time periods. In a scenario tree structure, if the simulation window has a number of T periods and a number of S scenarios are modeled for each time period, then the total number of scenarios in the scenario tree is S^T. The standard deviation is chosen such that the resulted forecast error is about 5% in the real-time operation [95].

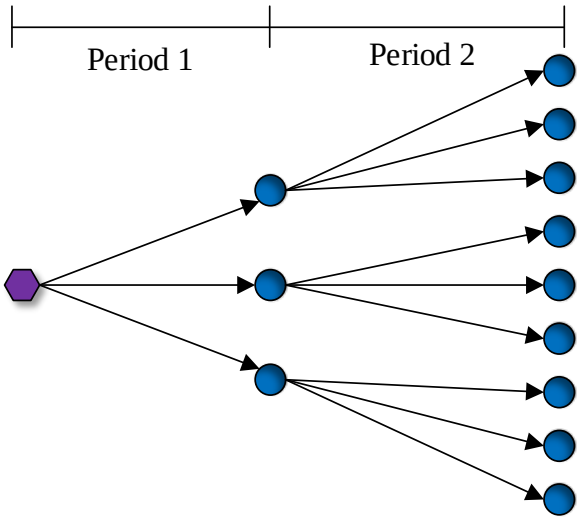

Fig. 6.1. Illustration of the Scenario Tree Structure

6.2.4. Simulation Procedure

The simulation methodology is described as follows. Stochastic simulations are first performed to generate four scenarios for each time period. Then a scenario tree is constructed using the generated scenarios. The resulted scenario tree has a total number of 4096 scenarios for the 15-minute interval. After the scenario tree is constructed, a real-time scheduling model is solved to determine the generation re-dispatch and the regulation reserves in the system. One wind scenario is used in the real-time scheduling problem, which is the actual wind forecast for the 15-mintue interval. After the solution is obtained from the real-time scheduling problem, the regulation reserve dispatch model is solved for all the wind scenarios in the scenario tree, one scenario at a time, to test if the

scheduled generation and reserves are sufficient for all the wind scenarios generated. If violations are reported, security corrections should be performed to make up for such violations in the system.

6.3. Case Study

The RTS96 one-zone model [87]-[88] is used as the test system. The total generation capacity in the system is 3402 MW, while the system peak load is 2850 MW. The load profile information is obtained from [87]-[88] and the resulted system load is 2422.5 MW. The system load is assumed to stay the same during the 15 minutes of operation. The value of reserve deployment factor γ^{DF} is chosen to be 0.5, implying that the 50% of the scheduled regulation reserve capacity will be activated. An initial commitment status is provided for each generator in the system. The commitment status for each generator is not allowed to change in the two-step problem. The cost for correcting involuntary load shedding is assumed to be 3000 $/MWh and the cost for correcting violations in reserve requirement is assumed to be 1100$/MWh. Note that these penalty prices are approximations; since the true cost for correcting security violations is difficult to obtain. If a different set of penalty prices is used, the result of the case study may be different; but the trend of the result is expected to stay the same.

The simulation is performed for wind penetration levels at 10%, 15%, and 20%; the wind penetration level is defined as the ratio of total daily wind generation to the total system daily demand. Wind data is collected from the NREL Wind Integration Database [78]. The original 10-min wind data is interpolated into 2.5-minute and 5-minute data. Wind curtailment is allowed when the system cannot accommodate all of the available wind production. In the simulation, a 20MW/15min flywheel storage unit is included.

The parameters used for the flywheel are obtained from [40]. A summary of the parameters is presented in Table 6.1. Since a flywheel has a fast ramping capability, the ramp rate for the flywheel is set at a high value such that the ramp rate constraint is never binding for the flywheel. An initial state of charge is provided for the flywheel. In the real-time scheduling problem, the state of the charge for the flywheel unit in the last time period is required to be the same as the initial value. The efficiencies for flywheels during production and consumption are assumed to be 1.

TABLE 6.1. FLYWHEEL PARAMETERS

Type	$P_b^{In\_max}, P_b^{Out\_max}$ (MW)	E_b^{Min} (MWh)	E_b^{Max} (MWh)
Flywheel	20	0.5	5

6.3.1. Result Analysis and Discussion

The results for the real-time scheduling problem and regulation reserve dispatch problem are shown in Table 6.2 and Table 6.3. The system total operating costs, involuntary load shedding, wind curtailment, and reserve requirement violations are reported for the 15-minute operation for each wind penetration level. The reserve requirement violations in Table 6.2 present the aggregate violations in reserve requirements including the up regulation, down regulation, and spinning reserves. In Table 6.3, the expected reserve requirement violations include only the spinning reserve, since regulation reserves are activated in the regulation reserve dispatch problem. The expected cost savings by incorporating flywheels in the system are summarized in Table 6.4.

TABLE 6.2. SYSTEM RESULTS FOR THE 15-MINUTE OPERATION IN THE FIRST-STEP

With Flywheel					
	Wind %	System Total Operating Cost ($)	Involuntary Load Shedding (MWh)	Wind Curtailment (MWh)	Reserve Requirement Violations (MWh)
1	10%	8672	0	0	0
2	15%	3989	0	0	0
3	20%	2886	0	2	0
No Flywheel					
	Wind %	Total System Operating Cost ($)	Involuntary Load Shedding (MWh)	Wind Curtailment (MWh)	Reserve Requirement Violations (MWh)
1	10%	10380	0	0	1.7
2	15%	3989	0	0	0
3	20%	2912	0	5	0

In the first-step, a real-time generation scheduling problem is formulated. In the real-time scheduling problem, the flywheel is considered as a unit that can only provide regulation reserve. For the 10% wind penetration case, since wind penetration is at a relatively low level, most of the online capacities from both slow and fast units are used to satisfy the load. As a result, fast units will be dispatched at higher output levels. As fast units have limited capacities left for ancillary services and slow units have limited ramping capabilities, the system does not have enough flexibility to meet the reserve requirements in the case without the flywheel. For the case with the flywheel, since the flywheel has a high ramp rate, it can provide regulation reserve as high as its maximum power rating. Therefore, at 10% wind penetration level, the case without the flywheel has about 1.7MWh of reserve requirement violations and, thus, results in a much higher cost than that the case with the flywheel. At higher wind penetration levels, fast units have more capacities to provide ancillary services and, thus, the system is able to meet the reserve requirement. Therefore, as shown in Table 6.4, the cost saving by having the

flywheel in the system is much lower in higher wind penetration levels than in the 10% wind level. However, it should be noted that only the reserve capacities are determined in the first-step. By only evaluating the benefits to provide regulation reserve capacity, the flexibility of the flywheel may not be fully utilized and the benefit of using the flywheel is not entirely realized.

To fully evaluate the attractiveness of the flywheel, the second-step is solved to simulate the deployment of the regulation reserves and analyze the fast-ramping capability of flywheels. The results for the second-step are shown in Table 6.3, where the expected system total operating costs, expected involuntary load shedding, expected wind curtailment, and expected violations in reserve requirement are reported. From Table 6.3, it can be noticed that for the cases with flywheel, the total system costs are reduced and less load and wind is curtailed in general. The operating cost savings by having the flywheel in the system are about 4% to 8% as shown in Table 6.4. Compared to the first-step, except for the 10% penetration level, the cost savings by using the flywheel are much higher in the second-step. In the second-step, the regulation reserve dispatch problem is solved sequentially and a desired dispatch point is provided for each generator. Therefore, if wind generation deviates away from the forecast, the thermal units in the system may not have enough ramping capabilities to meet the ramping requirements. However, as flywheels have fast-ramping capabilities and fast-response times, they can effectively compensate for renewable uncertainty and thus improve system reliability. This explains why the cost savings by using flywheel are generally higher in the second-step than those in the first-step.

TABLE 6.3. SYSTEM EXPECTED RESULTS FOR THE 15-MINUTE OPERATION IN THE SECOND-STEP

With Flywheel					
	Wind %	System Total Operating Cost ($)	Involuntary Load Shedding (MWh)	Wind Curtailment (MWh)	Reserve Requirement Violations (MWh)
1	10%	10816	0	0	1.90
2	15%	5676	0.27	0	0.71
3	20%	7336	1.42	1	0.09
No Flywheel					
	Wind %	Total System Operating Cost ($)	Involuntary Load Shedding (MWh)	Wind Curtailment (MWh)	Reserve Requirement Violations (MWh)
1	10%	11744	0	0	2.75
2	15%	5933	0.35	0	0.72
3	20%	7919	1.60	2	0.11

TABLE 6.4. OPERATING COST SAVINGS IN DOLLARS AND PERCENTAGE FOR THE 15-MINUTE

	Wind %	First-Step		Second-Step	
		Savings ($)	Savings (%)	Savings ($)	Savings (%)
1	10%	1707	16.4%	928	7.9%
2	15%	0	0	257	4.3%
3	20%	25	0.9%	583	7.4%

A box plot for the system total operating costs in the second-step is presented in Fig. 6.2. The edges of the boxes are the 25th and 75th percentiles and the whiskers represent the maximum and minimum not considered outliers. The horizontal red lines inside each box represent median values and outliers are plotted in red "+". The plot illustrates the variation in samples of system's total costs for each case. The cases labeled "with x%" are the cases with the flywheel and the rest are the cases without the flywheel. For 10% wind penetration, the cost range for the cases with the flywheel is much lower than that for the cases without the flywheel, which suggests that the flywheel reduces the system total costs in most cases. For 15% and 20% wind penetration levels, the cases with the

flywheel have lower medium values and lower maximum total costs, showing that the flywheel is a valuable resource for providing regulation reserves. Also, as the plots for the cases with flywheel span shorter ranges under 15% and 20% wind penetration levels, it indicates that the variance is smaller for the cases with flywheel for 15% and 20% wind penetration levels.

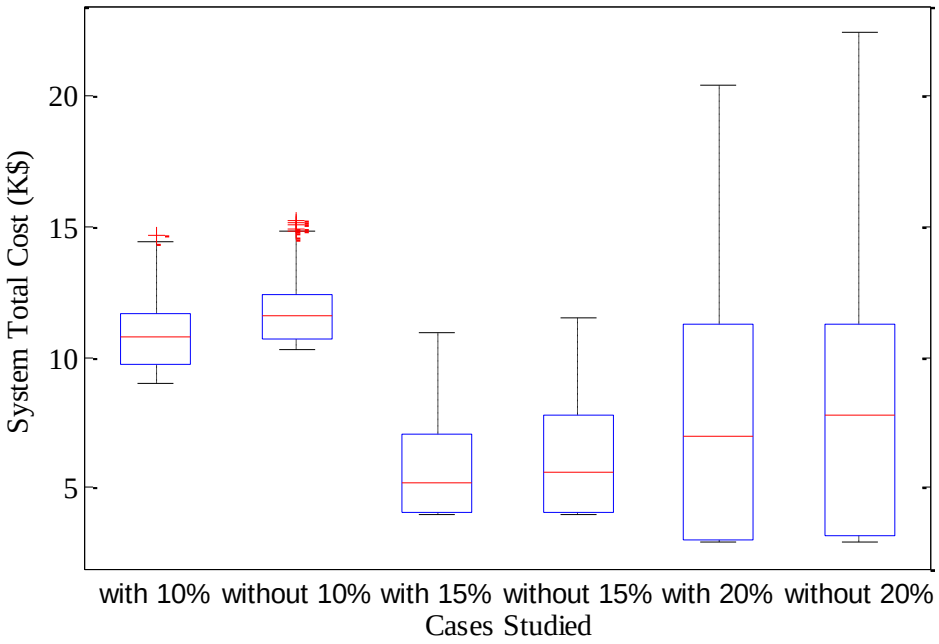

Fig. 6.2. Box Plot for System Total Operating Costs for Each Case in the Second-Step

6.3.2. Conclusions

Energy storage technologies are an attractive solution for maintaining the generation-demand balance in power systems. Flywheels, like most energy storage technologies, have high ramp rates and fast response times. As such, flywheels have characteristics that match well with the needs of frequency regulation applications. In this chapter, the attractiveness of flywheels for providing regulation services is evaluated in the proposed two-step approach. In the first-step, the scheduling problem evaluates the benefits of the

flywheel to provide high capacity of regulation services. In the second-step, a regulation reserve dispatch program, with a finer time resolution, is implemented to assess the fast ramping capability of the flywheel. Results from the two-step analysis demonstrate the effectiveness of the flywheel storage technology to provide fast acting regulation reserves.

CHAPTER 7.

FLEXIBLE OPERATION OF BATTERY STORAGE IN POWER SYSTEM SCHEDULING WITH RENEWABLE ENERGY

As a fast developing storage technology, battery storage has received growing interests in recent years. In this chapter, a two-step modeling framework is used to evaluate the benefits of battery storage in systems with renewable resources. A flexible operating range approach is proposed to improve the operational scheme of energy storage in real-time operations.

7.1. Introduction

With increasing concerns about climate change and the need for a more sustainable grid, power systems have seen a fast expansion of renewable resources in recent years. The variability and uncertainty of renewable resources have increased the complexities in balancing load with generation and have introduced new challenges in regards to maintaining system reliability. As a result, more flexible resources are needed to meet the increasingly stringent ramping requirements in the system.

Driven by the need to integrate higher penetration levels of renewable energy and to reduce the costs for serving peak demands, recent interests have been focused on energy storage technologies. Energy storage can shift energy from peak-demand hours to off-peak-demand hours, or absorb excess renewable energy to provide it back to the grid when desired. The fast-ramping capability also makes energy storage a competitive resource to compensate for the variability and uncertainty in renewable energy. By using

energy storage, the cycling of thermal units can be reduced, which is an advantage since many thermal units are not designed to be ramped up and down frequently.

Among all existing storage technologies, there is substantial interest in batteries as an emerging solution to manage intermittent renewable resources. Compared with thermal units, batteries do not have a no-load cost and they are generally considered to not have a minimum production level. Compared to other storage technologies, such as PHS and CAES, batteries have higher power densities. Even though the main barrier with battery technologies is their high capital costs, efforts are being made to reduce the capital costs and improve the cost-effectiveness of different battery solutions [96].

While the study of battery storage in systems with renewable resources is not new, much of the previous work is based on day-ahead models or short-term look-ahead scheduling models [41], [98], [99]. In such look-ahead scheduling problems, scheduling for future time periods are optimized together in one model based on forecast information. However, with a look-ahead type of scheduling model, the challenges associated with managing the state of charge (SOC) of the battery are not properly captured. Different from thermal units, the dispatch of batteries is constrained by their SOC. In real-time operation, as look-ahead functionality is limited, decisions for time period t have to be made in advance without having perfect information about future uncertainties. An inappropriate decision made for battery storage in the current time period could potentially result in insufficient capacity to charge or discharge in future time periods. These challenges are not adequately captured in independent day-ahead or short-term look-ahead scheduling models.

In this chapter, we study battery storage under the assumption that it is a system asset operated by the system operator. A two-step modeling framework is presented to study the operation and the benefit of battery storage in transmission systems with renewable generation. In the first-step, a stochastic UC model is formulated for the day-ahead stage where wind power generation is uncertain. In the second-step, the challenge associated with utilizing energy storage in real-time operation is investigated. An improved approach is proposed to provide a flexible operating strategy for energy storage in real-time operation. Analysis is conducted using the IEEE RTS system with wind power uncertainty data obtained from a numeric weather predictions (NWP) model.

7.2. Mathematical Model and Methodology

The two-step modeling framework is structured as follows. In the first-step, which is referred to as the day-ahead scheduling, a two-stage stochastic day-ahead UC model is formulated. In the second-step, a Monte-Carlo based simulation, which is later referred to as the stochastic simulation, is performed to test the day-ahead solution against wind scenarios that are not included in the day-ahead stochastic UC. The second-step is later referred to as the post-stage analysis. The formulation used in the two-step framework is described in the following subsections.

7.2.1. Day-Ahead Scheduling and Stochastic Unit Commitment

The stochastic UC is formulated as a mixed integer linear program based on the formulation in [100]. A lossless dc power flow formulation is used. In [100], the scheduling horizon is divided into several time blocks. Within each time block, wind scenarios are grouped into different “buckets” based on their average wind forecast value.

The non-anticipativity constraints are then enforced for scenarios that are in the same bucket in each time block. The advantage of this formulation is that it can provide a more flexible schedule for the thermal generators as the commitment schedule is dependent on each bucket rather than being the same for all the scenarios in the stochastic UC. It should be noted that the day-ahead UC model is still solved for the full 24-hour time horizon. The introduction of time blocks is primarily to introduce flexibility in the solution by allowing commitment decisions for thermal units to vary between buckets and time blocks, as a function of the wind power level.

The complete formulation of the stochastic UC with energy storage is presented in (7.1)-(7.29), where the objective (7.1) is to minimize the system total costs and the costs of security violations (e.g., the cost of involuntary load shedding and violations of the reserve requirements). In the formulation, constraint (7.2) guarantees the power balance at every bus. Constraint (7.3) represents the dc power flow on each line and (7.4) is the line-flow limit constraint. Limits on the power output for each generator are presented in (7.5) and (7.6). The non-anticipativity constraints are shown in (7.7), where e is the index for buckets and β is an assignment function that matches each scenario to its corresponding bucket. Note that the non-anticipativity constraints are only modeled for the slow units and enforced for each individual bucket, i.e., not across all the scenarios. The minimum up and down time constraints are shown in (7.8)-(7.10). Constraints (7.11)-(7.14) represent the ramp rates constraints for regulation, spinning and non-spinning reserves provided by thermal units. The hourly ramp rate constraints are shown in (7.15) and (7.16).

The model for the battery is shown in (7.17)-(7.24). Constraints (7.17)-(7.20) represent the limits on regulation and spinning reserves provided by batteries. Constraints (7.18) and (7.20) indicate that a battery should be able to maintain its output for duration of α_b^S and α_b^R hours to be qualified to provide spinning and regulation reserves respectively. Constraint (7.21) is the power balance constraint for energy storage. Regulation reserve variables are included in (7.21) to estimate the change in SOC as a result of the deployment of the regulation reserves. Parameter γ^{DF} is included to estimate the actual regulation deployment in time period *t.* Parameter γ_b^{DF} is assumed to be 0.2 in the model, based on the assumption that 20% of the scheduled regulation reserve capacity will be activated. The limits on consumption and production for the battery are presented in (7.22) and (7.23). Constraint (7.24) represents the energy capacity for the battery.

The constraints for system-wide regulation and spinning reserve requirements are presented in (7.25)-(7.29). In the model, the regulation reserve requirement is set to be 2% of the load, while the operating reserve (sum of spinning and non-spinning reserve) is required to be greater or equal to the single largest generator contingency. It is also required that half of the system operating reserve should come from spinning reserve. The reserves needed to compensate renewable uncertainties are addressed endogenously by the stochastic UC model. The reserve requirement constraints can be violated for a predetermined penalty price, as reflected in the objective function.

Minimize:

$$\sum_s \pi_s \{\sum_g \sum_t \left[C_g\left(P_{gst}\right) + c_g^{NL} u_{gst} + c_g^{SU} v_{gst}\right] + \sum_n \sum_t c^{vL} s_{nst}^{L} + \sum_t \left(c^{vR+} s_{st}^{R+} + c^{vR-} s_{st}^{R-} + c^{vSP} s_{st}^{SP} + c^{vOR} s_{st}^{OR}\right)\} \quad (7.1)$$

Subject to:

$$\sum_{\forall g(n)} P_{gst} + \sum_{k\in\delta^{+}(n)} P_{kst} - \sum_{k\in\delta^{-}(n)} P_{kst} + \sum_{\forall b(n)}(P_{bst}^{Out} - P_{bst}^{In}) = d_{nt} - s_{nst}^{L} -$$

$$\sum_{\forall w(n)}(P_{wst}^{Wind} - s_{wst}^{W}), \forall n, t, s \tag{7.2}$$

$$P_{kst} - B_k(\theta_{kst}^{+} - \theta_{kst}^{-}) = 0, \forall k, t, s \tag{7.3}$$

$$-P_k^{max} \leq P_{kst} \leq P_k^{max}, \forall k, t, s \tag{7.4}$$

$$P_{gst} + r_{gst}^{R+} + r_{gst}^{S} \leq P_g^{max} u_{gst}, \forall g, t, s \tag{7.5}$$

$$P_g^{min} u_{gst} \leq P_{gst} - r_{gst}^{R-}, \forall g, t, s \tag{7.6}$$

$$u_{gst} = u_{get}, \forall g \in \Omega_{Gs}, t, e = \beta(s,t), \forall g \in \Omega_{Gs}, t, s \tag{7.7}$$

$$\sum_{q=t-UT_g+1}^{t} v_{gsq} \leq u_{gst}, \ \forall g, t \in \{UT_g, \dots, T\}, s \tag{7.8}$$

$$\sum_{q=t-DT_g+1}^{t} w_{gsq} \leq 1 - u_{gst}, \ \forall g, t \in \{DT_g, \dots, T\}, s \tag{7.9}$$

$$v_{gst} - w_{gst} = u_{gst} - u_{g,s,t-1}, \ \forall g, t, s \tag{7.10}$$

$$r_{gst}^{R+} \leq R_g^{5+} u_{gst}, \forall g, t, s \tag{7.11}$$

$$r_{gst}^{R-} \leq R_g^{5-} u_{gst}, \forall g, t, s \tag{7.12}$$

$$r_{gst}^{S} \leq R_g^{10+} u_{gst}, \forall g, t \tag{7.13}$$

$$r_{gst}^{NS} \leq R_g^{NS}(1 - u_{gst}), \forall g, t, s \tag{7.14}$$

$$P_{g,s,t} - P_{g,s,t-1} \leq R_g^{60+} u_{g,s,t-1} + R_g^{SU} v_{gst}, \forall g, t, s \tag{7.15}$$

$$P_{g,s,t-1} - P_{g,s,t} \leq R_g^{60-} u_{gst} + R_g^{SD} w_{gst}, \forall g, t, s \tag{7.16}$$

$$r_{bst}^{S} + r_{bst}^{R+} \leq P_b^{Out\_max} - P_{bst}^{Out} + P_{bst}^{In}, \forall b, t, s \tag{7.17}$$

$$\alpha_b^S r_{bst}^S + \alpha_b^R r_{bst}^{R+} \leq \eta_b^{Out}(E_{bst} - E_b^{Min}), \forall b, t, s \tag{7.18}$$

$$r_{bst}^{R-} \leq P_b^{In\_max} - P_{bst}^{In} + P_{bst}^{Out}, \forall b, t, s \tag{7.19}$$

$$\alpha_b^R r_{bst}^{R-} \leq (E_b^{Max} - E_{b,s,t})/\eta_b^{In}, \forall b, t, s \tag{7.20}$$

$$E_{bst} = E_{b,s,t-1} + P_{bst}^{In}\eta_b^{In} - P_{bst}^{Out}/\eta_b^{Out} + \gamma_b^{DF}\alpha_b^R(r_{bst}^{R-}\eta_b^{In} - r_{bst}^{R+}/\eta_b^{Out}), \forall b, t, s \quad (7.21)$$

$$0 \le P_{bst}^{Out} \le P_b^{Out\_max} z_{bst}, \forall b, t, s \quad (7.22)$$

$$0 \le P_{bst}^{In} \le P_b^{In\_max}(1 - z_{bst}), \forall b, t, s \quad (7.23)$$

$$E_{min} \le E_{bst} \le E_{max}, \forall b, t, s \quad (7.24)$$

$$\sum_g r_{gst}^{R+} + \sum_b r_{bst}^{R+} \ge 0.02 \sum_n d_{nt} - s_{st}^{R+}, \forall t, s \quad (7.25)$$

$$\sum_g r_{gst}^{R-} + \sum_b r_{bst}^{R-} \ge 0.02 \sum_n d_{nt} - s_{st}^{R-}, \forall t, s \quad (7.26)$$

$$Q_{st}^{OR} \ge P_{gst} + r_{gst}^{S}, \forall g, t, s \quad (7.27)$$

$$\sum_g r_{gst}^{S} + \sum_b r_{bst}^{S} + \sum_g r_{gst}^{NS} \ge Q_{st}^{OR} - s_{st}^{OR}, \forall t, s \quad (7.28)$$

$$\sum_g r_{gst}^{S} + \sum_b r_{bst}^{S} \ge 0.5 Q_{st}^{OR} - s_{st}^{SP}, \forall t, s \quad (7.29)$$

7.2.2. Post-Stage Analysis and Hourly-Dispatch Problem

In the second-step, which is referred to as the post-stage analysis, stochastic simulation is performed to test the day-ahead solution against wind scenarios that are not included in the day-ahead UC. In the post-stage analysis, only the uncertainty in renewable generation is considered; load forecast uncertainty and generator outages are not included. The post-stage analysis is formulated using an hourly-dispatch model. The complete formulation for the hourly-dispatch model is presented in (8.30)-(8.33). A deterministic formulation is used and only one scenario is included in each dispatch problem. In (8.30)-(8.33), index *t*' represents the current time period and T_{LA} represents the number of look-ahead time periods included. Each dispatch run solves for the current hour and looks T_{LA} hours ahead (T_{LA}=1 as default assumption), for which a *persistence* wind power forecast is assumed. The objective is to minimize the total cost in the current

hour and the look-ahead period, as shown in (8.30). The hourly dispatch problem is solved sequentially for 24 hours using a rolling window. The hourly-dispatch model is formulated to approximate the real-time operation, but with a lower time resolution than what is typically used in U.S. energy markets. The commitment schedules for slow (slow-start) units are given by the day-ahead UC, as shown in (8.31). Parameter $\overline{u}_{gt}$ is the commitment status obtained from day-ahead UC. Fast (fast-start) units are allowed to change commitment status in the hourly-dispatch problem. Slow units are defined as the generators that have minimum up and down time greater than one hour. Fast units are defined as the generators that have minimum up and down time smaller or equal to one hour. The other constraints for the hourly-dispatch model are similar to those used in the day-ahead UC,

Minimize:

$$\sum_g \sum_t \left(C_g\left(P_{gt}\right) + c_g^{NL} u_{gt} + c_g^{SU} v_{gt}\right) + \sum_n \sum_t \; c^{vL} s_{nt}^{L} + \sum_t \left(c^{vR+} s_t^{R+} + c^{vR-} s_t^{R-} + c^{vSP} s_t^{SP} + c^{vOR} s_t^{OR}\right) \quad (7.30)$$

Subject to:

$$u_{gt} = \overline{u}_{gt}, \forall g \in \Omega_{Gs}, t \in \{t', \dots, t' + T_{LA}\} \quad (7.31)$$

$$\text{Eqs. (8.2)-(8.6), (8.10)-(8.29)}, t \in \{t', \dots, t' + T_{LA}\} \quad (7.32)$$

$$P_{wt}^{Wind} = P_{w,t-1}^{Wind}, \forall w, t \in \{t' + 1, \dots, t' + T_{LA}\}. \quad (7.33)$$

7.2.3. Battery Operation with a Fixed Operating Schedule

To address the limited look-ahead functionality in real-time operation, one approach is to use the solution obtained through a look-ahead scheduling stage. However, as the SOC is a second-stage decision in the day-ahead stochastic UC, one battery schedule is

obtained for each scenario. Therefore, in the post-stage analysis, for each wind scenario to be tested, the most appropriate battery schedule should be selected from the day-ahead solution. In this work, the battery schedule is selected based on the similarity between the post-stage wind scenario and the day-ahead wind scenario. The similarity between the two wind scenarios is measured by the Euclidean distance. Therefore, for each post-stage wind scenario s, the day-ahead wind scenario s_0, which is closest to scenario s, is identified. Then the battery schedule that corresponds to the scenario s_0 is used in the post-stage scenario s. Denote this battery schedule as $\overline{\boldsymbol{E}}_b^{\boldsymbol{s0}}$, where $\overline{\boldsymbol{E}}_b^{\boldsymbol{s0}}$ is a vector with each element representing a target SOC in each time period.

For each post-stage scenario, the corresponding battery schedule has to be determined before the first time period is solved. To reflect the fact that wind generation cannot be perfectly forecasted while not over-complicating the simulation process, the wind generation profiles in the first six hours of each post-stage scenario are used to determine the closest day-ahead wind scenario. The underlying assumption is that the wind forecast for the first six hours has relatively low forecast errors and can be used as an acceptable approximation to determine which day-ahead schedule should be used. The battery schedule obtained using the above method is later referred to as the "fixed schedule" and will be used as a benchmark approach to be compared with our proposed method.

7.2.4. Battery Operation with a Flexible Operating Range

Next, an approach that aims at flexibly operating battery storage in real-time operation while taking into account future uncertainties is proposed. Two goals are to be achieved by the proposed method. First, the approach should be able to provide

instructions to the battery of when to charge, discharge, and provide reserves, so that the battery will have enough capability in current as well as future time periods to charge or discharge. Second, the proposed method should provide enough room for adjustments in real-time operation, such that the fast-ramping capability of the battery can be utilized when renewable generation deviates away from its planned production. The proposed method is referred to as the flexible operating range approach and constitutes an improvement to the fixed-schedule approach. In the proposed method, an operating range is determined for the battery in each time period. The fundamental idea of the proposed method is to use the day-ahead UC solution to generate an operating range around the fixed schedule for the battery in real-time operation. The detailed procedure for determining the flexible operating range is described as follows.

Firstly, obtain a fixed schedule for the battery for each post-stage scenario *s* using the procedure described in the previous subsection. This is done prior to the beginning of the simulation for each post-stage scenario. Denote this fixed schedule as $\bar{\boldsymbol{E}}_b^{\boldsymbol{s_0}}$. Secondly, prior to solving the hourly-dispatch problem for each time period, find the day-ahead scenarios that are in the same bucket as the post-stage scenario *s* and denote the corresponding day-ahead battery schedules as $\bar{\boldsymbol{E}}_b^{\boldsymbol{s_1}}, \dots, \bar{\boldsymbol{E}}_b^{\boldsymbol{s_m}}$. Then the upper and lower limit of the flexible operating range are determined as

$$E_{b,t}^{Up} = max \ \{\bar{E}_{b,t}^{s_0}, \bar{E}_{b,t}^{s_1}, \dots, \bar{E}_{b,t}^{s_m}\}, \forall b, t \tag{7.34}$$

$$E_{b,t}^{Low} = min \ \{\bar{E}_{b,t}^{s_0}, \bar{E}_{b,t}^{s_1}, \dots, \bar{E}_{b,t}^{s_m}\}, \forall b, t \tag{7.35}$$

$$E_{b,t}^{Low} - s_{b,t}^{Low} \leq E_{b,t} \leq E_{b,t}^{Up} + s_{b,t}^{Up}, \forall b, t \tag{7.36}$$

where $E_{b,t}^{Low}$ and $E_{b,t}^{Up}$ are the lower and upper bounds for the flexible operating range in time period *t* for the battery. The flexible operating range is formulated as a pair of limits on the SOC. Variables $s_{b,t}^{Low}$ and $s_{b,t}^{Up}$ are the slack variables used to relax the flexible operating range when necessary by incurring a penalty cost. The objective function of the flexible operating range approach is formulated as

Minimize:

$$\sum_g \sum_t \left(C_g\left(P_{gt}\right) + c_g^{NL} u_{gt} + c_g^{SU} v_{gt}\right) + \sum_n \sum_t \; c^{vL} s_{nt}^{L} + \sum_t \left(c^{vR+} s_t^{R+} + c^{vR-} s_t^{R-} + c^{vSP} s_t^{SP} + c^{vOR} s_t^{OR}\right) + \sum_b \sum_t (c_{bt}^{Low} s_{b,t}^{Low} \eta_b^{Out} + c_{bt}^{Up} s_{b,t}^{Up} / \eta_b^{In}). \quad (7.37)$$

In (8.37), the penalty prices c_{bt}^{Low} and c_{bt}^{Up} are both assumed to be the highest marginal costs of all the online slow units. The reason for using such a penalty price is that constraint (7.36) should be relaxed if it can avoid the commitment of an additional fast unit, which typically happens when all the slow units are fully dispatched. As turning on an additional fast unit will incur not only marginal fuel cost but also no-load cost and start-up cost, the commitment of an additional fast unit is expected to be more expensive than using the energy stored in the battery.

7.2.5. Renewable Scenario Generation

Wind power forecasts are affected by several sources of uncertainty that include data and physics modeling. In this study the wind scenarios that account for the errors in the NWP are generated using Gaussian process (GP) regression [101]. The GP is built to estimate the differences between a state-of-the-art NWP forecasts, WRF v3.6 [102], and the observations (corresponding to NOAA Surfrad network). The NWP forecasts are initialized using North American Regional Reanalysis fields. Simulations are started

every day during August 2012 and cover the continental U.S. on a grid of 25x25 Km. A GP is calibrated to reproduce the discrepancy between forecasts and observations at 10m height (mean and variance). Samples from this distribution are extrapolated from 10m to 100m hub height and passed through a standard power curve to obtain the wind scenarios for representative locations [103].

7.2.6. Simulation Process

Firstly, wind scenarios are generated based on the approach outlined above. The scenario reduction approach in [86] is applied to select a predetermined number of scenarios to be used in the day-ahead UC. Secondly, the stochastic UC is solved with the reduced scenario set. The day-ahead solution is then tested against wind scenarios that are not included in the day-ahead UC (i.e. out-of-sample) in the post-stage analysis. In the post-stage, the scenarios tested are provided with equal probabilities. Lastly, the performance of the proposed flexible operating range approach is compared with other benchmark methods.

7.3. Case Study

The case study is conducted using the IEEE RTS 24-bus system [87], [88]. The RTS 24-bus system has 35 branches, 32 generators, and 21 loads. The load in the system is decreased such that the peak load is 2565 MW. Similar to [104], the capacity of line (14-16) is reduced to 350 MW to create congestion in the system. One 50MW, 150MWh battery storage is placed at bus 13, i.e., at the location of one of the two wind farms in the system (the second is at bus 22). The parameters used for the battery are summarized in Table 7.1 [6]. The power rating of the battery is about 2% of the system peak load. In the

day-ahead UC, an initial SOC of 90 MWh is assumed for the battery. It is required in the day-ahead UC that at the end of the day, the SOC of the battery should be the same as the initial SOC. Parameters α_b^S and α_b^R are assumed to be 0.5, which indicates that battery storage should have enough energy to maintain its output for half an hour in order to be qualified to provide spinning and regulation reserves. It is assumed that there are no losses associated to storing the energy.

TABLE 7.1. SUMMARY OF THE PARAMETERS USED FOR BATTERY STORAGE [6]

$\eta_b^{In}, \eta_b^{Out}$	$P_b^{In\_max}, P_b^{Out\_max}$ (MW)	E_b^{Min} (MWh)	E_b^{Max} (MWh)
0.9	50	30	150

Two hundred wind scenarios are generated for day 236 in 2012 and 40 scenarios are selected for the day-ahead UC. In the post-stage analysis, the day-ahead solution is tested against 150 scenarios. The simulation is conducted for wind penetration levels from 15% to 30%, with an increment of 5%. The wind penetration level is defined as the ratio of total daily wind generation (assuming a capacity factor of 100% for wind generators) to the total daily demand. Wind curtailment is allowed when the system cannot accommodate all of the available wind production. The cost of involuntary load shedding is assumed to be 9000 $/MWh, and the cost for violations of reserve requirements is assumed to be 3300 $/MWh. Note that these penalty prices are approximations; since the true cost for correcting security violations is difficult to obtain. If a different set of penalty prices is used, the result of the case study may be different; but the trend of the result is expected to stay the same. In the stochastic UC, the planning horizon is divided into four time blocks, with each to be six hours. In each time block, two buckets are modeled.

Wind scenarios are assigned to each bucket based on their average wind generation in the corresponding time block.

7.3.1. Day-Ahead Scheduling

In the day-ahead scheduling stage, the stochastic UC is solved. Four metrics are used to evaluate the operational benefits of battery storage, which are the expected involuntary load shedding, expected wind curtailment, expected reserve requirement violations and expected total generator commitment hours (ETCH). The metric "expected reserve requirement violations" is the sum of violations of regulation and operating reserves. The metric "expected total generator commitment hours" is computed as

$$ETCH = \sum_{g,t,s} \pi_s u_{gst} \tag{7.38}$$

which is the weighted average of the sum of the commitment hours for all the generators in a day. If this metric is low, it means that thermal units are committed less frequently in the system. The metric ETCH is shown for slow units and fast units separately in Table 7.2.

TABLE 7.2. EXPECTED DAILY SYSTEM RESULTS FOR DAY-AHEAD UNIT COMMITMENT

Wind %	Involuntary Load Shedding (MWh)	Wind Curtailment (MWh)	Reserve Violations (MWh)	ETCH for Slow Units (h)	ETCH for Fast Units (h)
With Battery					
15%	0	4	0	297	144
20%	0	99	0.4	282	140
25%	0	221	0.2	271	137
30%	0	1036	0.1	278	135
No Battery					
15%	0	5	0.3	369	144
20%	0	56	5.4	345	147
25%	0	468	4.1	331	147
30%	0	1460	2.9	311	146

As shown in Table 7.2, with battery storage in the system, the ETCH for both the slow units and fast units are much lower than the cases without battery storage. With battery storage in the system, fewer slow units are needed to address the variability in renewable resources. At the same time, the need for fast units to compensate the uncertainty in renewable generation is also reduced. Meanwhile, more wind generation is dispatched in general when battery storage is included in the system due to reduced wind curtailment. The expected system total operating costs for the cases with and without battery storage are presented in Table 7.3. It is shown in Table 7.3 that the system total operating costs are significantly reduced when battery storage is included. The day-ahead result shows that the battery is a valuable resource in accommodating high levels of renewable resources, especially when considering that the battery in the system is relatively small compared to the system load and wind generation. As renewable penetration levels increase, the value of the flexibility that battery storage provides also increases.

TABLE 7.3. EXPECTED DAILY SYSTEM TOTAL OPERATING COSTS AND COST SAVINGS FOR DAY-AHEAD UNIT COMMITMENT

Wind %	Total Operating Cost with Battery ($)	Total Cost without Battery ($)	Cost Savings ($)	Cost Savings (%)
15%	806,287	930,440	124,154	13.3%
20%	765,307	887,480	122,173	13.8%
25%	733,779	849,963	116,184	13.7%
30%	712,808	827,570	114,762	13.9%

7.3.2. Post-Stage Analysis with the Fixed Operating Schedule

In the post-stage analysis, the fixed-schedule approach, where the battery is not allowed to deviate from the given schedule, is first tested. The same metrics used in the day-ahead scheduling stage are used in the post-stage analysis. The results for the post-

stage analysis are reported in Table 7.4 and Table 7.5. From Table 7.4 and Table 7.5, the same trend as in the day-ahead scheduling stage can be seen, as battery storage can help dispatch more wind generation, decrease the total number of hours that slow and fast units are committed and reduce the system total operating costs. The security violations are also reduced for the cases with the battery in general.

TABLE 7.4. EXPECTED DAILY SYSTEM RESULTS FOR POST-STAGE ANALYSIS

Wind %	Involuntary Load Shedding (MWh)	Wind Curtailment (MWh)	Reserve Violations (MWh)	ETCH for Slow Units (h)	ETCH for Fast Units (h)
With Battery					
15%	0	0	4.0	297	145
20%	0	7	9.0	282	145
25%	0.4	130	9.9	272	140
30%	2.0	741	30.4	279	138
No Battery					
15%	0	0	5.1	367	146
20%	0	8	16.1	339	147
25%	0	124	22.4	321	147
30%	1.3	1009	31.0	313	147

TABLE 7.5. EXPECTED DAILY SYSTEM TOTAL OPERATING COSTS AND COST SAVINGS FOR POST-STAGE ANALYSIS

Wind %	Total Operating Cost with Battery ($)	Total Cost without Battery ($)	Cost Savings ($)	Cost Savings (%)
15%	847,874	971,823	123,948	12.8%
20%	827,291	943,955	116,664	12.4%
25%	808,768	936,378	127,610	13.6%
30%	876,424	957,140	80,715	8.4%

However, comparing the day-ahead results with those for the post-stage analysis, it can be observed that the cost savings by having battery storage in the system are much lower in the post-stage analysis than those in the day-ahead scheduling. The reason is as follows. The post-stage analysis is formulated to approximate the real-time operation,

where each dispatch problem is solved with limited foresight of future information (i.e. one hour look-ahead forecast) using a rolling horizon. When the realized wind generation deviates from the day-ahead forecast, the day-ahead battery schedule may not be able to address the unexpected deviation. Therefore, as shown in Table 7.4, the system reserve violations and the expected generator commitment hours are higher in the post-stage analysis than those in the day-ahead scheduling, especially at higher wind penetration levels. The increase in expected total generator commitment hours is the result of the commitment of additional fast units in the post-stage analysis. As the flexibility of the battery cannot be fully utilized with a fixed-schedule approach, fast units have to be committed to address the intermittency in wind generation. Therefore, as renewable penetration level increases, a more flexible operating approach is needed for battery storage.

It should be noted that this work simplifies the generation scheduling process adopted in industry today, where a short-term UC is usually solved between the day-ahead scheduling stage and the real-time economic dispatch stage [46]. This is also one of the reasons that the benefit provided by the battery is much lower in the post-stage analysis than that in the day-ahead scheduling. During such an intermediate stage, the day-ahead schedule for the battery could be updated based on the short-term wind forecast. Even though such a short-term UC stage is not formulated in this chapter, the two-step framework still captures the main challenges in scheduling battery storage in a system with increased uncertainties: 1) real-time operation has limited look-ahead functionalities and 2) the schedule obtained from a look-ahead scheduling process may not be able to fully utilize the flexibility of battery storage when uncertainties increase.

7.3.3. Cost-Benefit Analysis of the Battery

The cost-benefit analysis of the battery is performed to analyze if the cost savings achieved by using the battery can offset the capital cost of the battery. The cost savings for the 20% wind penetration level are used to analyze the cost-benefit of the battery. The operating cost savings from the day-ahead stage are used in the cost-benefit analysis and it is assumed that all the day-ahead cost savings can be achieved during the real-time operation. The operating cost savings from the six representative days are summarized in Table 7.6. The yearly total cost saving is computed using the cost savings from the six representative days. In Table 7.6, the six representative days are labeled as "D219", "D225", "D230", "D236", "D237", and "D243" respectively.

TABLE 7.6. SUMMARY OF THE OPERATING COST SAVINGS ($K)

D219	D225	D230	D236	D237	D243	Six-Day Sum	Yearly Sum
103.1	110.4	124.3	121.7	122.2	102.4	684.2	41619.4

As battery storage has limited discharging cycles, the impact of discharging on the cycle life of the battery should be taken into account. The expected daily and yearly discharging cycles are computed for the battery and summarized in Table 7.7. The daily expected discharging cycle is computed using (7.39). The depth of discharge of a full discharge is assumed to be 80%, since the battery has a minimum energy capacity of 30 MWh and a maximum capacity of 150 MWh. As shown in (7.39), the daily expected discharging cycle is calculated on an aggregation base. For simplicity, it is assumed in the cost-benefit analysis that the life time of the battery is sensitive only to the total number of equivalent full discharging cycles, i.e. the DOD of each discharging cycle has little to

no effect on the life time of the battery. This is a reasonable assumption for some battery technologies [105], [106]. Since the initial SOC is required to be the same as the final SOC in the day-ahead UC, the number of daily discharging cycles will be the same as the daily charging cycles,

$$Daily\_Discharge\_Cycle = \pi_s \sum_s \frac{\sum_t P_{bst}^{Out}/\eta_b^{Out}}{E_b^{Max} - E_b^{Min}}. \quad (7.39)$$

TABLE 7.7. EXPECTED DISCHARGING CYCLES FOR THE BATTERY (CYCLES)

D219	D225	D230	D236	D237	D243	Six-Day Sum	Yearly Sum
2.1	3.0	2.9	2.3	3.0	2.8	16.2	988.2

Assuming the battery used in the study is a lithium-ion (Li-ion) battery. The life cycle and the capital cost data is obtained from the DOE/EPRI energy storage handbook [6]. In [6], the life cycle for a Li-ion battery is assumed to be $365 \times 15 = 5475$ cycles. Assuming the battery can be fully discharged at most 5475 cycles, the expected life time (number of years) can be calculated using the expected yearly discharging cycle obtained from Table 7.7. The expected life time for the battery is calculated as

$$ExpLifeTime = \frac{5475}{988.2} \approx 5.5 \text{ years}. \quad (7.40)$$

Therefore, using the results obtained from the six representative days, it is expected that the battery can last for about five years. Assume the yearly cost saving obtained by using the battery is the same for the five years, which is 41.6 million dollars per year as shown in Table 7.6. Also assume the discount factor is 6% per year. Following the theory of future value of money, the present value (PV) of the cost saving over the five-year period is computed as

$$PV_{+} = \sum_{t=1}^{5} \frac{yearly\_cost\_saving}{(1+i_d)^t} = 191{,}387{,}407\ (\$). \quad (7.41)$$

With an assumption of 3000 $/kW for the present value of the capital cost of the battery [6], the net present value (NPV) of the battery is computed as

$$NPV = PV_{+} + PV_{-} = 191{,}387{,}407 - 150{,}000{,}000 = 41{,}387{,}407\ (\$). \quad (7.42)$$

This result indicates that by using the battery, the total cost savings over the five-year period is about 41 million dollars in present value.

The result of the cost-benefit analysis shows that battery storage is beneficial to the system when the capital cost and the degradation effect of the battery are considered. However, it should be noted that as the costs for batteries can vary depending on the battery configurations (energy to power ratio) and technologies, the result of the cost-benefit analysis may not apply to all the battery storage technologies. However, with that being said, the study in this section provides an adequate analysis to demonstrate the benefits and the cost-effectiveness of battery storage in systems with renewable resources. As the cost of battery storage is expected to be further reduced in the next five to ten years [96], the benefit of battery storage will be more profound in systems with renewable resources.

7.3.4. Evaluation of the Proposed Flexible Operating Range Approach

To better utilize the flexibility of battery storage in systems with increased renewable resources, the flexible operating range approach is proposed. In this subsection, the performance of the proposed method is compared with the other two benchmark methods. The first benchmark compared is the fixed-schedule approach, which is described in section 7.2.3. The second benchmark is referred to as the no-schedule

approach. In the no-schedule approach, no predetermined schedule is provided for the battery. The dispatch of the battery in each time period is only based on the system conditions in time period t and t+1. The decisions made in time period t do not take into account any forecast information beyond time period t+1. Such an approach is also referred to as a myopic policy [117].

The performance of the three approaches is evaluated using wind scenarios for six days in 2012. For each representative day, the day-ahead stochastic UC is solved and the hourly-dispatch problem is solved with 150 different wind scenarios. The generator commitment schedules for slow units used in the three approaches are the same. The expected operating cost savings in percentage for the proposed approach to the fixed-schedule and the no-schedule methods are presented in Fig. 7.1 and Fig. 7.2 respectively.

As shown in Fig. 7.1, compared to the fixed-schedule benchmark, the proposed approach can provide about 1%-3% cost savings for most of the cases. The cost savings tend to be larger at higher wind penetration levels. This is because as wind penetration level increases, the intermittency in wind generation increases in terms of MWs. Therefore, at higher wind levels, with the proposed approach, the battery can be used to compensate for the deviations in wind generation and provide more cost savings. In Fig. 7.1, there is only one case in which the performance of the proposed method is worse than the fixed-schedule case; the cost difference is about 1%.

Compared with the no-schedule method, the costs savings provided by the proposed method are higher than those of the fixed-schedule. This is consistent with our intuition, since the no-schedule method does not account for future uncertainties when making decisions for the battery in each time period. The high cost savings shown in Fig. 7.2 are

a result of the high security violations in the no-schedule case and the high penalty prices used in the simulation, since the decisions in the no-schedule benchmark are made based on only the current operating condition.

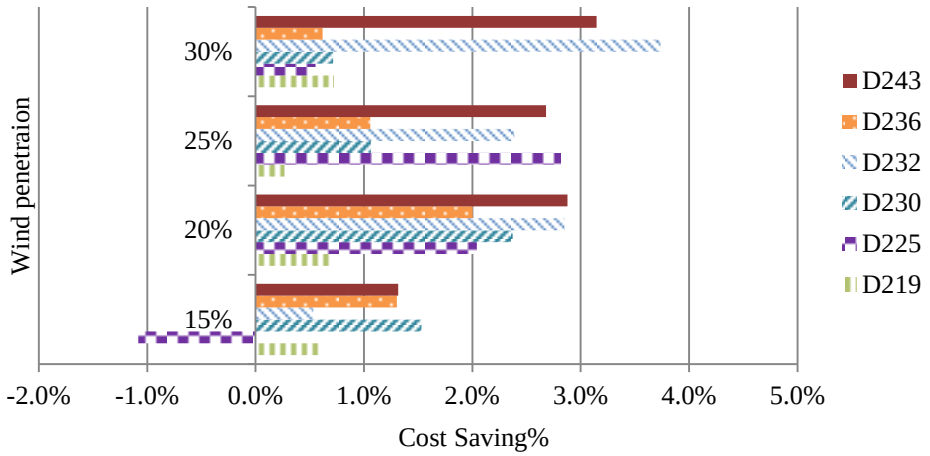

Fig. 7.1. Daily Operating Cost Savings in Percentage of the Proposed Method to the Fix-Schedule Method

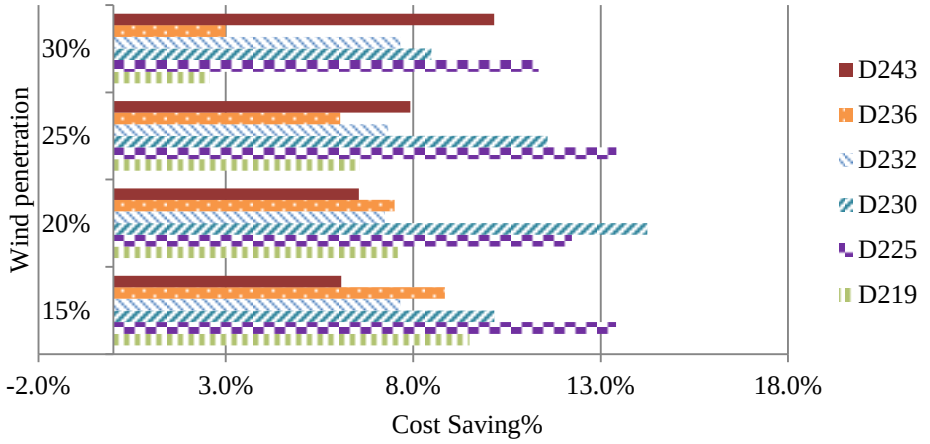

Fig. 7.2. Daily Operating Cost Savings in Percentage of the Proposed Method to the No-Schedule Method

In Fig. 7.3, the result for day 236, scenario 3 with 30% wind penetration level is presented. The dashed lines in Fig. 7.3 represent the operating range determined by the proposed method, which is modeled as a pair of limits on the SOC of the battery. The red solid line (with square markers) shows the schedule obtained using the proposed

approach. The blue solid line (with triangle markers) represents the schedule obtained by the fixed-schedule method. In Fig. 7.3, for the time periods in which the SOC of the battery is outside the limits, such as hour 20, 21 and 22, the SOC limits are relaxed by incurring the penalty cost. For most of the time periods, the battery is operated within the range provided by the proposed method. As the flexible operating range is obtained using the day-ahead schedules, it provides a policy for the battery of when to discharge and charge. As shown in Fig. 7.3, the battery is forced by the limits to increase its SOC level during hours 10 to 13, and to decrease its SOC level during hours 14 to 15. Compared to the fixed-schedule approach, the proposed method can provide an operating range for the battery in each time period rather than a fixed operating point. As renewable generation deviates from forecasts, the battery is allowed to be operated within the operating range, and even possibly exceed the range, to compensate for renewable uncertainties. By using the proposed approach, the flexibility of the battery can be better utilized to address the intermittency in renewable resources.

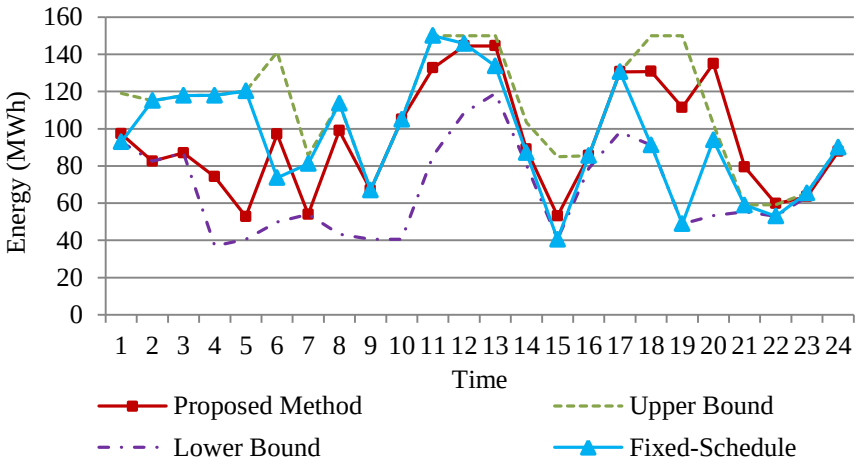

Fig. 7.3. Illustration of the Proposed Flexible Operating Range Approach (Day 236, Scenario 3, 30% Wind Level)

In Fig. 7.4, the energy and ancillary services scheduled for the battery for day 236, scenario 3 with 30% wind level are presented. The solid blue bars in Fig. 7.4 represent the power output of the battery, where positive value indicates discharging and negative value indicates charging. From Fig. 7.4, it can be seen that the battery is scheduled mainly to provide ancillary services, which is because of its fast-ramping capability. Also, it can be noted from Fig. 7.4 that the ancillary services provided by the battery are sometimes larger than its maximum power rating of 50 MW. This result occurs because the battery requires a short transition time between charging and discharging mode. In charging mode, a battery can stop charging and transition to discharging mode to provide up reserves. The maximum up reserve that the battery can provide in this case is $P_{bst}^{In} + P_{bst}^{Out\_max}$. This result suggests that the flexibility of battery storage will be more valuable when providing ancillary services.

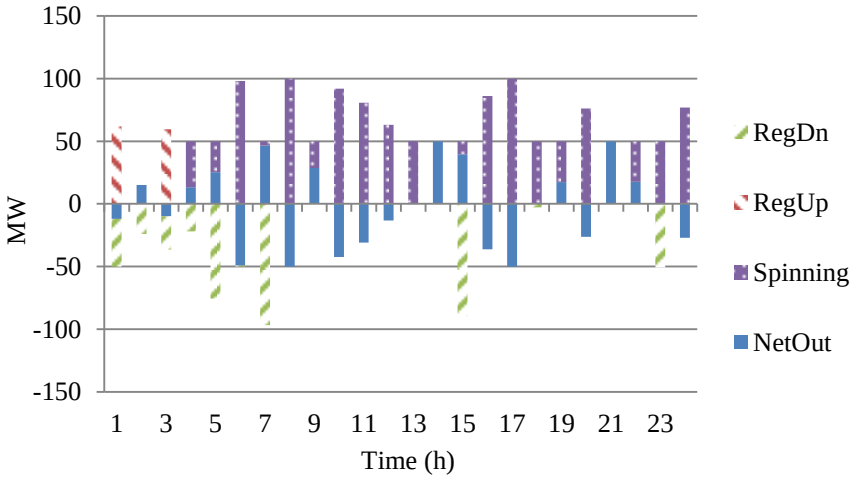

Fig. 7.4. Schedule for the Battery Using the Proposed Method (Day 236, Scenario 3, 30% Wind Level)

7.4. Conclusion

With its energy-shifting and fast-ramping capabilities, battery storage has a great potential to facilitate the integration of high levels of renewable resources. In this chapter,

a two-step framework is used to evaluate the benefits of battery storage in power system operation with renewable resources. In the day-ahead scheduling stage, it is shown that battery storage can decrease the curtailment of wind generation, reduce the commitment of thermal units and reduce system total operating costs. In the post-stage analysis, the challenge with operating battery in real-time is illustrated. The result in the post-stage analysis indicates that using a fixed-schedule approach cannot make full use of the flexibility of the battery. To address this problem, a flexible operating range approach is proposed for battery storage. The case study demonstrates that the proposed approach is more effective in utilizing battery storage in real-time operations compared to the fixed-schedule and no-schedule benchmark methods. The proposed method is able to take advantage of the flexibility of energy storage to address the variability and uncertainty in renewable resources.

CHAPTER 8.

ENHANCED UTILIZATION OF PUMPED HYDRO STORAGE IN POWER SYSTEM OPERATION USING POLICY FUNCTION

In chapter 7, a stochastic programming approach is proposed to improve the operational scheme of energy storage in real-time operation. However, because of the high computational requirement, such stochastic programming models may not be computationally tractable for large-scale power systems. In this chapter, a policy function approach is proposed to enhance the utilization of energy storage with minimal added computational difficulty. The study is focused on the operation of PHS. The performance of the approach is evaluated and compared with other benchmark approaches using the IEEE RTS 24-bus test system.

8.1. Introduction

Driven by the rapid integration of high levels of renewable energy, power system has experienced an increasing need for flexible generation resources. As energy storage technologies have the capability to shift energy across hours and follow fast-ramping signal, it provides an attractive solution to facilitate high levels of renewable resources in power systems. In California, an energy storage mandate has been adopted to require the utility companies to install 1325 MW of energy storage by 2020 [7]. As renewable penetration level increases, energy storage is expected to be more valuable to the grid.

As the most commercially matured large-scale energy storage technology, the PHS has the largest installed capacity around the world, which is about 127 GW by 2010 [8]. Recently, the focus is to use PHS to manage intermittent renewable resources [31]-[36].

While there are growing interests in storage, existing energy management systems (EMS) and market management systems (MMS) do not make full use of storage flexibility; schedules are frequently determined and fixed at a look-ahead time stage with limited real-time adjustments. Such approaches do not fully utilize storage as the actual characteristics of the storage are not fully modeled, across sufficient look-ahead time periods, while also accounting for uncertainties.

For energy storage, the consumption and production capabilities are constrained by its storage level. As real-time operation has limited look-ahead functionality, an inappropriate decision made for the current time period may potentially reduce the consumption and production capabilities in the future. Therefore, a computationally efficient decision tool that optimally schedules PHS across multiple time periods is needed. In this chapter, a policy function based approach is proposed to enhance the utilization of the PHS in real-time operation. The main contributions are: 1) a policy function approach that improves real-time utilization of PHS with minimal added computational difficulty; 2) use classification techniques to construct the policy function; 3) communicate the idea and the philosophy behind policy functions and illustrate the advantages of policy functions.

One interesting thing to note is the similarity between the PHS operation problem and classic inventory control problems. In [108], the two problems are described to have "cosmetic similarities" as both of them try to minimize cost by optimally managing the inventory level. However, the two problems still have fundamental differences. Firstly, the supply and demand in an inventory control problem generally come from different sources and do not directly interact with each other. However, the supply and demand for

the PHS are correlated, as both of them can be seen as net injections to the grid. Secondly, in inventory control problems, an exogenous demand is met by controlling the supply of the product. However, compared to inventory control, the challenge in PHS operation is to *coordinate* the generation schedule and pumping schedule, as the PHS will either produce or consume in each time period.

8.2. Policy Function and the Proposed Framework

In dynamic programming, a policy function is a rule that describes the control action as a function of the state [107]. In this chapter, policy function has a broader meaning, which refers to a policy (function) that returns an action for the given operating condition, taking into account the uncertainty in the system and the future value of the resource. The motivation to use policy function can be illustrated as follows. In this paper, a policy function has a similar meaning, which refers to a policy (function) that returns an action for a given operating condition. The motivation to use a policy function is illustrated as follows. In power systems, reserve requirements are policy functions, which are used to protect the system from contingencies. However, ad-hoc reserve policies do not guarantee the procured reserve is deliverable since congestion is not always acknowledged during the recourse, post-contingency state. Such reserve policies are a proxy for *N*-1 except when contingencies are explicitly represented. Reserve zones are used today for the very purpose to improve reserve deliverability. While stochastic programming models explicitly formulate *N*-1 contingency requirements and implicitly determine the quantity and location of reserves, such models are not scalable for large-scale power systems. The use of proxy reserve requirements is a policy choice to

approximate the function of stochastic programs, while keeping the computational complexity tractable for large-scale power systems.

From the above example, it can be understood that policy functions have three primary merits: 1) return a decision for a given state using knowledge obtained during a prior offline study; 2) use embedded information to overcome model approximations and limitations (in this paper, we enhance a deterministic program with limited look ahead capability to account for uncertainty and future time period operations); 3) shift the computational difficulty to offline stages.

8.2.1. Literature Review

Policy functions have been applied to different powers system applications. In [109], NYISO proposes to use a reserve demand curve to determine the amount of the operating reserve needed in the system. The reserve demand curve can be seen as one form of policy function. It is used in a deterministic model to help the optimization program find a balance between the future needs of the reserve and the cost to hold the reserves, given the uncertainties in the system. In [110] and [111], the amount of the reserve needed in the system is modeled as a function of the load and renewable resources. In [112], a dynamic reserve zone approach is proposed to address the locational aspect of the day-ahead reserve scheduling. The approaches in [110]-[112] derive reserve proxy constraints (policy functions) offline to enhance a deterministic model to account for uncertainty with limited added computational complexity. In [113], a policy function is used to determine the optimal operational strategy of an energy storage facility. In the study, a value function approximation is constructed to capture the future value of the storage. Policy functions are also found in water reservoir management applications [114]-[116].

In [114]-[116], different forms of policy functions are implemented, such as operating rule, value function and adaptive network-based fuzzy inference system.

This work differs from the previous studies from the following aspects. While [113] uses a policy function to determine the operational strategy of energy storage, [113] takes the viewpoint of an independent power producer that maximizes its profits whereas the work in this chapter takes the viewpoint of a central system operator who maximizes social welfare. The prior work does not address many challenges faced by the system operator (e.g., network flow constraints or commitment binary variables), which makes the prior methodology not applicable for this case. In [114]-[116], studies are conducted to determine the optimal water release for water reservoirs. However, the focus of [114]-[116] is on the water flow in river systems, rather than the power flow in transmission systems, which is different from this work.

8.2.2. A Policy Function Approach

An overview of the policy function based approach is illustrated in Fig. 8.1 and consists of three phases. The first phase is the policy function derivation; Monte-Carlo simulations, which are referred to as the stochastic simulation, are performed to obtain PHS schedules for possible wind realizations. The stochastic simulation data is used to construct the policy function. The construction of the policy function is carried out prior to actual operations; it can be constructed offline based on historical data or at a look-ahead stage while relying on forecasts. In the second phase, updated wind forecasts are obtained and then the policy function provides an action. For this chapter, the second phase is after the day-ahead market (DAM) and before the real-time market (RTM), though the timing of such implementation can be revised. The action returned by the

policy function is converted to a set of constraints used in the real-time market model. In the third phase, the real-time market is solved with the additional constraints provided by the policy function.

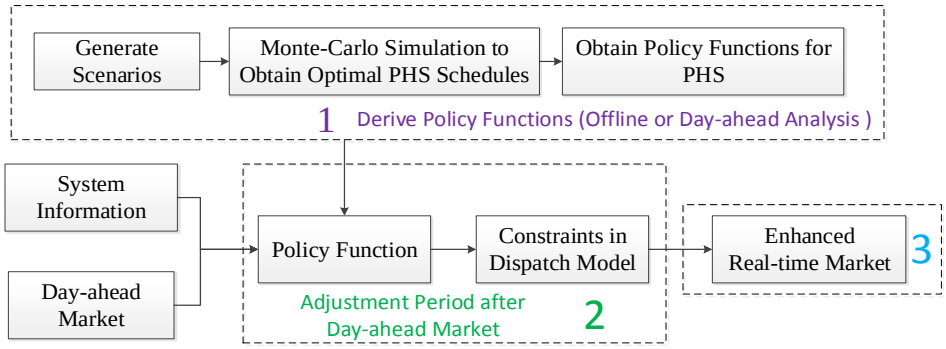

Fig. 8.1. Overview of the Proposed Approach

Policy functions have different forms; the proposed one is a policy function approximation (PFA). For a given state, a PFA returns an action without using the information of future forecast or resorting to any form of imbedded optimization [117]. Different from two-stage stochastic programs, which simultaneously optimize over multiple scenarios, a PFA returns an action for the given state based on the knowledge extracted from prior state-and-action pairs. By using PFA, the computational burden is shifted from real-time to an offline stage. The motivation is, thus, to enhance a deterministic model to perform comparably to a stochastic program without the computational burden. While our focus is on PHS, the same philosophy is generalizable for other power system applications.

8.3. Simulation Setup and Mathematical Formulations

8.3.1. Overview of the Simulation Process

In this work, the PFA is generated using the day-ahead wind forecasts. The simulation process is presented in Fig. 8.2. Wind scenarios are first generated and the day-ahead UC is solved. Stochastic simulations are performed, based on the UC solution, to determine the optimal PHS schedules for different wind scenarios. The data obtained from the stochastic simulation is used to construct the PFA. After the PFA is obtained, the performance of the PFA is evaluated and compared with other benchmark approaches. The mathematical models involved are described in the following subsections.

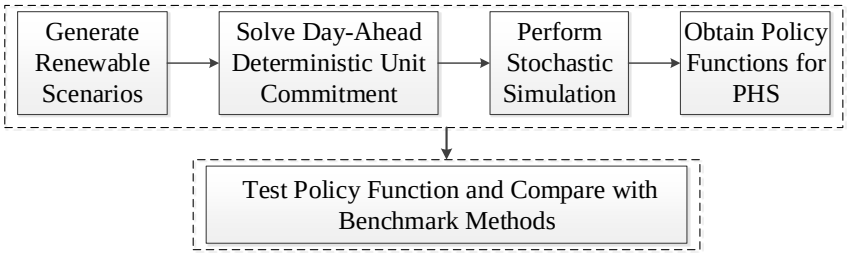

Fig. 8.2. Flowchart for the Simulation Process

8.3.2. Day-Ahead Unit Commitment

The day-ahead UC model is formulated as a mixed integer linear program. The formulation of the UC model is shown in (8.1)-(8.29), where the objective (8.1) is to minimize total system operating costs and violation costs. The violation costs include the costs of involuntary load shedding and the costs of not meeting the reserve requirements. Constraint (8.2) guarantees the power balance at every bus. Constraint (8.3) represents the dc power flow on each line and (8.4) is the line-flow limit constraint. Limits on the power output for each generator are presented in (8.5) and (8.6). The minimum up and down time constraints are shown in (8.7)-(8.9). Constraints (8.10)-(8.12) represent the

ramp rates for regulation, spinning and non-spinning reserves for the thermal units. The hourly ramp rate constraints are shown in (8.13) and (8.14). The model for the PHS is shown in constraints (8.15)-(8.23). The PHS included in the study is assumed to be an adjustable-speed PHS. Constraints (8.15)-(8.18) represent the limits on regulation and spinning reserves provided by the PHS. Constraint (8.19) is the energy balance constraint. The limits on consumption and production for the PHS are presented in (8.20) and (8.21). Constraint (8.22) requires that the PHS can only be in one mode at one time period. Constraint (8.23) formulates the limits on the water reservoir of the PHS. The system-wide regulation and spinning reserve requirements constraints are presented in (8.24)-(8.29). The regulation reserve requirement is set to be 2% of the hourly load. The operating reserve (sum of spinning and non-spinning reserves) is required to be greater or equal to the single largest generator contingency, or the NREL's "3+5" reserve rule [110], whichever is greater. The NREL's "3+5" reserve rule is used to address the uncertainty in renewable resources. The reserve requirements can be violated for a predetermined penalty price.

Minimize:

$$\sum_g \sum_t \left[C_g\left(P_{gt}\right) + c_g^{NL} u_{gt} + c_g^{SU} v_{gt}\right] + \sum_t \left(c^{vR+} s_t^{R+} + c^{vR-} s_t^{R-} + c^{vSP} s_t^{SP} + c^{vOR} s_t^{OR}\right) + \sum_n \sum_t c^{vL} s_{nt}^{L} \quad (8.1)$$

Subject to:

$$\sum_{\forall g(n)} P_{gt} + \sum_{k \in \delta^+(n)} P_{kt} - \sum_{k \in \delta^-(n)} P_{kt} + \sum_{\forall b(n)} (P_{bt}^{Out} - P_{bt}^{In}) = d_{nt} - s_{nt}^{L} - \sum_{\forall w(n)} (P_{wt}^{Wind} - s_{wt}^{W}), \forall n, t \quad (8.2)$$

$$P_{kt} - B_k(\theta_{kt}^{+} - \theta_{kt}^{-}) = 0, \forall k, t \quad (8.3)$$

$$-P_k^{max} \leq P_{kt} \leq P_k^{max}, \forall k, t \quad (8.4)$$

$$P_{gt} + r_{gt}^{R+} + r_{gt}^{S} \leq P_g^{max} u_{gt}, \forall g, t \tag{8.5}$$

$$P_g^{min} u_{gt} \leq P_{gt} - r_{gt}^{R-}, \forall g, t \tag{8.6}$$

$$\sum_{q=t-UT_g+1}^{t} v_{gq} \leq u_{gt}, \ \forall g, t \in \{UT_g, \dots, T\} \tag{8.7}$$

$$\sum_{q=t-DT_g+1}^{t} w_{gq} \leq 1 - u_{gt}, \ \forall g, t \in \{DT_g, \dots, T\} \tag{8.8}$$

$$v_{gt} - w_{gt} = u_{gt} - u_{g,t-1}, \ \forall g, t \tag{8.9}$$

$$r_{gt}^{R+} \leq R_g^{5+} u_{gt}, \ r_{gt}^{R-} \leq R_g^{5-} u_{gt}, \ \forall g, t \tag{8.10}$$

$$r_{gt}^{S} \leq R_g^{10+} u_{gt}, \forall g, t \tag{8.11}$$

$$r_{gt}^{NS} \leq R_g^{NS}(1 - u_{gt}), \forall g, t \tag{8.12}$$

$$P_{g,t} - P_{g,t-1} \leq R_g^{60+} u_{g,t-1} + R_g^{SU} v_{gt}, \forall g, t \tag{8.13}$$

$$P_{g,t-1} - P_{g,t} \leq R_g^{60-} u_{gt} + R_g^{SD} w_{gt}, \forall g, t \tag{8.14}$$

$$r_{bt}^{S} + r_{bt}^{R+} \leq P_b^{Out\_max} - P_{bt}^{Out} + P_{bt}^{In}, \forall b, t \tag{8.15}$$

$$\alpha_b^S r_{bt}^S + \alpha_b^R r_{bt}^{R+} \leq \eta_b^{Out}(E_{bt} - E_b^{Min}), \forall b, t \tag{8.16}$$

$$r_{bt}^{R-} \leq P_b^{In\_max} - P_{bt}^{In} + P_{bt}^{Out}, \forall b, t \tag{8.17}$$

$$\alpha_b^R r_{bt}^{R-} \leq (E_b^{Max} - E_{b,t})/\eta_b^{In}, \forall b, t \tag{8.18}$$

$$E_{bt} = E_{b,t-1} + P_{bt}^{In}\eta_b^{In} - P_{bt}^{Out}/\eta_b^{Out}, \forall b, t \tag{8.19}$$

$$P_b^{Out\_min} z_{bt}^{Out} \leq P_{bst}^{Out} \leq P_b^{Out\_max} z_{bt}^{Out}, \forall b, t \tag{8.20}$$

$$P_b^{In\_min} z_{bt}^{In} \leq P_{bt}^{In} \leq P_b^{In\_max} z_{bt}^{In}, \forall b, t \tag{8.21}$$

$$z_{bt}^{Out} + z_{bt}^{In} \leq 1, \forall b, t \tag{8.22}$$

$$E_b^{Min} \leq E_{bt} \leq E_b^{Max}, \forall b, t \tag{8.23}$$

$$\sum_g r_{gt}^{R+} + \sum_b r_{bt}^{R+} \geq \ 0.02 \sum_n d_{nt} - s_t^{R+}, \forall t \tag{8.24}$$

$$\sum_g r_{gt}^{R-} + \sum_b r_{bt}^{R-} \geq \ 0.02 \sum_n d_{nt} - s_t^{R-}, \forall t \tag{8.25}$$

$$Q_t^{OR} \geq P_{gt} + r_{gt}^S, \forall g, t \tag{8.26}$$

$$Q_t^{OR} \geq 0.03 \sum_n d_{nt} + 0.05 \sum_w P_{wt}^{Wind}, \forall t \tag{8.27}$$

$$\sum_g r_{gt}^S + \sum_b r_{bt}^S + \sum_g r_{gt}^{NS} \geq Q_t^{OR} - s_t^{OR}, \forall t \tag{8.28}$$

$$\sum_g r_{gt}^S + \sum_b r_{bt}^S \geq 0.5 Q_t^{OR} - s_t^{SP}, \forall t \tag{8.29}$$

$$z_{bt}^{In}, z_{bt}^{Out} \in \{0,1\}, \forall b, t \tag{8.30}$$

$$0 \leq v_{gt}, w_{gt} \leq 1, \forall g, t \tag{8.31}$$

8.3.3. Stochastic Simulation and the 24-Hour Dispatch Model

After the day-ahead UC is solved, the stochastic simulation is performed to obtain the optimal schedules of the PHS with different wind scenarios. In the stochastic simulation, each wind scenario is solved using a 24-hour dispatch model. In the 24-hour dispatch model, the 24 time periods are solved together in one optimization program. The primary function of the stochastic simulation is to obtain PHS schedules with different wind scenarios assuming that the entire path of the wind scenario is known. After the stochastic simulation is performed, an optimal PHS schedule is determined for each wind scenario. The obtained PHS schedules are then used to construct the PFA that returns an action for each realized operating condition.

The formulation of the 24-hour dispatch model is presented in (8.32)-(8.34). The commitment statuses for slow units are fixed the same as the ones from the day-ahead solution, as shown in (8.33). Also, as shown in (8.34), a desired dispatch point is provided for each slow unit and the slow units can deviate from the desired dispatch point within the 10-minute ramp rate. In the 24-hour dispatch problem, only the generator contingency reserve requirement is modeled. It is assumed that the reserve scheduled to

address renewable uncertainty is deployed in the 24-hour dispatch problem. The other constraints used in the 24-hour dispatch model are similar to those used in the day-ahead UC model,

Minimize:

$$\sum_g \sum_t \left(C_g\left(P_{gt}\right) + c_g^{NL} u_{gt} + c_g^{SU} v_{gt}\right) + \sum_n \sum_t \; c^{vL} s_{nt}^{L} + \sum_t \left(c^{vR+} s_t^{R+} + c^{vR-} s_t^{R-} + c^{vSP} s_t^{SP} + c^{vOR} s_t^{OR}\right) \quad (8.32)$$

Subject to:

Eqs. (8.2)-(8.26), (8.28)-(8.31)

$$u_{gt} = \overline{u}_{gt}, v_{gt} = \overline{v}_{gt}, w_{gt} = \overline{w}_{gt}, \forall g \in \Omega_{Gs}, t \quad (8.33)$$

$$(\bar{P}_{gt} - R_g^{10-}) u_{gt} \leq P_{gt} \leq (\bar{P}_{gt} + R_g^{10+}) u_{gt}, \forall g \in \Omega_{Gs}, t. \quad (8.34)$$

8.3.4. Performance Evaluation and the Hourly-Dispatch Model

Once the stochastic simulation is performed, the PFA is trained using PHS schedules and the corresponding operating conditions obtained from the stochastic simulation. The construction procedure of the PFA is presented in Section IV. After the PFA is obtained, the performance of the PFA is evaluated and compared with other benchmark approaches. An hourly-dispatch model is formulated for the performance evaluation process. The hourly-dispatch model approximates real-time operations. Each hourly-dispatch problem is solved for two consecutive time periods: the current time period and the look-ahead time period. Each time period represents a one-hour interval. The look-ahead period is included primarily to ensure the feasibility of the problem, since generators are required to ramp to the desired dispatch point in the next time period. The hourly-dispatch problem is solved sequentially with a rolling horizon for 24 hours. The formulation for

the hourly-dispatch problem is similar to that used for the 24-hour dispatch model (8.32)-(8.34), but with the difference that only two time periods are included. For the proposed policy function approach, two additional constraints are needed in the hourly-dispatch problem to model the generation/pumping power range determined by the PFA, which are formulated as,

$$L_{bt}^{Out} - s_{bt}^{Out-} \le P_{bt}^{Out} \le U_{bt}^{Out} + s_{bt}^{Out+}, \forall b, t \tag{8.35}$$

$$L_{bt}^{In} - s_{bt}^{In-} \le P_{bt}^{In} \le U_{bt}^{In} + s_{bt}^{In+}, \forall b, t. \tag{8.36}$$

In constraint (8.35), L_{bt}^{Out} and U_{bt}^{Out} are the proxy lower and upper generation limits determined by the PFA; s_{bt}^{Out-} and s_{bt}^{Out+} are the slack variables used to relax the limits when necessary. Similarly is for constraint (8.36), which represents the limits on the pumping power. If the PFA determines that the PHS should be in generation mode with output power between 40% and 70% of the maximum power rating, then $L_{b,t}^{Out}$ and U_{bt}^{Out} will take on value $0.4P_b^{Out\_max}$ and $0.7P_b^{Out\_max}$ respectively. At the same time, both L_{bt}^{In} and U_{bt}^{In} are set to be zero.

The relaxation of (8.35) and (8.36) are penalized in the objective function. The objective function of the hourly-dispatch problem is formulated as

Minimize:

$$\sum_g \sum_t \left(C_g(P_{gt}) + c_g^{NL} u_{gt} + c_g^{SU} v_{gt}\right) + \sum_n \sum_t c^{vL} s_{nt}^{L} + \sum_t \left(c^{vR+} s_t^{R+} + c^{vR-} s_t^{R-} + c^{vSP} s_t^{SP} + c^{vOR} s_t^{OR}\right) + \sum_b \sum_t \left[c_{bt}^{In}(s_{b,t}^{In-} + s_{b,t}^{In+}) + c_{bt}^{Out}(s_{b,t}^{Out-} + s_{b,t}^{Out+})\right] \tag{8.37}$$

where the last summation term in (8.37) represents the penalty costs of relaxing the proxy limits on the water storage level. The penalty prices c_{bt}^{In} and c_{bt}^{Out} are assumed to be the highest marginal cost of the slow unit that is online in time period *t*. The reason for

choosing such a penalty price is based on the intuition that constraints (8.35) and (8.36) should be relaxed if all the committed slow units are operating at their maximum output levels or do not have any available ramp-up capability; otherwise, a fast unit may have to be committed. The incurred no-load cost and start-up cost for committing an additional fast unit are expected to be more expensive than the future value of water that the PHS has stored.

8.4. Constructing the Policy Function

After the stochastic simulation is performed, the PHS schedules and the corresponding operating conditions are used to construct the PFA. In this section, the design and construction of the PFA are presented.

8.4.1. Policy Function and Classification Technique

The PFA is constructed using classification techniques. Classification is a task to learn a classification model, also called a classifier, which maps each input attribute set to one of the predicted output class labels [120]. Previously, classification techniques have been applied in a number of power system applications. In [121], decision trees are implemented to provide online security assessment and preventive control guidelines. In [122], support vector machine classification algorithm is used to improve the performance of the smart relays. In [123], neural network based classification models are used for nonintrusive harmonic source identification.

With the data obtained from the stochastic simulation, a classifier is built to identify patterns between the operating conditions and the corresponding PHS actions. The classifier is used to determine the PHS decisions for the given operating states. The

structure of the classifier is shown in Fig. 8.3. The input of the classifier is a set of attributes describing the operating conditions at the end of time period *t*-1 and the output is the generation/pumping power range for the PHS in period *t*. In real-time operations, before solving the dispatch problem for each time period *t*, the attributes describing the operating condition are first computed. Then the attributes are provided as the input of the classifier and an operational decision for the PHS in time period *t* is returned by the classifier.

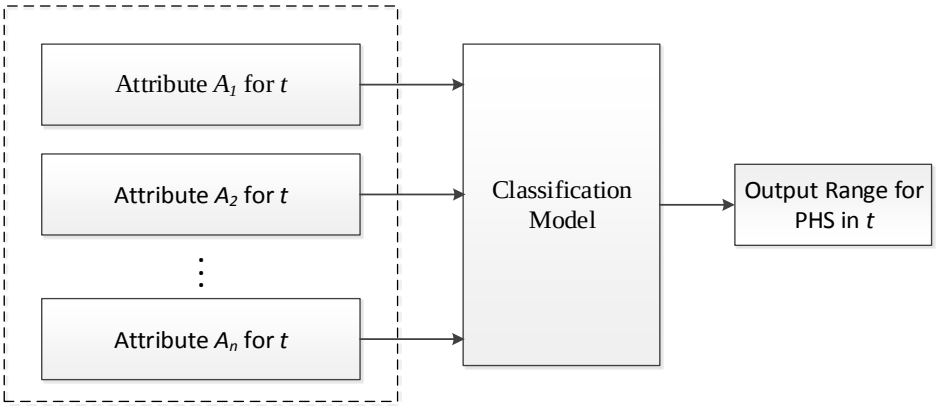

Fig. 8.3. Illustration of the Classifier

8.4.2. Attributes Design and Selection

As aforementioned, the input of the classifier is a set of attributes describing the system operating condition. To construct an effective policy function, the attributes should be an adequate and comprehensive description of the system operating condition. The process to design attributes has been referred to as "feature engineering" in data mining and machine learning societies [124], [125]. In this chapter, the attributes are designed using domain knowledge.

Initially, about 27 attributes are designed. To improve the performance of the classifier, redundant and unnecessary attributes should be removed from the attribute set.

In other words, attributes that are most descriptive and effective should be selected from the initial attribute set. To perform a thorough and comprehensive attribute selection, feature selection techniques [126], [127] can be implemented. However, as a large number of feature selection methods are heuristics, they do not guarantee a global optimum. Also, as suggested in [126], domain knowledge is an important tool in feature selection. As the attribute set is relative small in the case study, domain knowledge and a trial-and-error phase are used to construct the "ad hoc" attribute set. After the attributes are designed, they are grouped into different sets using domain knowledge and the performance for each set is compared. After the comparison, the attribute set that has the best performance is used in the case study. The detailed feature selection process is not presented.

The attributes selected to be used in the case study are in Table 8.1. Attribute A_1 is the coming operating time period. Attributes A_2 and A_3 are the differences between system-wide available capacity to provide up (down) reserve and system up (down) reserve requirements. Attributes A_4 and A_5 are the ratios of the system-wide available capacity to provide up (down) reserve to system up (down) reserve requirement. Attributes A_2 to A_5 describe the relationship between the system reserve requirement and the capability of thermal units to provide reserves. These four attributes provide a measurement of the residual reserve requirement in the system. It indicates how much reserve should be provided by PHS. Attributes A_6 and A_7 are the available pumping and generation capacity of the PHS. Attribute A_8 is the water storage level of the PHS at the end of time period *t*-1. Attributes A_6 to A_8 describe the operating state and the available ramping capability of PHS in each hour. Attributes A_9 and A_{10} are the number of online generators

in time period *t*-1 and *t*. Attribute A_{11} is the difference between the number of committed generators in time periods *t* and *t*-1. Attributes A_{12} is the difference between the water reservoir level in the current scenario and that in the day-ahead UC solution. Attribute $A_{13}$is the difference between the system-wide available capacity to provide up reserves in the current scenario and that in day-ahead solution. Variables R^{+}_{sys} and $R^{+}_{sys\_DA}$ are the system-wide available capacity to provide up reserves in the current scenario and day-ahead solution respectively. Variables R^{+}_{sys} and $R^{+}_{sys\_DA}$ are computed using (8.38). Attribute A_{14} is the Euclidian distance between the current wind scenario and the scenario used in the day-ahead UC. Attributes A_{12} to A_{14} measure the similarity between the system state in the current scenario and that in the day-ahead solution. The motivation of including attributes A_{12} to A_{14} is to use the day-ahead UC solution as a reference case to describe the relative state of the operating condition. The inclusion of attributes A_{12} to A_{14} adds another dimension of information to the input attribute set to describe the pattern between the operating condition and the optimal PHS action. In Table 8.1, variables R^{+}_{sys} and R^{-}_{sys} represent the system-wide available capacity to provide up and down reserves, which are computed as:

$$R^{+}_{sys} = min(\sum_g P^{max}_g u_{gt} - \sum_n d_{nt} + \sum_w P^{Wind}_{wt}, \sum_g (R^{10+}_g + R^{5+}_g) u_{gt}) \quad (8.38)$$

$$R^{-}_{sys} = min(\sum_n d_{nt} - \sum_w P^{Wind}_{wt} - \sum_g P^{min}_g u_{gt}, \sum_g R^{-}_g u_{gt}). \quad (8.39)$$

TABLE 8.1. SUMMARY OF THE INPUT ATTRIBUTES TO THE CLASSIFIER

Attribute	Formulation to Calculate the Attribute
A_1	t
A_2	$R_{sys}^{+} - (Q_t^{R+} + Q_t^{OR})$
A_3	$R_{sys}^{-} - Q_t^{R-}$
A_4	$R_{sys}^{+}/(Q_t^{R+} + Q_t^{OR})$
A_5	R_{sys}^{-}/Q_t^{R-}
A_6	$\text{Min}((E_b^{Min} - E_{b,t-1})/\eta_b^{In}, P_b^{In\_max})$
A_7	$\text{Min}((E_{b,t-1} - E_b^{Min})\eta_b^{Out}, P_b^{Out\_max})$
A_8	$E_{b,t-1}$
A_9	$\sum_g u_{gt}$
A_{10}	$\sum_g u_{g,t-1}$
A_{11}	$\sum_g u_{gt} - \sum_g u_{g,t-1}$
A_{12}	$E_{b,t-1} - \bar{E}_{b,t-1}$
A_{13}	$R_{sys}^{+} - R_{sys\_DA}^{+}$
A_{14}	$\|\boldsymbol{\omega_s} - \boldsymbol{\omega_0}\|_2$

8.4.3. Classification Algorithm

The random forest classification algorithm is used to construct the classifier. Random forest is a class of ensemble classifiers, which combines the prediction outcomes of multiple base learners. Each base learner is a classifier itself. For an ensemble classifier such as random forest, it consists of a large number of base learners and utilizes a "voting" scheme to determine the final prediction outcome. In a random forest classifier, a base learner is a decision tree classifier. A decision tree is a tree-like structure. At each internal node, a testing rule is applied to the attributes. The outcome of the test is represented by a branch in the tree. At each terminal node, a class label is assigned. The obtained classification rules are implied by the paths from root to each terminal node.

In a random forest classifier, each decision tree is built differently by using different data records or different attributes. As decision trees are constructed using heuristic methods, they cannot guarantee a global optimum. Therefore, by introducing a little bit

randomness, the idea of random forest classifier is to overcome the drawbacks of decision trees by growing a large number of decision tress differently and using a voting scheme to determine the class label. To classify an unseen data record, the data record is run down all the trees in the random forest classifier and each tree makes a prediction. A "voting" scheme is then used to determine the class label for the data record. Further discussion on random forests and their algorithms can be found in [120] and [129]. In this chapter, the random forest algorithm with random attribute selection is used.

8.4.4. Hierarchical Classification

In this work, the classification problem involved is a multi-class problem, in which the data records have more than two class labels. To address the multi-class classification problem, a hierarchical classification approach is used [128]. The hierarchical classification is a "decomposition" type of approach. Instead of using one model to determine the operational mode and the corresponding generation/pumping power at the same time, the hierarchical classification divides the classification task into two separate steps. An illustration of the hierarchical classification problem in this work is presented in Fig. 8.4.

As shown in Fig. 8.4, the involved problem consists of two levels of classifications. At the first level, one classifier is constructed to determine the operational mode of the PHS in time period *t*. This classifier is built using all the data records obtained from the stochastic simulation. At the second level, two classifiers are built for the generation and pumping mode respectively. Given the operation mode determined at the first level, the classifiers at the second level are used to determine the generation/pumping power range

for the PHS. The classifiers at the second level are built using only the data records that belong to the corresponding operation mode.

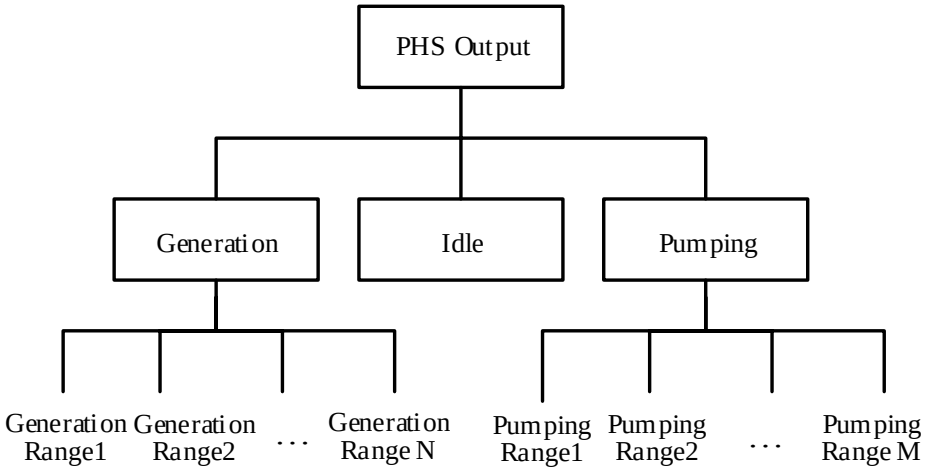

Fig. 8.4. Illustration of the Hierarchical Class Structure

8.5. Case Study and Result Analysis

8.5.1. Data Preparation

One primary reason to adopt a policy function approach is that it is a scalable approach in *comparison* to other approaches that add more complexity (many variables and constraints) in order to capture future time periods and uncertainties. For this work, we have chosen to use the IEEE RTS 24-bus model [87]. While this is a small test case, we are able to demonstrate the substantial benefits that occur by using policy functions. More importantly, the real-time computational complexity for our approach is primarily driven by the number of large energy storage resources and not as much by the size of the system. For that reason, we expect to find similar results (savings with limited added computational complexity) for large systems with limited sizeable storage resources, which is common today, and we leave the problem of policy functions for large systems with many storage resources to future work.

The case study is conducted using the IEEE RTS 24-bus system [87]. The 24-bus system has 35 branches, 32 generators, and 21 loads. The total generation capacity in the system is 3402 MW and the system peak load is 2850 MW. The capacity of line (14-16) is reduced to 350 MW to create congestion in the system. One 100 MW, 500MWh adjustable-speed PHS unit is located at bus 22. The parameters used for the PHS are summarized in Table 8.2. Following the assumptions in [119], the minimum generation level for the PHS is assumed to be 30% of the maximum generation capacity. In the day-ahead UC, an initial water storage level of 200 MWh is assumed for the PHS. It is required in the day-ahead UC and 24-hour dispatch model that at the end of the day, the water storage level should be the same as the initial value. Parameters α_b^S and α_b^R are assumed to be 0.5, with the assumption that a unit should be able to maintain its output for half an hour in order to be qualified to provide spinning and regulation reserves. It is assumed that there are no losses associated to storing the energy (e.g., water evaporation). The cost for correcting involuntary load shedding is assumed to be 3000 $/MWh and the cost for correcting violations in reserve requirement is assumed to be 1100 $/MWh. Note that these penalty prices are approximations; since the true cost for correcting security violations is difficult to obtain. If a different set of penalty prices is used, the result of the case study may be different; but the trend of the result is expected to stay the same.

TABLE 8.2. SUMMARY OF THE PARAMETERS FOR THE PHS

$\eta_b^{In}, \eta_b^{Out}$	$P_b^{Out\_min}$ (MW)	$P_b^{In\_min}$ (MW)	$P_b^{Out\_max}, P_b^{In\_max}$ (MW)	E_b^{Min} (MWh)	E_b^{Max} (MWh)
0.85	30	70	100	100	500

8.5.2. Modeling of Renewable Scenarios

Following the methodology described in [104], an autoregressive integrated moving average (ARIMA) model based approach [131] is used to generate the wind scenarios. Historical wind data for March 2006 is taken from NREL Wind Integration Datasets [78]. The wind data for three different areas are obtained to produce three different wind farms in the system (bus #13, #21 and #23). The original 10-mintue wind speed data is aggregated to produce the hourly wind speed. The hourly ARIMA models are fit for each wind farm and the corresponding scenarios are generated. To reflect the typical day-ahead wind forecast errors reported in [80] and [81], the generated wind scenarios are normalized with the average such that the resulted forecast error is about 20%. The mean value of the time series is used in the day-ahead UC.

Using the approach described above, 700 wind scenarios are generated. Four hundred scenarios are randomly selected to be used in the stochastic simulation. The other 300 scenarios are used to evaluate the performance of the PFA based approach. The case study is conducted for 25% wind penetration level. The wind penetration level is defined as the ratio of total daily wind generation to the total daily demand. Wind curtailment is allowed when the system cannot accommodate all of the available wind production.

8.5.3. Construction of the Classifiers

As the output of the classifier is a class label, which is a categorical value, the generation/pumping power capacity of the PHS are discretized. In Table 8.3, the discretized intervals for generation/pumping power capacity are summarized. When designing a discretization strategy, tradeoffs between various factors should be considered. On one hand, if the power range of PHS is discretized into very fine intervals,

the computational requirement may be increased for the stochastic simulation; since enough data records should be generated so that there are training data falling into each discretized segment. Meanwhile, small discretized intervals also limit the operation of PHS to small ranges of adjustment. As a result, a large number of class labels are created, which could negatively impact the performance of the classifier as well as the operation of PHS. Since when the number of class labels is too large, it will be difficult for the classifier to accurately classify each class, especially when the classes are imbalanced (which means some classes have a large number of instances, while the others only have a few instances). On the other hand, a coarse discretization may cause the policy function to be uninformative, which can degrade the functionality of the policy function. To find a balance between the aforementioned tradeoffs, the power capacity of the PHS is discretized into medium intervals in the case study. This discretization results in three class labels in the generation mode and two class labels in the pumping mode. Please note that the distribution of data records has also been taken into account, as the generation capacity of the PHS is not discretized evenly.

TABLE 8.3. DISCRETIZATION OF THE GENERATION/PUMPING CAPACITY OF THE PHS

Generation Mode		Pumping Mode	
Range 1	0 - 40%	Range 1	0 - 85%
Range 2	40% - 70%	Range 2	85% - 100%
Range 3	70% - 100%	–	–

For the proposed approach, three classifiers are built. One classifier is built to predict the PHS operation mode; the other two are built to determine the generation and pumping power range respectively. The parameters used for the three classifiers are selected using

the grid-search approach [130]. The construction of the classifier is implemented using the Scikit-learn machine learning package [132].

Besides random forests, other classification algorithms, such as support vector machine (SVM) and boosting, can also be used to construct the classifier. In the case study, we have compared the performance of random forest to that of a SVM classifier and a boosting classifier [120]. The parameters for the classifiers are determined using the grid search approach. The comparison result shows that the three classifiers have close performance and the random forest classifier performs slightly better than the others. The detailed comparison result is not presented.

As most of the classification algorithms are heuristic which do not guarantee a global optimum, one classification algorithm may not always out-perform the others. To implement the policy function approach, historical data can be used to identify the classifier with the best performance for the given system. To further improve the proposed approach, the classifier can be updated on a monthly or seasonal basis. In this chapter, we focus on using random forest classifier to demonstrate the effectiveness of the policy function approach.

8.5.4. Performance Evaluation of the Proposed PFA

The policy function's performance is compared with four benchmarks. The same unit commitment schedule, the one determined by the day-ahead UC, is used for all five approaches tested. For the policy function approach, the operation of PHS is *not* coordinated with day-ahead decisions. The operation of PHS is only determined by the policy function and the hourly-dispatch model.

The first benchmark is referred to as the fixed-schedule approach, where the PHS schedule determined by the day-ahead UC is used for the PHS. In this benchmark, a water storage target is provided for the PHS in each time period and the PHS is not allowed to deviate. This benchmark represents a common approach to operate PHS units. The second benchmark is referred to as the fixed-mode approach. For this benchmark, the PHS operation mode in each time period is fixed to the same as the one from the day-ahead UC solution. No constraint is enforced on the generation/pumping power of the PHS. Both the fixed-schedule and fixed-mode approaches are solved using the hourly-dispatch model.

The third benchmark is referred to as the perfect foresight benchmark. In the perfect foresight benchmark, all the time periods are solved together using the 24-hour dispatch model. The perfect foresight benchmark represents an ideal case where all the uncertainties can be perfectly forecasted. The solution obtained by the perfect foresight benchmark is the best lower bound solution of the wind scenarios tested.

The fourth benchmark is a two-stage stochastic program formulated with 200 wind scenarios. The 200 wind scenarios are selected from the wind scenarios used in the stochastic simulation using backward scenario reduction [133]. The operation mode of the PHS is modeled as a *first-stage* decision. Meanwhile, one scenario is selected from the 200 scenarios as the base scenario in the stochastic program using backward reduction. In each time period, the output/input power of the PHS in each scenario can only deviate from the one in the base scenario within a certain range in the stochastic program. The generation power of the PHS in each scenario can deviate from the generation power in the base scenario by $0.4P_b^{Out\_max}$.The pumping power in each

scenario can deviate from the one in the base scenario by $0.2P_b^{In\_max}$. After the stochastic program is solved, in the hourly-dispatch problem, the generation/pumping power obtained from the base scenario is provided as the desired dispatch point for the PHS. In each time period, the PHS can deviate from the desired dispatch point by $0.4P_b^{Out\_max}$ if in generation mode and $0.2P_b^{In\_max}$ if in pumping mode. The duality gap of the stochastic program is set to be 0.5%.

The expected results for each approach are summarized in Table 8.4. Please note that only the results from the performance evaluation phase are reported in Table 8.4. The day-ahead UC cost, which is the same for all the approaches compared, is not presented. Three metrics are reported, which are the expected system total operating cost, expected violation cost, and expected wind curtailment. The metric expected violation cost is the sum of the involuntary load shedding cost and the reserve requirement violation cost.

TABLE 8.4. EXPECTED DAILY SYSTEM RESULTS FOR EACH METHOD

Method	System Total Operating Cost ($K)	Violation Cost ($K)	Wind Curtailment (MWh)
PFA	761.9	34.3	337
Fixed-Schedule	778.5	50.2	303
Fixed-Mode	777.5	48.8	299
Stochastic Program	771.2	44.8	377
Perfect Foresight	757.3	51.1	264

As shown in Table 8.4, the PFA approach reduces the violation costs and the system total costs compared to the fixed-schedule and fixed-mode approaches; the operating cost savings are reported in Table 8.5. Compared to the fixed-schedule and the fixed-mode benchmarks, the proposed PFA provides cost savings at 2.1% and 2.0% respectively. In Fig. 8.6, a statistical description of total system costs for the PFA, the fixed-schedule and

the fixed-mode approaches is presented. Compared to the fixed-schedule and the fixed-mode benchmarks, the standard deviation as well as the maximum value are lower in the cases of the proposed PFA approach.

TABLE 8.5. OPERATING COST SAVINGS BY USING THE PROPOSED APPROACH

Method	Relative Savings to Fixed Schedule (%)	Relative Savings to Fixed Mode (%)
PFA	2.1%	2.0%

TABLE 8.6. STATISTICAL DESCRIPTION OF SYSTEM TOTAL OPERATING COSTS FOR EACH METHOD ($)

	PFA	Fixed-Schedule	Fixed-Mode
Standard Deviation	124864	147753	148708
Minimum	601614	600865	600865
Maximum	1349057	1489466	1511773

One critical result in Table 8.4 is that the total system cost for the PFA approach is lower than that of the stochastic program. It is known that the stochastic program will provide the best solution if all scenarios are modeled and the problem is solved to optimality. However, for scalability purposes, a stochastic program also requires simplifications, e.g., scenario reduction techniques. The PFA approach should not be expected to always beat a stochastic program approach but this result is crucial; well-designed offline approaches can compete with stochastic programs without the added computational burden and without the market pricing complications.

In Fig. 8.5, the relative performance of the PFA approach is presented and it is computed as

$$RltP_i\% = \frac{C_{ref} - C_{PFA}}{C_{ref} - C_{bm}} \cdot 100\%. \tag{8.40}$$

In (8.40), C_{PFA} is the expected total cost for the PFA approach, C_{bm} is the expected total cost for the benchmark approach, and C_{ref} is the expected total cost for the reference approach. In Fig. 8.5, the solid blue bar represents the relative performance with fixed schedule as the reference and dotted red bar shows the relative performance of the PFA approach with fixed mode as the reference. The perfect foresight approach is used as the benchmark in Fig. 8.5.

The relative performance measures the percentage of the cost savings due to the PFA approach. This metric also indicates how close the PFA performance is to that of the perfect foresight benchmark. A relative performance of 100% means that the PFA approach has the same performance as the idealistic benchmark approach. As shown in Fig. 8.5, compared to the perfect foresight approach, the relative performance of the proposed approach is about 78% and 77% with respect to the reference approaches of fixed schedule and fixed mode. This observation indicates that the PFA approach achieves the majority of the potential savings that an ideal, perfect foresight approach could achieve. Such results demonstrate that the proposed PFA approach effectively improves the utilization of the PHS in real-time operations.

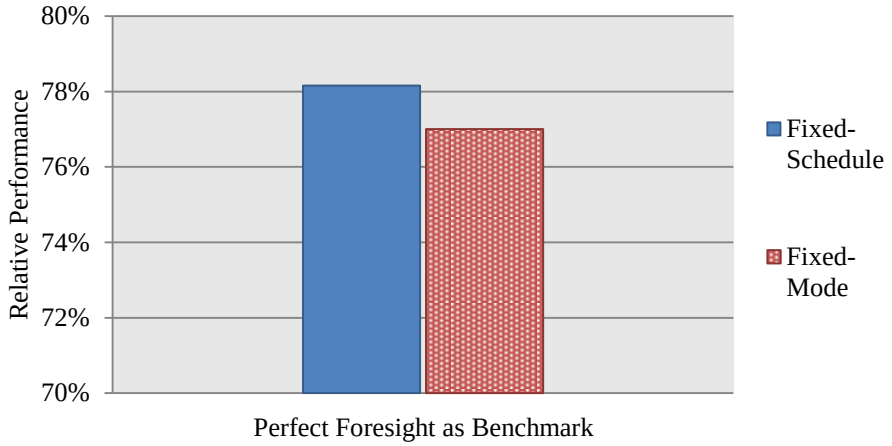

Fig. 8.5. Relative Performance of the Policy Function Approach to the Fixed-Schedule and the Fixed-Mode Approaches

The average solution times to solve one hourly-dispatch problem for the fixed-schedule benchmark and the PFA approach are in Table 8.7. In Table 8.7, the preprocessing time for the fixed-schedule represents the time to build the optimization model. For the PFA approach, the preprocessing time also includes the time to calculate the input attributes and the time to run the policy function (the classifier) to obtain the action for the PHS. The solver time in Table 8.7 represents the execution time for the solver to solve the optimization program and reflects the time to solve the real-time model.

TABLE 8.7. AVERAGE SOLUTION TIME FOR THE FIXED-SCHEDULE AND THE POLICY FUNCTION APPROACH (SECOND)

	Fixed-Schedule	PFA
Preprocessing Time	0.02	0.22
Solver Time	0.12	0.16
Total Time	0.14	0.38

As shown in Table 8.7, the solver times are very close for the two approaches, which are 0.12 s and 0.16 s respectively. For the preprocessing time, it is larger for the PFA

approach than that for the fixed-schedule approach. For the PFA approach, the bulk part of the preprocessing time is spent on running the classifier to get the operation decision for the PHS. It should be noted that the computational time to run the classifier only depends on the type of the classifier, the number of data records used during the training stage, and the number of attributes used, but not the size of the system. Even for a large-scale power system, the preprocessing time of the PFA approach will not increase much if the same classification strategy described in this chapter is used. Therefore, the preprocessing time is not a concern regarding the impact on the real-time market solution time as the solver time is the time that would indicate the impact on the real-time market. The results in Fig. 8.5 and Table 8.7 demonstrate that the PFA approach can enhance the utilization of PHS with minimal added computational difficulty.

To further evaluate the performance of the proposed approach, the policy function approach is tested on wind scenarios for four additional days. The relative performance and the relative cost saving metrics are presented in Fig. 8.6 and Fig. 8.7 respectively. As shown in Fig. 8.6, the policy function approach has relative performance of about 60% to 80%, which indicates that the policy function approach can achieve the bulk part of the cost savings that a perfect foresight approach can obtain. Compared to the fixed-schedule and the fixed-mode benchmarks, the relative cost savings obtained by using the policy function approach are about 1% to 4%.

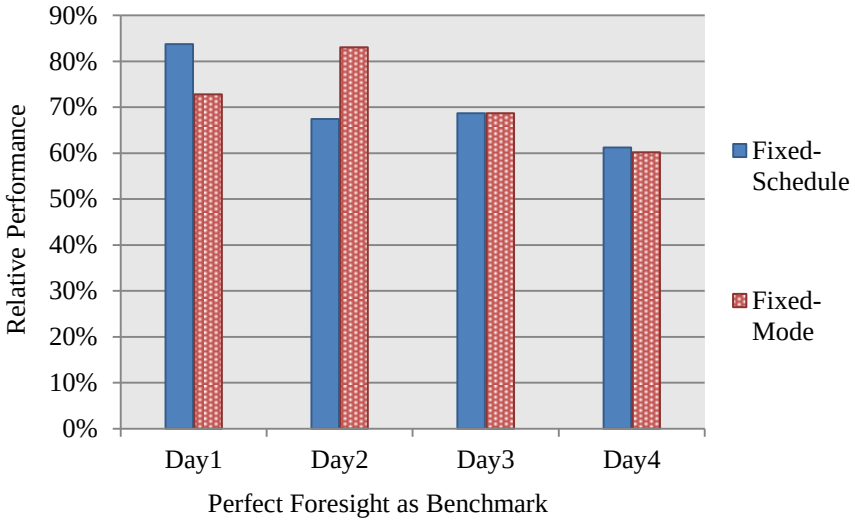

Fig. 8.6. Relative Performance of the Policy Function Approach

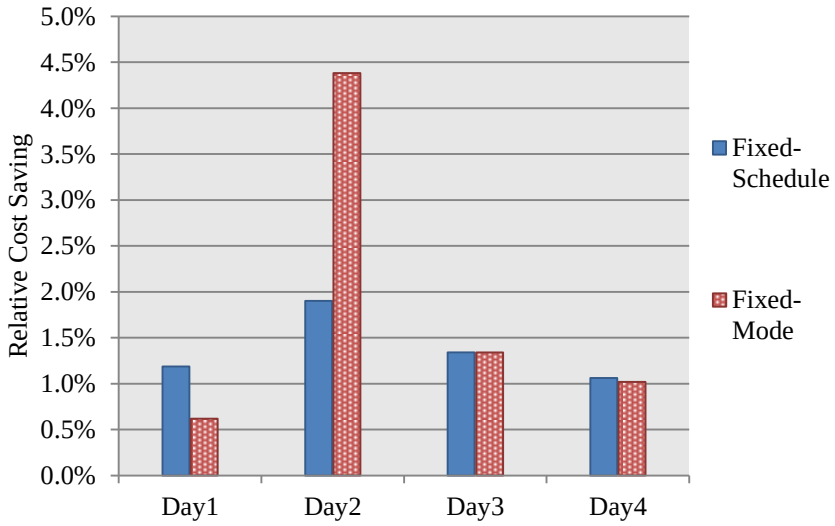

Fig. 8.7. Relative Cost Savings by Using the Proposed Approach

Finally, while the savings may not seem very high, note that this is for a single PHS facility; it is critical to acknowledge that the proposed approach have saved roughly 60% to 80% of the overall potential cost savings. For systems with more PHS resources, the overall impact will be more profound.

8.6. Conclusion

While energy storage provides a solution to manage intermittent renewable resources, the flexibility of energy storage is not being fully utilized by existing EMS and MMS. In this chapter, a policy function is used to enhance the utilization of PHS in settings with a limited look-ahead horizon. The proposed policy function is shown to have performance close to an ideal perfect foresight benchmark. Meanwhile, the proposed approach has minimal added computational difficulty for the real-time market. While the policy function is developed for PHS operation, the same philosophy can be generalized to other power-system applications. As stochastic programming is still not computationally tractable for large-scale power systems today, policy functions provide attractive solutions to achieve the main benefits of a two-stage stochastic program. Furthermore, while the chosen policy function is used to improve a deterministic program, they can also be used to enhance two-stage stochastic programs, both in terms of savings and computational time.

The primary merits of policy functions can be summarized as: 1) return a decision for a given state using knowledge obtained during prior offline studies; 2) overcome model limitations using embedded information; 3) shift the computational difficulty to offline stages.

CHAPTER 9.

CONCLUSIONS AND FUTURE WORK

9.1. Conclusions

The fast expansion of renewable resources has introduced new challenges to power system operations. To mitigate the renewable uncertainty and maintain the reliability of the system, there has been a growing need for flexible resources in the system. Under such circumstances, recent interests have been focused on energy storage technologies. In the dissertation, the attractiveness of bulk energy storage in transmission systems with increasing penetrations of renewable resources is analyzed. Enhanced models are developed to improve the utilization of energy storage in systems with renewable resources. The contributions of this dissertation are summarized as follows.

Firstly, a two-stage stochastic UC model is designed to study the attractiveness of conventional generators and energy storage with increasing renewable penetrations. To capture the impact of high penetration levels of renewable resources in the system, a ramping cost term is included in the stochastic UC to represent the costs incurred during the ramping processes. The result shows that, as renewable penetration level increases, the role of conventional generators will transition to primarily providing backup generation and ancillary services. As a result, conventional generators will have increased average costs and decreased utilization rates. As wind can be considered as a “free” energy with zero fuel cost, the increase of wind generation will decrease the LMPs in the system. Therefore, conventional generators will have decreased profits on top of increased average costs. With energy storage in the system, the expected hourly average costs for conventional generators are decreased, while the expected capacity factors and

the hourly utilization rates for conventional generators are improved. The use of energy storage also decreases the number of committed generators in the system. The above results indicate that the use of energy storage improves the efficiencies for conventional generators. With energy storage in the system, the total system operating costs are also reduced compared to the cases without energy storage.

Secondly, the benefit of using energy storage to provide ancillary services is evaluated. A two-step approach is developed to analyze the performance of flywheels in providing regulation services from two aspects: the regulation reserve capacity flywheels can provide and the accuracy in following dispatch signals. In the two-step approach, the first-step represents the reserve scheduling while the second-step simulates the deployment of reserves. The result shows that flywheels are an effective resource to provide regulation services and mitigate renewable uncertainties.

Thirdly, a two-step framework is proposed in chapter 7 to evaluate the benefits of battery storage in system with renewable resources and investigate the challenges associated with the real-time operation of energy storage. The two-step framework captures the day-ahead generation scheduling stage as well as the real-time dispatch stage. The case study result shows that battery storage can improve the system reliability and reduce the system total operating costs by about 8% to 13%. The result also demonstrates that the cost saving obtained by using the battery is able to justify the investment cost of the battery. In chapter 7, the challenges with operating battery storage across multiple time periods are also studied. In the case study, it is shown that using a traditional fixed-schedule approach cannot fully utilize the flexibility of energy storage. To improve the operational scheme for energy storage, a flexible operating range

approach is developed. The flexible operating range approach utilizes the solution from the day-ahead stochastic UC to construct an operating policy for battery storage in real-time. By using the proposed approach, battery storage can provide more operating cost savings compared to the cases where a fixed-schedule approach and a no-schedule approach (a myopic policy) is used.

Lastly, in chapter 8, a policy function approach is designed to enhance the utilization of PHS in systems with renewable resources. While the flexible operating range approach developed in chapter 7 is shown to be effective, such an approach may not be computationally tractable for large-scale power systems; since it requires solving a stochastic UC model which is computationally challenging. However, for the policy function approach, all the computationally extensive tasks are shifted from real-time to an offline analysis stage. During the offline analysis stage, data mining techniques are utilized to determine the patterns between the system operating conditions and the optimal decisions for the PHS. Once the data mining model is constructed, it is used in real-time to determine dispatch decisions for energy storage for each realized operating condition. Compared to a traditional approach where the schedule of the PHS is determined and fixed at a prior look-ahead stage, the policy function approach can improve the utilization of the PHS by efficiently operate the PHS across multiple time horizons. Meanwhile, the policy function approach has been shown to have minimal added computational complexity to the real-time market, which makes it a scalable approach for large-scale power systems especially when compared to two-stage stochastic programs.

9.2. Future Work

In the dissertation, energy storage has been demonstrated to be an attractive solution to facilitate the integration of high levels of renewable resources. In order to further exploit and harness the potentials of energy storage, the following work is suggested for future study.

9.2.1. Improved Policy Function Approach for PHS

In chapter 8, the policy function based approach is tested on the IEEE 24-bus testbed system. Future work may extend the policy function approach to a large-scale power system. For large-scale power systems, zonal partition techniques can be applied to divide the system into multiple zones based on the congestion information, the locations of PHS units or the locations of wind farms. The policy function approach can then be applied on a locational basis and the attributes for the classifier can be computed using the information within each zone.

Another direction is to develop policy functions for multi PHS cases, where multiple PHS units are included in the system. Under multi-entity situations, the policy function should be able to enhance the utilization of each PHS facility, while taking into account the interactions between the PHS facilities. The policy functions constructed for each PHS entity should be coordinated such that they do not provide conflicting decisions with each other.

There is also potential to incorporate the policy functions into a market structure. In deregulated energy markets, PHS entities are market participants who bid into the market and try to maximize their profits. To utilize policy functions in such market settings, the existing market structure may need to be redesigned such that enough incentive is

provided for the PHS units to follow the dispatch instructions provided by the system operator.

9.2.2. Generalization of Policy Functions to Other Power-system Applications

The future work described in this section is in collaboration with Nikita Ghanshyam Singhal.

While the policy function is used to enhance PHS real-time operation in this dissertation, the same design philosophy can be generalized to other power-system applications. One potential application is to improve the reserve scheduling and allocation in the day-ahead market.

The primary motivation to utilize the policy function approach is to efficiently and effectively allocate reserves in the system such that reserves are deliverable after uncertainties are realized in the system, while maintaining the computational tractability of the UC model. A flowchart of the policy function approach is illustrated in Fig. 9.1. The proposed framework is primarily designed to improve the deliverability of reserves in the post-contingency state for systems with renewable resources.

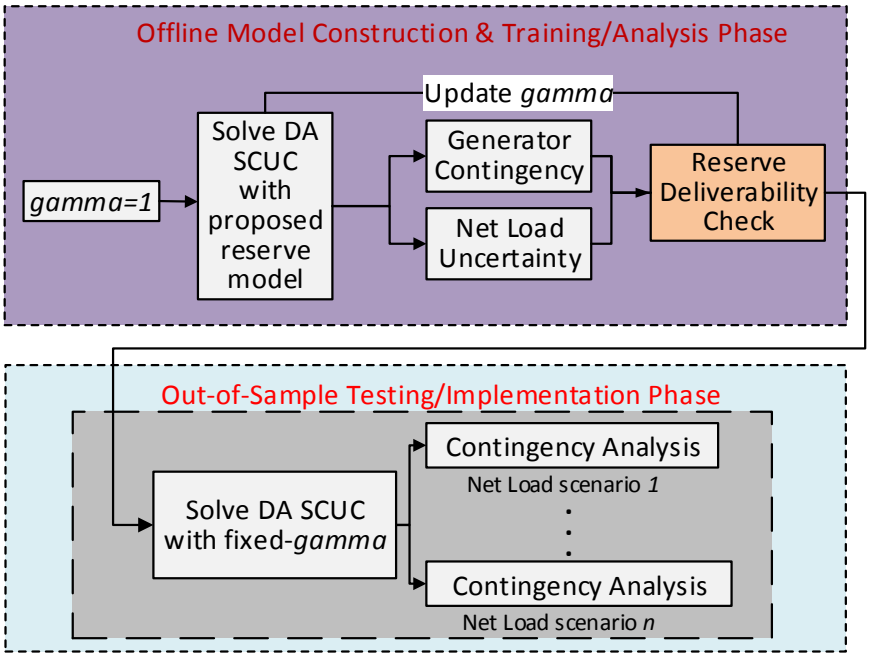

Fig. 9.1. Flowchart for the Policy Function Approach

The proposed policy function approach consists of two phases. The first phase is the offline training phase, where a security-constraint unit commitment (SCUC) is solved to determine the quantity and location of reserves for each generator contingency. Once the SCUC is solved, a reserve deliverability check is performed to analyze the deliverability of the reserve that each generator provides in each scenario. During the deliverability check, two types of uncertainties are considered. One type of uncertainties is the single generator failures in the system; the other is the renewable uncertainties, which is modeled as net load uncertainties in this work. After the deliverability check, a reserve activation factor Γ_{gt}^{c} is updated to reflect the deliverability of the reserve provided by each generator in each scenario. The reserve activation factor Γ_{gt}^{c} measures the portion of the reserve that is potentially deliverable when the reserve is deployed in the post-contingency state. The activation factor will be later used in the second phase.

The second phase of the proposed approach is the testing phase, which represents the day-ahead scheduling stage. In the testing phase, a SCUC is solved with a responsive reserve model. The parameter Γ_{gt}^{c} obtained from the offline training phase is utilized in the SCUC to allocate reserves (provided by each generator) at prime locations (i.e., the locations that deliver reserves in the post-contingency state) in the system. After the SCUC is solved, contingency analysis is conducted to test the SCUC solution against generator contingencies combined with net load scenarios in the system.

The formulation of the responsive reserve model used in the testing phase SCUC is shown in (9.1)-(9.3). Constraint (9.1) represents the contingency-based reserve requirement. By incorporating the reserve activation factor Γ_{gt}^{c} into the reserve model, constraint (9.1) identifies a response set for each contingency event. The response sets defined by (9.1) identify the locations where reserves are potentially deliverable as well as the required quantity of reserves in each contingency event. Constraint (9.2) models the post-contingency line flows on critical transmission paths. In constraint (9.2), P_{kt} represents the pre-contingency power flow on line *k*. The second component, $P_{ct}PTDF_{n(c),k}$, represents the change in the power flow on line *k* due to the loss of generator *c*. The third component $\sum_g PTDF_{n(g),k}\Gamma_{gt}^{c}r_{gt}^{c}$ represents the change in the line flow due to reserve deployment on line *k* in contingency *c*. Constraint (9.2) explicitly models the post-contingency line flows and aims to ensure reserves can be potentially transferred through critical transmission paths in the post-contingency state. Constraint (9.3) indicates that Γ_{gt}^{c} is a parameter taking on values between zero and one,

$$\sum_g \Gamma_{gt}^{c} r_{gt} \geq P_{ct} + r_{ct}, \forall c, t \tag{9.1}$$

$$-P_k^{MaxC} \leq P_{kt} - P_{ct}PTDF_{n(c),k} + \sum_g PTDF_{n(g),k}\Gamma_{gt}^c r_{gt} \leq P_k^{MaxC},$$

$$\forall c \in \Omega_{G^c}, l \in \Omega_{L^c}, t \tag{9.2}$$

$$\Gamma_{gt}^c \in [0,1], \forall c, g, t. \tag{9.3}$$

In the testing stage, the post-contingency line flow constraints (9.2) are only formulated for the critical transmission paths and the critical generators in the system, which is to strike a balance between model accuracy and model complexity. The critical transmission paths can be identified using historical data or stochastic simulations that utilize forecast information. The primary motivation to use a policy function approach is to improve the allocation of reserves so that reserves are deliverable through critical transmission lines post-contingency, while keeping the added computational difficulty to the day-ahead market at minimum.

REFERENCES

[1]. Global Wind Energy Council, "Global wind report: annual market update 2012," April 2013. [Online]. Available: http://www.gwec.net/wp-content/uploads/2012/06/Annual_report_2012_LowRes.pdf

[2]. World Wind Energy Association, "2012 Half-year report," [Online]. Available: http://www.wwindea.org/webimages/Half-year_report_2012.pdf

[3]. Earth Techling, "Global solar, wind energy growth continues to impress," [Online]. Available: http://www.earthtechling.com/2013/07/global-solar-wind-energy-growth-continues-to-impress/

[4]. U.S Energy Information Administration, "Most states have renewable portfolio standards," February 2012. [Online]. Available: http://www.eia.gov/todayinenergy/detail.cfm?id=4850

[5]. Energy Information Administration, "Existing capacity by energy source," 2011. [Online]. Available: http://www.eia.gov/electricity/annual/html/epa_04_03.html

[6]. Sandia National Laboratories, "DOE/EPRI 2013 electricity storage handbook in collaboration with NRECA," July 2013. [Online]. Available: http://energy.gov/oe/downloads/doeepri-2013-electricity-storage-handbook-collaboration-nreca-july-2013

[7]. California Public Utilities Commission, "CPUC sets energy storage goals for utilities," [Online]. Avalable: http://docs.cpuc.ca.gov/PublishedDocs/Published/G000/M079/K171/79171502.PDF

[8]. Electric Power Research Institute, "Electricity energy storage technology options – a white paper primer on applications, costs, and benefits," December 2010. [Online]. Available: http://www.electricitystorage.org/images/uploads/static_content/technology/resources/ESA_TR_5_11_EPRIStorageReport_Rastler.pdf

[9]. U.S. Department of Energy, "Grid energy storage," December 2013. [Online]. Available: http://energy.gov/sites/prod/files/2013/12/f5/Grid%20Energy%20Storage%20December%202013.pdf

[10]. National Hydropower Association, "Challenges and opportunities for new pumped storage development," July 2012. [Online]. Available: http://www.hydro.org/wp-content/uploads/2012/07/NHA_PumpedStorage_071212b1.pdf

[11]. Electric Power Research Institute, “MISO energy storage study phase 1 report,” Power Delivery & Utilization, February 2012. [Online]. Available: http://www.epri.com/abstracts/Pages/ProductAbstract.aspx?ProductId=000000000001024489

[12]. General Commission, “Texas dispatchable wind 1, LLC,” [Online]. Available: http://www.generalcompression.com/index.php/tdw1

[13]. Xtreme Power, “About Xtreme Power,” [Online]. Available: http://www.xtremepower.com/about

[14]. Alaska Energy Wiki, “Lead-acid batteries,” [Online]. Available: http://energy-alaska.wikidot.com/lead-acid-batteries

[15]. Torresol Energy, “Gemasolar,” [Online]. Available: http://www.torresolenergy.com/TORRESOL/gemasolar-plant/en

[16]. Torresol Energy, “Central-tower technology,” [Online]. Available: http://www.torresolenergy.com/TORRESOL/central-tower-technology/en

[17]. Ivanpah Solar Electric Generating System, “Ivanpah project facts,” [Online]. Available: http://ivanpahsolar.com/about

[18]. Highveiw Power Storage, “Cryo energy storage,” [Online]. Available: http://highview-power.com/wordpress/?page_id=8

[19]. Electricity Storage Association, “Liquid air energy storage (LAES),” [Online]. Available: http://www.electricitystorage.org/technology/tech_archive/laes_storage

[20]. Institution of Mechanical Engineers, “Electricity storage,” [Online]. Available: https://custom.cvent.com/2A4273FF30A84F3194B3668DAC5E13F7/files/d6022910c6e749d5908ef249bfa2d640.pdf

[21]. J. A. Suul, “Variable speed pumped storage hydropower plants for integration of wind power in isolated power system,” [Online]. Available: http://www.intechopen.com/books/renewable-energy/variable-speed-pumped-storage-hydropower-plants-for-integration-of-wind-power-in-isolated-power-syst

[22]. Department of Energy, “DOE global energy storage database,” [Online]. Available: http://www.energystorageexchange.org/

[23]. J. R. Ruggiero and G. T. Heydt, “Making the economic case for bulk energy storage in electric power systems,” *North American Power Symposium*, September 2013.

[24]. R. J. Kerestes, G. F. Reed, and A. R. Sparacino, “Economic analysis of grid level energy storage for the application of load leveling,” *IEEE Power and Energy Society General Meeting*, July 2012.

[25]. K. Aoki, M. Itch, T. Satoh, K. Nara, and M. Kanezashi, “Optimal long-term unit commitment in large scale systems including fuel constrained thermal and pumped-

storage hydro," *IEEE Transactions on Power Systems*, vol. 4, no. 3, pp. 1065-1063, August 1989.

[26]. G. H. McDaniel and A. F. Garbrielle, "Dispatching pumped storage hydro," *IEEE Transactions on Apparatus and Systems*, vol. PAS-85, no. 5, pp. 465- 461, May 1966.

[27]. B. Y. Lee, Y. M. Park, and K. Y. Lee, "Optimal generation planning for a thermal system with pumped-storage based on analytical production costing model," *IEEE Transactions on Power Systems*, vol. PWRS-2, no. 2, pp. 486-493, May 1987.

[28]. R. Siohansi, P. Denholm, T. Jenkin, and J. Weiss, "Estimating the value of electricity storage in PJM: arbitrage and some welfare effects," *Energy Economics*, vol. 32, no. 2, pp. 269-277, March 2009.

[29]. R. Walawalkar, J. Apt, and R. Mancini, "Economics of electric energy storage for energy arbitrage and regulation in New York," *Energy Policy*, vol. 35, no. 4, pp. 2558-2568, November 2006.

[30]. G. Gross, A. Dominguez-Garcia, C. Singh, and A. Sprintson, "Integration of storage devices into power systems with renewable energy sources," PSERC Publication 12-24, September 2012. [Online]. Avalable: http://www.pserc.wisc.edu/documents/publications/reports/2012_reports/gross_pserc_project_s-40_2012.pdf

[31]. A. Tuohy and M. O'Malley, "Impact of pumped storage on power system with increasing wind penetration," *IEEE Power & Energy Society General Meeting*, July 2009.

[32]. J. P. Deane, E. J. Mckeogh, and B. P. O. Gallachoir, "Derivation of intertemporal targets for large hydro energy storage with stochastic optimization," *IEEE Transactions on Power Systems*, vol. 28, no. 3, pp. 2147-2155, August 2013.

[33]. M. E. Khodayar and M. Shahidehpour, "Enhancing the dispatchability of variable wind generation by coordination with pumped-storage hydro units in stochastic power systems," *IEEE Transactions on Power Systems*, vol. 28, no. 3, pp. 2808-2818, August 2013.

[34]. D. J. Swider, "Compressed air energy storage in an electricity system with significant wind power generation," *IEEE Transactions on Energy Conversion*, vol. 22, no. 1, pp. 95-102, March 2007.

[35]. H. Daneshi, A. K. Srivastava, and A. Daneshi, "Generation scheduling with integration of wind power and compressed air energy storage," *IEEE Transmission and Distribution Conference and Exposition*, April 2010.

[36]. H. Daneshi and A. K. Srivatava, "Impact of battery energy storage on power system with high wind penetration," *IEEE Transmission and Distribution Conference and Exposition*, May 2012.

[37]. J. Garcia-Gonzalez, R. M. R. Muela, L. M. Santos, and A. M. Gonzalez, "Stochastic joint optimization of wind generation and pumped-storage units in an electric-

ity market," *IEEE Transactions on Power Systems*, vol. 23, no. 2, pp. 460-469, May 2008.

[38]. A. A. Thatte, F. Zhang, and L. Xie, "Coordination of wind farms and flywheels for energy balancing and frequency regulation," *IEEE Power and Energy Society General Meeting*, July 2011.

[39]. L. Xie, A. A. Thatte, and Y. Gu, "Multi-time-scale modeling and analysis of energy storage in power system operations," *IEEE Energytech*, May 2011.

[40]. N. Lu, M. R. Weimar, Y. V. Makarov, F. J. Rudolph, S. N. Murthy, and J. Arseneaux, "An evaluation of the flywheel potential for providing regulation services in California," *IEEE Power and Energy Society General Meeting*, July 2010.

[41]. B. Lu and M. Shahidehpour, "Short-term scheduling of battery in a grid-connected PV/battery system," *IEEE Transactions on Power Systems*, vol. 29, no. 2, pp. 1053-1051, May 2005.

[42]. M. E. Khodayar, L. Abreu, and M. Shahidephour, "Transmission-constrained intra-hour coordination of wind and pumped-storage hydro units," *IET Generation, Transmission and Distribution*, vol. 7, no. 7, pp. 755-765, October 2012

[43]. Z. Hu, F. Zhang, and B. Li, "Transmission expansion planning considering the deployment of energy storage systems," *IEEE Power and Energy Society General Meeting*, July 2012.

[44]. K. A. Zach and H. Auer, "Bulk energy storage versus transmission grid investments: bringing flexibility into future electricity systems with high penetration of variable RES-electricity," *9th International Conference on the European Energy Market (EEM)*, May 2012.

[45]. ISO New England, "Unit commitment and dispatch," May 2013. [Online]. Available: http://www.iso-ne.com/support/training/courses/wem201/01_wem201_unit_commitment_and_dispatch_coutu.pdf

[46]. California ISO, "Market process," [Online]. Available: http://www.caiso.com/market/Pages/MarketProcesses.aspx

[47]. H. B. Gooi, D. P. Mendes, K. R. W. Bell, and D. S. Kirschen, "Optimal scheduling of spinning reserve," *IEEE Transactions on Power Systems*, vol. 14, no. 4, pp. 1485-1483, November 1999.

[48]. R. Billinton and R. Karki, "Capacity reserve assessment using system well-being analysis," *IEEE Transactions on Power Systems*, vol. 14, no. 2, pp. 433-438, May 1999.

[49]. M. Foruhi-Firuzabad and R. Billinton, "Generating unit commitment using a reliability framework," *Proceedings of IEEE Canadian Conference on Electrical and Computer Engineering*, May 1999.

[50]. S. J. Wang, S. M. Shahidehpour, D. S. Kirschen, S. Mokhtari, and G. D. Irisarri, "Short-term generation scheduling with transmission and environmental constraints using an augmented Lagrangian relaxation," *IEEE Transactions on Power Systems*, vol. 10, no. 3, pp. 1294-1301, August 1995.

[51]. D. Bertsimas, E. Litvinov, X. A. Sun, J. Zhao, and T. Zheng, "Adaptive robust optimization for the security constrained unit commitment problem," *IEEE Transactions on Power Systems*, vol. 28, no. 1, pp. 52-53, February 2013.

[52]. S. Takriti, J. R. Birge, and E. Long, "A stochastic model for the unit commitment problem," *IEEE Transactions on Power Systems*, vol. 11, no. 3, pp. 1497-1507, August 1996.

[53]. A. Shapiro and A. Philpott, "A tutorial on stochastic programming," [Online]. Available: http://stoprog.org/stoprog/SPTutorial/TutorialSP.pdf

[54]. S. A. H. Bahreyni, M. A. Khorsand, and S. Jadid, "A stochastic unit commitment in power systems with high penetration of smart grid technologies," *2nd Iranian Conference on Smart Grid (ICSG)*, May 2012.

[55]. J. M. Arroyo and F. Galiana, "Energy and reserve pricing in security and network-constrained electricity markets," *IEEE Transactions on Power Systems*, vol. 20, no. 2, pp. 634-643, May 2005.

[56]. T. Alvey, D. Goodwin, X. Ma,D. Streiffert, and D. Sun, "A security-constrained bid-clearing system for the New Zealand wholesale electricity market," *IEEE Transactions on Power Systems*, vol. 13, no. 2, pp. 340–346, May 1998.

[57]. J. Wang, M. Shahidehpour, and Z. Li, "Security-constrained unit commitment with volatile wind power generation," *IEEE Transactions on Power Systems*, vol. 23, no. 3, pp. 1319-1327, August 2008.

[58]. A. Botterud, et al., "Wind power trading under uncertainty in LMP markets," *IEEE Transactions on Power Systems*, vol. 27, no. 2, pp. 894-893, May 2012.

[59]. J. M. Morales, A. J. Conejo, and J. Perez-Ruiz, "Economic valuation of reserves in power systems with high penetration of wind power," *IEEE Transactions on Power Systems*, vol. 24, no. 2, pp. 900-910, May 2009.

[60]. F. Bouffard, F. D. Galiana, and A. J. Conejo, "Market-clearing with stochastic security- Part I: formulation," *IEEE Transactions on Power Systems*, vol. 20, no. 4, pp. 1818-1826, November 2005.

[61]. F. Bouffard, F. D. Galiana, and A. J. Conejo, "Market-clearing with stochastic security- Part II: case studies," *IEEE Transactions on Power Systems*, vol. 20, no. 4, pp. 1827-1835, November 2005.

[62]. F. Bouffard and F. D. Galiana, "Stochastic security for operations planning with significant wind power generation," *IEEE Power and Energy Society General Meeting*, July 2008.

[63]. A. Papavasiliou, S. S. Oren, and R. P. O'Neil, "Reserve requirements for wind power integration: a scenario-based stochastic programming framework," *IEEE Transactions on Power Systems*, vol. 26, no. 4, pp. 2197-2206, November 2011.

[64]. N. Gröwe-Kuska, H. Heitsch, and W. Römisch, "Scenario reduction and scenario tree construction for power management problems," in *Proc. IEEEE Power Tech Conf.*, June 2003.

[65]. H. Heitsch and W. Romisch, "Scenario tree reduction for multistage stochastic programs," *Computational Management Science*, vol. 6, no. 2, pp. 117-133, May 2009.

[66]. S. M. Ryan, R. J.-B. Wets, D. L. Woodruff, C. Silva-Monroy, and J.-P Watson, "Toward scalable, parallel progressive hedging for stochastic unit commitment," University of California Davis. [Online]. Available: http://www.math.ucdavis.edu/~rjbw/mypage/Stochastic_Optimization_files/FGRWWW12_ph_1.pdf

[67]. A. J. Wood, B. F. Wollenberg, and G. B. Sheble, *Power generation, operation, and control*, 3rd edition. New Jersey: Wiley-Interscience, 2013.

[68]. T. Das, V. Krishnan, Y. G, and J. D. McCalley, "Compressed air energy storage: state space modeling and performance analysis," *IEEE Power and Energy Society General Meeting*, July 2011.

[69]. K. W. Hedman, M. C. Ferris, R. P. O'Neil, E. B. Fisher, and S. S. Oren, "Co-optimization of generation unit commitment and transmission switching with N-1 reliability," *IEEE Transactions on Power Systems*, vol. 25, no. 2, pp. 1052-1064, May 2010.

[70]. California ISO, "Spinning reserve and non-spinning reserve," Settlements Guide, January 2006. [Online]. Available: http://www.caiso.com/docs/2003/09/08/2003090815135425649.pdf

[71]. D. Milborrow, "Forecasting for scheduled delivery," *Windpower Monthly*, December 2003. [Online]. Available: http://www.windpowermonthly.com/article/955591/forecasting-scheduled-delivery

[72]. L. Landberg, "A mathematical look at a physical power prediction model," *Wind Energy*, vol. 1, no. 1, pp. 23-28, September 1998.

[73]. J. S. Hong, "Evaluation of the high-resolution model forecasts over the Taiwan are during GIMEX," *Weather and Forecasting*, vol. 18, no. 5, pp. 836-846, October 2003.

[74]. W. Guoyang, X. Yang, and W. Shasha, "Discussion about short-term forecast of wind speed on wind farm," *Jilin Electric Power*, vol. 181, no. 5, pp. 21-24, 2005.

[75]. K. Lalarukh and Z. Yasmin, "Time series models to simulate and forecast hourly averaged wind speed in Quetta, Pakistan," *Solar Energy*, vol. 61, no. 1, pp. 23-32, July 1997.

[76]. I. G. Damousis, and P. Dokopoulos, "A fuzzy expert system for the forecasting of wind speed and power generation in wind farms", *IEEE Power Engineering Society International Conference on Power Industry Computer Applications*, pp. 63-69, May 2001.

[77]. C. W. Potter and M. Negnevitsky, "Very short-term wind forecasting for Tasmanian power generation", *IEEE Transactions on Power Systems*, vol. 21, no. 2, pp. 965-972, May 2006.

[78]. National Renewable Energy Laboratory, "Wind integration datasets," 2006. [Online]. Available: http://www.nrel.gov/electricity/transmission/wind_integration_dataset.html

[79]. CAISO, "Integration of renewable resources: technical appendices for California ISO renewable integration studies – version 1," October 2010. [Online]. Available: http://www.caiso.com/282d/282d85c9391b0.pdf

[80]. W. Yuan-Kang and H. Jing-Shan, "A literature review of wind forecasting technology in the world," *IEEE Power Tech*, pp. 504 -509, July 2007.

[81]. S. Fan, J. R. Liao, R. Yokoyama, L. Chen, and W. Lee, "Forecasting the wind generation using a two-stage network based on meteorological information," *IEEE Transactions on Energy Conversion*, vol. 24, no. 2, pp. 474-482, June 2009.

[82]. G. M. Masters, *Renewable and Efficient Electric Power Systems*. New York, NY, USA: Wiley Interscience, 2004.

[83]. K. Dietrich, J. M. Latorre, L. Olmos, A. Ramos, and I. J. Perez-Arriaga, "Stochastic unit commitment considering uncertain wind production in an isolated system," in *Proc. 4th Conference on Energy Economics and Technology*, April 2009.

[84]. H. Bludzuweit, J. A. Dom ńguez-Navarro, and A. Llombart, "Statistical analysis of wind power forecast error," *IEEE Transactions on Power Systems*, vol. 23, no. 3, pp. 983–991, Aug. 2008.

[85]. F. Bouffard and F. D. Galiana, "Stochastic security for operations planning with significant power generation," *IEEE Transactions on Power System*, vol. 23, no. 2, pp. 306–316, May 2008.

[86]. J. Dupacov á, N. Gr öwe-Kuska, and W. Römisch, "Scenario reduction in stochastic programming: An approach using probability metrics," *Mathematical Program, series A*, vol. 3, pp. 493–511, February 2003.

[87]. University of Washington, "Power systems test case archive," Department of Electrical Engineering, 1999. [Online]. Available: http://www.ee.washington.edu/research/pstca/rts/pg tcarts.htm

[88]. J. M. S. Pinheiro, C. R. R. Dornellas, M. Th. Schilling, A. C. G. Melo, and J. C. O. Mello, "Probing the new IEEE reliability test system (RTS-96): HL-II Assessment," *IEEE Transactions on Power Systems*, vol. 13, no. 1, pp. 171-176, February 1998.

[89]. T. Aigner and T. Gjengedal, "Detailed wind power production in northern Europe," in *Proc. Renewable Energy Conf. 2010*, Yokohoma, July 2010.

[90]. Sandia National Laboratories, "Characteristics and technologies for long- vs. short-term energy storage: A study by the DOE energy storage systems program," SAND2001-0765, March 2001. [Online]. Available: http://prod.sandia.gov/techlib/access-control.cgi/2001/010765.pdf

[91]. Sandia National Laboratories, "Energy storage system cost update: A study by the DOE energy storage systems program," SAND2011-2730, April 2011. [Online]. Available: http://prod.sandia.gov/techlib/access-control.cgi/2011/112730.pdf

[92]. North American Electric Reliability Corporation, "Balancing and frequency control," January 2011. [Online]. Available: http://www.nerc.com/docs/oc/rs/NERC%20Balancing%20and%20Frequency%20Control%20040520111.pdf

[93]. Y. V. Makarov, "Wide-area storage and management system to balance intermittent resources in the Bonneville Power Administration and California ISO control areas," Pacific Northwest National Laboratory, June 2008. [Online]. Available: http://www.pnl.gov/main/publications/external/technical_reports/PNNL-17574.pdf

[94]. Y. Chen, M. Keyser, M. H. Tackett, and X. Ma, "Incorporating short-term stored energy resource into Midwest ISO energy and ancillary service market," *IEEE Transactions on Power Systems*, vol. 26, no. 2, pp. 829-838, May 2011.

[95]. Pacific Gas and Electric, "Renewable generation model – results and model demonstration," October 2010. [Online]. Available: http://www.cpuc.ca.gov/NR/rdonlyres/7462FECF-81A3-490A-AAE7-56AB0A7D8EFE/0/PGECPUCWorkshopOct22v8Final.ppt

[96]. DOE, "DOE energy innovation hub – batteries and energy storage," Mar, 2013. [Online]. Available: http://science.energy.gov/~/media/bes/pdf/hubs/JCESR_Fact_Sheet.pdf

[97]. D. Pudjianto, M. Aunedi, P. Djapic, and G. Strbac, "Whole-systems assessment of the value of energy storage in low-carbon electricity systems," *IEEE Transactions on Smart Grid*, vol. 5, no. 2, pp. 1098-1109, March 2014.

[98]. H. Daneshi and A. K. Srivatava, "Impact of battery energy storage on power system with high wind penetration," *IEEE Transmission and Distribution Conference and Exposition*, May 2012.

[99]. T. Logenthiran and D. Scrinivasan, "Short term generation scheduling of a microgrid," *IEEE Region 10 Conference*, January 2009.

[100]. C. Uckun, A. Botterud, and J. Birge, "An improved stochastic unit commitment formulation to accommodate wind power," *IEEE Transactions on Power Systems,* vol. 31, no. 4, pp. 2507-2517, September 2015.

[101]. Stein, M., Interpolation of spatial data: some theory for Kriging. Berlin: Springer Verlag, 1999.

[102]. W. Skamarock, J. Klemp, J. Dudhia, D. Gill, D. Barker, M. Duda, X.-Y. Huang, W. Wang, and J. Powers, "A description of the advanced research WRF version 3", NCAR, Boulder, CO. June 2008. [Online]. Available: http://www2.mmm.ucar.edu/wrf/users/docs/arw_v3.pdf

[103]. E. M. Constantinescu, V. M. Zavala, M. Rocklin, S. Lee, and M. Anitescu, "A computational framework for uncertainty quantification and stochastic optimization in unit commitment with wind power generation," *IEEE Transactions on Power Systems*, vol. 26, no. 1, pp. 431-441, February 2011.

[104]. J. D. Lyon, F. Wang, K. W. Hedman, and M. Zhang, "Market implications and pricing of dynamic reserve policies for systems with renewables," *IEEE Transactions on Power Systems*, vol. 30, no. 3, pp. 1593-1602, January 2015.

[105]. M. A. Ortega-Vazquez, "Optimal scheduling of electric vehicle charging and vehicle-to-grid services at household level including battery degradation and price uncertainty," *IET Generation, Transmission & Distribution*, vol. 8, no. 6, pp. 1007-1016, June 2014.

[106]. International Renewable Energy Agency, "Battery storage for renewables: market status and technology outlook," January. 2015. [Online]. Available: http://www.irena.org/DocumentDownloads/Publications/IRENA_Battery_Storage_report_2015.pdf

[107]. R. E. Bellman, *Dynamic Programming*. Princeton, NJ: Princeton University Press, 2003.

[108]. J. H. Kim and W. B. Powell, "Optimal energy commitment with storage and intermittent supply," *Operations Research*, vol. 59, no. 6, pp. 1347-1360, January. 2011.

[109]. NYISO, "Ancillary services manual," March 2015. [Online]. Available: http://www.nyiso.com/public/webdocs/markets_operations/documents/Manuals_and_Guides/Manuals/Operations/ancserv.pdf

[110]. GE Energy, "Western wind and solar integration study," National Renewable Energy Lab., Golden, CO, May 2010. [Online]. Available: http://www.nrel.gov/docs/fy10osti/47434.pdf

[111]. S. Eftekharnejad, G. T. Heydt, and V. Vittal, "Optimal generation dispatch with high penetration of photovoltaic generation," *IEEE Transactions on Sustainable Energy*, vol. 6, no. 3, pp. 1013-1020, July 2015.

[112]. F. Wang and K. W. Hedman, "Dynamic reserve zones for day-ahead unit commitment with renewable resources," *IEEE Transactions on Power Systems*, vol. 30, no. 2, pp. 612-620, March 2015.

[113]. D. F. Salas and W. B. Powell, "Benchmarking a scalable approximate dynamic programming algorithm for stochastic control of multidimensional energy storage problems," Department of Operations Research and Financial Engineering, Princeton Univ., Princeton, NJ, USA, Tech. Rep. 2004, 2015. [Online]. Available: http://castlelab.princeton.edu/Papers/Salas%20Powell%20-

%20Benchmarking%20ADP%20for%20multidimensional%20energy%20storage%20problems.pdf

[114]. P. Liu, S. Guo, X. Xu, and J. Chen, "Derivation of aggregation-based joint operating rule curves for cascade hydropower reservoirs," *Water Resource Management*, vol. 25, no. 13, pp. 3177-3200, June 2011.

[115]. I. Nalbantis and D. Koutsoyiannis, "A parametric rule for planning and management of multiple-reservoir systems," *Water Resource Research*, vol. 33, no. 9, pp. 2165-2177, September 1997.

[116]. Y. Chang, L. Chang, and F. Chang, "Intelligent control for modeling of real-time reservoir operation, part II: artificial neural network with operating rule curves," *Hydrological Processes*, vol. 19, no. 7, pp. 1431-1444, December 2004.

[117]. W. B. Powell, Approximate dynamic programming: solving the curses of dimensionality, 2nd edition. New York: Wiley, 2001.

[118]. V. Koritarov, *et al*., "Modeling ternary pumped hydro storage units," Argonne National Laboratory, Argonne, IL, August 2013. [Online]. Available: http://www.ipd.anl.gov/anlpubs/2013/10/77293.pdf

[119]. V. Koritarov, *et al*., "Modeling and analysis of value of advanced pumped hydro storage hydropower in the United States," Argonne National Laboratory, Argonne, IL, June 2014. [Online]. Available: http://www.dis.anl.gov/projects/psh/ANL-DIS-14-7_Advanced_PSH_Final_Report.pdf

[120]. P. Tan, M. Steinbach, and V. Kumar, *Introduction to data mining*, 1st edition. Boston: Addison-Wesley, 2006.

[121]. K. Sun, S. Likhate, V. Vittal, S. Kolluri, and S. Mandal, "An online dynamic security assessment scheme using phasor measurements and decision trees", *IEEE Transactions on Power Systems*, vol. 22, no. 4, pp. 1935-1943, November 2007.

[122]. Y. Zhang, M. Ilic, and O. Tonguz, "Application of support vector machine classification to enhanced protection relay logic in electric power grids," *Large Engineering Systems Conference on Power Engineering*, October 2007.

[123]. D. Srinivasan, W. S. Ng, and A. C. Liew, "Neural-network based signature recognition for harmonic source identification," *IEEE Transactions on Power Delivery*, vol. 2, no. 1, pp. 398-405, January 2006.

[124]. Z. Zabokrtsky, "Feature engineering in machine learning," Institute of Formal and Applied Linguistics, Charles University in Prague, Czech Republic. [Online]. Available: https://ufal.mff.cuni.cz/~zabokrtsky/courses/npfl104/html/feature_engineering.pdf

[125]. B. Severtson, "Feature engineering and selection in Azure Machine Learning," Microsoft Azure. [Online]. Available: https://azure.microsoft.com/en-us/documentation/articles/machine-learning-feature-selection-and-engineering/

[126]. I. Guyon and A. Elisseeff, "An introduction to variable and feature selection," *Journal of Machine Learning Research*, vol. 3, pp. 1157-1182, March 2003.

[127]. M. A. Hall and G. Holmes, "Benchmarking attribute selection techniques for discrete class data mining," *IEEE Transactions on Knowledge and Data Engineering*, vol. 15, no. 3, pp. 1-16, May 2003.

[128]. C. N. Sillar Jr. and A. A. Freitas, "A survey of hierarchical classification across different application domains," *Data Mining and Knowledge Discovery*, vol. 22, no. 1-2, pp. 31-72, January 2011.

[129]. L. Breiman, "Random forests," *Machine Learning*, vol. 45, no. 1, pp. 5-32, October 2001.

[130]. C. Hsu, C. Chang, and C. Lin, "A practical guide to support vector machine," National Taiwan University, Taipei, Taiwan, April 2010. [Online]. Available: http://www.csie.ntu.edu.tw/~cjlin/papers/guide/guide.pdf

[131]. J. M. Morales, R. Minguez, and A. J. Conejo, "A methodology to generate statistically dependent wind speed scenarios," *Applied Energy*, vol. 87, pp. 843-855, September 2009.

[132]. Pedregosa *et al*., "Scikit-learn: maching learning in Python," *Journal of Machine Learning Research*, vol. 12, pp. 2825-2830, October 2011.

[133]. J. Dupacová, N. Gröwe-Kuska, and W. Römisch, "Scenario reduction in stochastic programming: an approach using probability metrics," *Math. Program, Series A*, vol. 3, pp. 493–511, February 2003.